pH-driven instabilities in chemical systems

Magdalena Maria Wróbel

Submitted in accordance with the requirements for the
degree of Doctor of Philosophy

University of Leeds
School of Chemistry

Supervisors: Dr Annette Taylor

Prof. Stephen Scott

October 2012

"The candidate confirms that the work submitted is his/her own, except where work which has formed part of jointly authored publications has been included. The contribution of the candidate and the other authors to this work has been explicitly indicated below. The candidate confirms that appropriate credit has been given within the thesis where reference has been made to the work of others."

Chapter 2 is based on:

Hu, G.; Pojman, J. A.; Wrobel, M. M.; Scott, S. K.; Taylor, A. F. Base-Catalyzed Feedback in the Urea-Urease Reaction J. Phys. Chem. B 2010, 114, 14059, where contribution of different authors is as follows:

- Pojman J. A. provided initial ideas,

- Hu G. ran the clock experiments with acetic acid, I ran the clock experiments with sulphuric acid and CSTR experiments with both sulphuric and acetic acids

- Taylor A. F. wrote the model, I ran the simulations

- All commented on the paper

Chapter 3 is based on:

Wrobel, M. M.; Bansagi, T. Jr.; Scott, S. K.; Taylor, A. F.; Bounds, C. O.; Carranzo, A.; Pojman, J. A.; pH WaveFront propagation in the Urea-Urease Reaction Biophys. J., 2012, 103, 1-6 where contribution of different authors is as follows:

- Pojman J. A.; Carranzo, A.; and Bounds, C.O. provided initial ideas,

- I prepared the set-up and ran the front experiments together with Bansagi, T. Jr.

- Taylor A. F. wrote the model, I ran the simulations

- All commented on the paper

Abstract

The main aim of my project is to find new feedback driven enzymatic systems and to develop new biochemical oscillators. Such systems help in the understanding of nonlinear behaviour in biological systems and may also find applications in, for example, drug delivery or material science.

The first step was to obtain a clock behaviour and bistability in a new enzymatic system, the urea/urease/sulphuric acid reaction. A kinetic model has been proposed and compared with the experimental results.

Secondly, front propagation has been also observed in space under specific range of conditions and the results have been analysed theoretically by expansion of the model into spatial dimension.

Additionally irregular oscillations in the urea/urease/acetic acid system in flow were observed. Attempts to explain this behaviour theoretically have been made and discussed.

In order to produce more robust, regular oscillations in the urea/urease reaction, literature and experimental investigations of reactions that could provide negative feedback were made. The most obvious strategy to obtain a pH oscillator is to find an H^+ autocatalytic reaction, in which case the best candidates from organic reactions was hydrolysis of esters to produce a carboxylic acid. Simple general models have been proposed and several examples of esters have been investigated experimentally.

Apparently one of the investigated esters, acetyl salicylic acid, exhibited very interesting behaviour from the perspective of chemical locomotion. The motion of aspirin has been analyzed qualitatively under different set of conditions.

Acknowledgments

I would like thank first my supervisors: Annette and Steve for giving me lots of opportunities to learn about the world and nonlinear dynamics, and also freedom to follow my intuition and respect to my decisions during my postgraduate time here.

Second thanks go to Tamas for his advice and support in professional recording of spatial results and great help in writing codes in Matlab.

Thanks go also to people from old 2.23 office and surroundings: Theo, Barney, Cassey and Warren for introducing me to Leeds and for a big lesson about English culture.

Вялікі дзякуй Аляксандру, за штодзённы подых Усходняй Еўропы, за натхненне ва ўсіх маіх пачынаннях, і за ўсё тое, што немагчыма выказаць у словах…

Największe podziękowania dla najwierniejszych kibiców w moim życiu – moich rodziców – którzy wspierali mnie we wszystkich moich marzeniach i często byli jedynymi, którzy wierzyli w ich spełnienie; a także za nauczenie mnie szacunku dla każdego człowieka i każdej kultury, dzięki czemu mogłam dobrze i owocnie przeżyć 3 lata mojego doktoratu w Leeds.

ZBIGNIEW HERBERT
Prayer Of Mr Cogito

Lord
thank you for creating the world beautiful and of such variety
and also for allowing me in your inexhaustible goodness
to visit places which were not the scene of my daily torments

– for lying at night near a well in a square in Tarquinia while the swaying
bronze declared from the tower your wrath and forgiveness

and a little donkey on the island of Corcyra sang to me from
its incredible bellowing lungs the landscape's melancholy

and in the very ugly city of Manchester I came across
very good and sensible people

nature reiterated her wise tautologies the forest was
forest the sea was sea and rock was rock

stars orbited and things were as they should be — Jovis omnia plena

- forgive me for thinking only of myself when the life of
others cruel and irreversible turned round me like the huge
astrological clock in the church at Beauvais

for being too cowardly and stupid because I did not understand
so many things

and also forgive me for not fighting for the happiness of
poor and vanquished nations and for seeing only moonrise and museums
— thank you for the works created to glorify you which
have shared with me part of their mystery so that in gross conceit

I concluded that Duccio Van Eyck Bellini painted for me too

and likewise the Acropolis which I had never fully understood
patiently revealed to me its mutilated flesh

— I pray that you do not forget to reward the white-haired old
man who brought me fruit from his garden in the bay of the island of Ithaca

and also the teacher Miss Hellen on the isle of Mull whose
hospitality was Greek or Christian and who ordered light
to be placed in the window facing Holy Iona so that human
lights might greet one another

and furthermore all those who had shown me the way and said
kato kyrie kato

[…]
— grant O Lord that I may forget my foolish and very weary
persecutors when the sun sets into the vast uncharted
Ionian sea

that I may comprehend other men other tongues other suffering
and that I be not stubborn because my limitations are
without limits

and above all that I be humble, that is, one who sees
one who drinks at the spring

thank you O Lord for creating a world very beautiful and varied
and if this is Your temptation I am tempted forever
and without forgiveness

Translated by: Adam Czerniawski

Contents

List of Figures:

List of Tables:

1. Background

1.1 Introduction

When scientists try to describe any living organism or a system, the first striking observation is its periodicity, from the macroscale of planetary systems through seasonal climate cycles on the Earth to anatomical cycles in humans and animals. The need to understand and control of biological processes led scientists to find many examples of periodical regular changes exhibiting a wide ranges of periods: from cardiac rhythms (1 s) to ovarian cycles (weeks). Many of these processes take place at the cellular level, such as calcium, glycolytic or cAMP oscillations.

Table 1.1 Biochemical and Cellular Rhythms[1]

Rhythm	Period
Membrane potential oscillators	10 ms – 10 s
Cardiac rhythms	1 s
Smooth muscle contraction	Seconds – hours
Calcium oscillations	Seconds – minutes
Protoplasmic streaming	1 min
Glycolitic oscillations	1 min – 1 h
cAMP oscillations	10 min
Insulin secretion	Minutes
Gonadotropic hormone secretion	Hours
Cell cycle	30 min – 24 hours
Circadian rhythms	24 h
Ovarian cycle	Weeks – months

Starting from the cellular level, chemistry begins to play an increasingly important role in governing the cyclic processes. The history of observations of chemical oscillations begins 400 years ago when Boyle observed oscillatory ignition of phosphorus[2], though not many more examples of chemical oscillations were found until the discovery of periodical changes of colours in a mixture of potassium bromate, cerium(IV) sulphate, propanedioic acid, citric acid and dilute sulphuric acid made by Belousov in late 1950s[3]. Although this finding was not considered seriously at that time, a rediscovery of this reaction by Zhabotinsky[3] increased the interest in studying this "exotic" system. From that moment both intensive

theoretical and experimental studies have been done on the Belousov – Zhabotinsky (BZ) reaction. The BZ reaction began to be used as a model system to investigate oscillatory behaviour in different modified set-ups, such as with application of an electric field[4], in silica gels[5], in microemulsions[6] or as coupled oscillators[7].

Later on, new chemical systems exhibiting oscillations were discovered and created; the group of pH oscillatory systems create one of the largest and the most well studied. This is explored more in detail in section 1.5.

Although the BZ reaction has many interesting properties, the main practical problem arising from this system is the toxicity of the bromine components of this system, which does not allow this reaction to be applied, for example, in drug delivery. The same problems appear in all of the other known inorganic oscillatory systems. This is one of the main reasons for an urgent need of the creation of a non-toxic organic-based pH oscillator. The most promising group of reactions that has been deeply studied are enzyme-catalyzed reactions that are described in detail in section 1.3 and 1.4.

Section 1.2 explains the basic theoretical background of nonlinearity and autocatalysis in chemical kinetics, especially clock reactions (section 1.2.1), bistability and oscillations (section 1.2.2), and fronts (section 1.2.3).

1.2 Nonlinearity and autocatalysis

In order to observe complex behaviour in chemical systems *in vitro* two general criteria have to be fulfilled: the presence of feedback in the chemical kinetics and far-from-equilibrium conditions.

Possibly the simplest type of chemical reaction is described by the equation:

$$A + BC \rightarrow AB + C \tag{1.1}$$

so that

$$\frac{-d[\text{A}]}{dt} = \frac{-d[\text{BC}]}{dt} = \frac{d[\text{AB}]}{dt} = \frac{d[\text{C}]}{dt} = k[\text{A}][\text{BC}] \qquad (1.2)$$

Keeping the concentration of A or BC in great excess of that of the other, a pseudo-first-order reaction is established. Thus all the other kinetic processes in chemistry are nonlinear which means that the vast majority of chemical reactions belong to this second group. Of particular interest here will be systems that show rate acceleration with extent of reaction.

The best way to visualise these considerations is to plot variation of the reaction rate with the extent of reaction as in Fig. 1.1[2]. The only linear dependence is seen in the middle curve (i) that describes a first order reaction. The reaction rate plots for simple cases of second- and half-orders show significant deviation from the linear case. Nevertheless in every case the reaction rate decreases with consumption of the reactants which means that it is a deceleratory process.
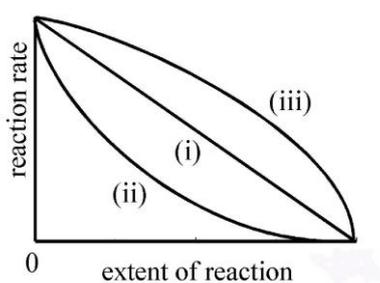
Figure 1.1 Dependence of reaction rate on extent of conversion for (ii) half-order, (i) first-order and (iii) second-order kinetics[2]

An additional source of deviation from linearity in chemical kinetics is the presence of feedback. Feedback is present when 'the products of later steps in the mechanism influence the rate of the earlier reaction, hence the rate of their own production'[2]. Then the processes can contain negative or positive feedback. The most widespread form of feedback is autocatalysis as in:

A + B → 2B $\qquad\qquad$ Rate = k[A][B] $\qquad$ (1.3)

or

A + 2B → 3B $\qquad\qquad$ Rate = k[A][B]^2 $\qquad$ (1.4)

where equation (1.3) represents quadratic and (1.4) cubic autocatalysis that can be visualised by plotting again the variation of the reaction rate with the extent of reaction. In Fig. 1.2 examples of acceleratory reactions are shown. In all the cases when autocatalysis is present the rate of reaction increases at the beginning until reaching a maximum before decreasing to zero.
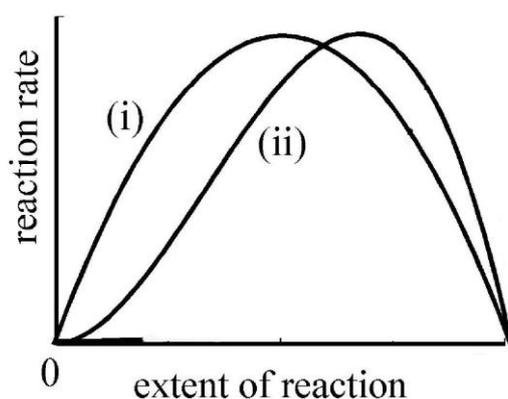
Figure 1.2 Dependence of reaction rate on extent of conversion for acceleratory systems with positive feedback: (i) quadratic autocatalysis, (ii) cubic autocatalysis[2]

Far-from-equilibrium conditions could be obtained in several ways. The first is to set up the initial concentrations in batch reactor in order to make the system approach the equilibrium. Another method is to perform the reaction in a flow reactor where continuous exchange of chemical species takes place through fresh inflow and matched outflow of reactants.

1.2.1 Clock reactions in a closed system

If a closed, thermostated reactor is considered as shown in Fig. 1.3, the system that contains positive feedback in its kinetics exhibits its autocatalytic character in clock behaviour[8].

Figure 1.3 Example of thermostated batch reactor

Clock reactions are characterized by a rapid acceleration of concentration of at least one of the species after an induction time (t_{ind}). In the case of a pH clock, the species are H^+ or OH^-. This behaviour is usually visualised by plotting concentration or reaction rate as a function of time, as in Fig. 1.4.
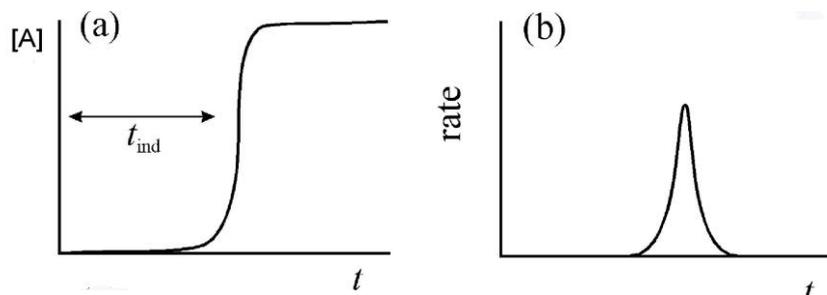
Figure 1.4 Dependence of (a) concentration of a reactant A, and (b) reaction rate on time for an autocatalytic reaction[2]

After the clock takes place, the system reaches its equilibrium state, then it is impossible to return to the initial state. There are known examples of reactions

displaying oscillations in closed system, such as the Belousov-Zhabotinsky or chlorite-iodide-malonic acid reaction[9], though the nature of all batch oscillations is transient and they eventually disappear in a relatively short timescale. Oscillations occur in intermediate concentrations, not reactants or products.

There is a possibility to observe a clock profile or an acceleration of the reaction without autocatalytic kinetics in the system[10]. This situation occurs when rapid removal of an inhibitor takes place or with phase transfer of one of the substrates. Then according to a simple model only one of the species exhibits acceleration in its rate of production (Fig. 1.5 d), whereas the other exhibits only a very slow exponential decrease (Fig. 1.5 c).
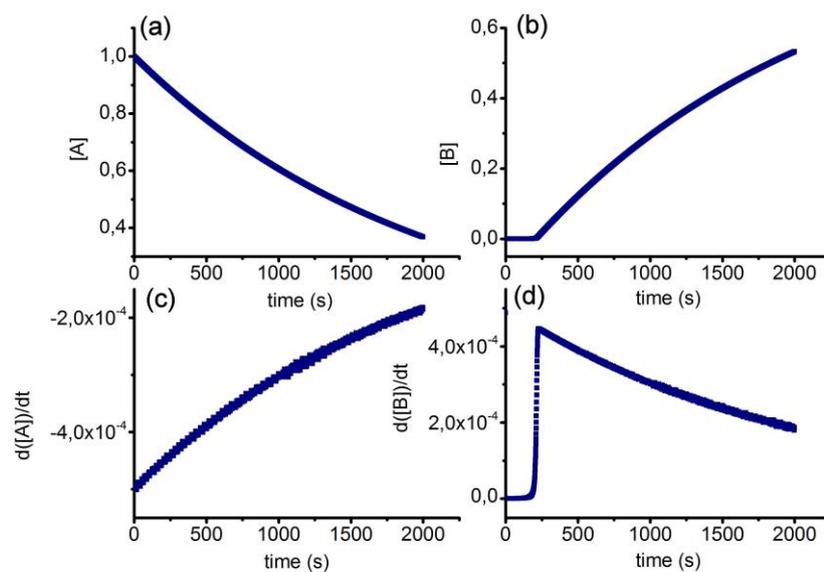
Figure 1.5 Illustration of changes of concentration of: (a) substrate [A], (b) product [B] and their derivatives in time (c) and (d) respectively for a simple model of inhibitor removal

Conversely, the classic model of a simple autocatalytic system shows that both the substrate and the product show an acceleration in their consumption (Fig. 1.6 a) and production (Fig. 1.6 b).
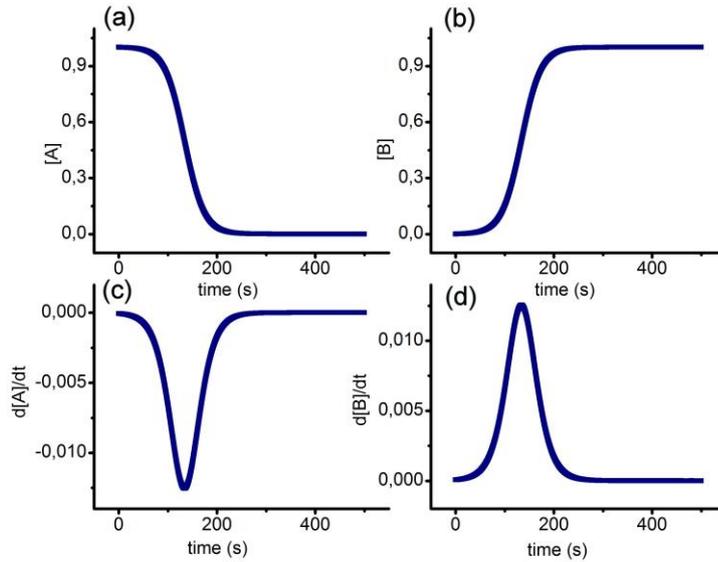
Figure 1.6 Illustration of changes of concentration of: (a) substrate [A], (b) product [B] and their derivatives in time (c) and (d) respectively for a simple model of autocatalytic production

Then to confirm positive feedback in the system requires either monitoring whether other species display acceleratory kinetics, or performing the reaction in CSTR in order to find bistability.

1.2.2 Bistability and oscillations in an open system

When a reaction that contains feedback in its kinetics is performed in a Continuous-Flow well-Stirred Tank reactor CSTR, as shown in Fig. 1.7, the system is kept in far-from-equilibrium conditions. The reactants are continuously pumped by a calibrated peristaltic pump into the well-stirred reactor through two or more channels. At the same time the outflow of products takes place in order to keep the volume of the reaction constant.
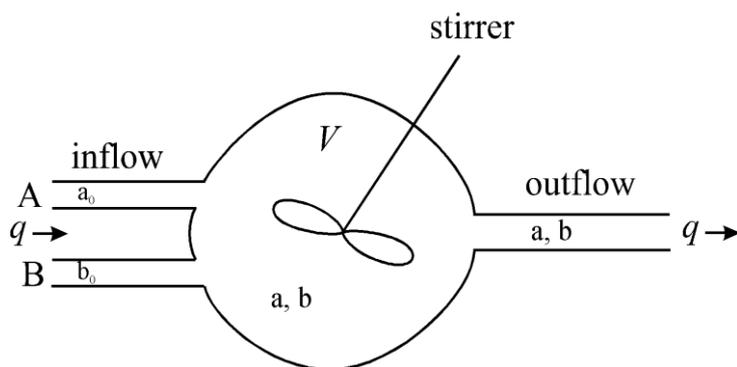
Figure 1.7 Example of the continuous-flow well-stirred tank reactor. A, B – inflow channels connected to peristaltic pump, q – flow, a_0, b_0 – initial concentration of A and B, a,b – concentration of A and B in the reactor

The rate of pumping and the size of reactor can influence the qualitative behaviour of the system. Depending on the flow rate and initial concentrations the system can be in one of three possible states. When the flow rate is very low the residence time of the molecules in the reactor is long enough to reach close to the chemical equilibrium state, called the thermodynamic state. When the flow rate is very high there is insufficient time for reaction to occur and an unreacted steady state is present, called the flow state. For a range of intermediate flow rates more complex behaviour is present as discontinuous changes in concentrations of reactants take place during continuous changes of the parameter (flow rate). This phenomenon is known as a bifurcation[2]. Depending on the kinetics of the system several types of bifurcations are possible. A saddle-node bifurcation causes the coexistence of two or more steady states i.e. multistability. The simplest scenario in a multistable system is bistability described above. It consists of two stable branches and one unstable branch as shown in Fig. 1.8. The interval of flow rates where we have either the flow or the thermodynamic branch depends on the history of the reaction; this is called hysteresis[2]. Thus if we start from the high flow rate and decrease it, we follow the flow branch, and if we start from the low flow rate and increase it, we follow the thermodynamic branch. In between those two branches a dashed line appears that represents an unstable steady state that can be calculated numerically but not

obtained experimentally as whenever the system is perturbed to the in unstable state it directly goes to a stable one. The range of flows where coexistence of two steady states takes place usually varies with initial concentrations of all substrates in the system.
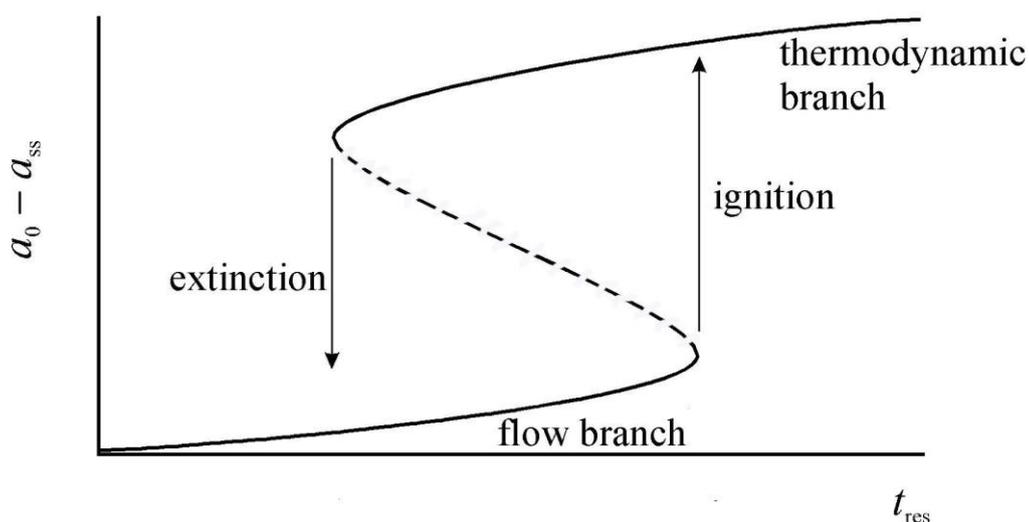
Figure 1.8 Representation of system displaying bistability: a bifurcation diagram where: t_{res} is residence time, a_{ss} is a steady state value of variable, for example pH, or concentration of substrate[2]

Another type of bifurcation that takes place in an open system is a Hopf bifurcation[2]. It is a transition from a steady state to oscillations when one parameter is varied. As with bistability, the region where oscillations are present depends on the initial concentration of substrates and flow rate. Also the amplitude and frequency of oscillations differs depending on the initial conditions in the system. A very useful tool for controlling the system is a cross-shape phase diagram, shown in Fig. 1.9. It is a plot of the dynamical behaviour as a function of two parameters. It could be a theoretical or an experimental map of a complex chemical system showing regions of steady states, bistability and oscillations. It was first theoretically constructed by De Kepper, Kustin and Epstein for the chlorite-iodate-arsenite reaction[11].
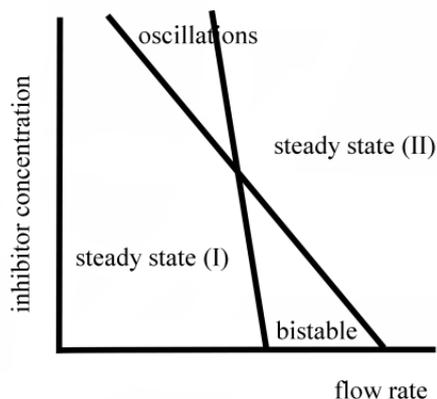
Figure 1.9 Schematic representation of bistability and oscillatory regions depending on flow rate and concentration of inhibitor: i.e. a phase diagram[12]

1.2.3 Fronts

Autocatalytic reactions are also known to display a number of characteristic spatial effects when coupled with diffusion. Chemical wavefronts and patterns are observed[2]. These phenomena are widespread in nature e. g. Lisegang structures in minerals[13], or mechanisms of biological morphogenesis[14].

The simplest nonlinear spatial phenomenon is a reaction-diffusion front. In a chemical front the reaction occurs at the boundary between the reactant and the product as it propagates through the mixture. The first chemical fronts were observed by Luther in a permanganate oxidation of oxalic acid in 1906[15]. Since that discovery many chemical fronts have been reported of which pH fronts are one of the most well-studied. A pH front is usually visualized by pH indicators that change colour significantly when the clock reaction takes place so that it is possible to observe the transitions between substrate and product solution. Propagation of the front may be either one-dimensional in a thin tube or two-dimensional in a Petri dish[8] or Hele-Shaw cell[16,17] (with a reasonably thin solution or gap width, otherwise the fronts becomes three-dimensional). The more dimensions, the more complex behaviour could be observed. Tubes, Hele-Shaw cells and Petri dishes are closed systems where after an initiation the front propagates until it reaches an equilibrium state. To study

more complex behaviour, chemical waves and fronts can be examined in an open system[8]. There is a number of examples of such different open reactors, e.g. continuously-fed unstirred reactor[18]. As biological and geological systems belong to a group of non-uniform media, a number of experiments exploring chemical waves performed in spatially modulated systems have been made.[19,20]

The typical chemical front is initiated by putting one drop of either the product solution or catalyst into the reactant solution. Depending on the spatial orientation of the tube/Hele-Shaw cell the front may propagate horizontally or vertically. An important parameter describing wavefronts is the front speed that is defined as the distance travelled per unit of time. In case of a system with quadratic autocatalysis planar front speed is constant and depends on the concentrations of substrates and the diffusion coefficient, expressed in equation 1.5:

$$c = A\sqrt{(Dk')}$$

(1.5)

where: c – wave speed, A – constant, D – diffusion coefficient, k' – pseudo-first rate order rate constant of autocatalysis.

Another important parameter describing a chemical front is the curvature[8]. In general, propagating fronts can be planar or curved, stable or unstable, as shown in Fig. 1.10.

Figure 1.10 Examples of a planar (a) and a curved (b) front in the bromate-sulphite reaction, $[BrO_3^-]_0 = 0.05$ M, $[HSO_3^-]_0 = 0.01$ M, $[SO_3^{2-}]_0 = 0.03$ M, indicator: bromocresol purple, tube diameter: (a) = 1 mm, (b) = 5 mm

The simplest method[12] of analysing the curvature K of the front in pseudo 2D system is in terms of radius, R, where:

K = 1/R   (1.6)

When K is positive, the front curves towards the direction of propagation. When K is negative, the front curves in the opposite direction. In a planar front K = 0 so it has an infinite radius of curvature[8]. Curvature effects depend on the effect of convection that arise from differences in the density between reactants and products[8]. As the density depends on the temperature and composition of the solution, both front speed and curvature vary with the concentration of substrates and also depend on whether the reaction is exo- or endothermic. From those differences, two types of convection – simple and double-diffusive (multicomponent) – can arise[8]. The first one appears when both thermal and volume changes are positive ($\Delta T > 0$ and $\Delta V > 0$) so that the reaction is exothermic and density decreases. An example is the iodate-arsenous reaction[21]. The other case is when the temperature rises but there is a volume contraction ($\Delta T > 0$ and $\Delta V < 0$) so the reaction is still exothermic but the density increases, as in the iron(II)-nitric acid reaction[22]. Double-diffusive convection may also appear when ΔT and ΔV have the same sign arising from differences in diffusion coefficients of reactants and products as the iodate-nitric acid[23] or the iodate-sulphite system[24]. Double-diffusive convection is a phenomenon widespread in nature and was studied primarily in mixing in currents in oceans[25].

1.3 Kinetics of enzymatic reactions

The same as other catalysts, enzymes provide an alternative path with lower free energy of activation of a specific reaction, though, as they are macromolecules sensitive to changes of many parameters, the kinetics of enzyme-catalyzed processes can be complex. One of the most well known and simplest models of enzyme

catalysis was proposed in 1913 by Michaelis and Menten[26]. They assumed that the enzyme catalyzed reaction proceeds through two steps:

$$E + S \xleftrightarrow{\;k_1,k_{-1}\;} ES \qquad\qquad (1.7)$$

$$ES \xrightarrow{\;k_2\;} E + P \qquad\qquad (1.8)$$

where: E – enzyme, ES – enzyme-substrate complex, P – product,

Assuming that $[S_0] \gg [E_0]$ and $k_{-1} \gg k_2$ so that the reaction (1.8) is a rate determining step and using steady state approximations so that the concentration of enzyme-substrate complex is constant in time, $\dfrac{d[ES]}{dt} = 0$, the initial velocity (v_0) of the enzymatic reaction is given by:

$$v_0 = \frac{V_M [S]}{K_M + [S]} \qquad\qquad (1.9)$$

where:

$$K_M = \frac{k_{-1} + k_2}{k_1} \text{ (Michaelis constant)}, \qquad\qquad (1.10)$$

$$V_M = k_2 [E]_0 \text{ (maximum initial rate)} \qquad\qquad (1.11)$$

The maximum velocity, V_M (1.11), gives information about the rate when the whole enzyme present in the system is converted to the enzyme-substrate complex. The constant k_2 in eq. 1.11 is called the turnover number. This constant gives information about the number of molecules of substrate converted into product per unit of time. As the turnover numbers could be measured only for pure enzymes, the activity of enzymes is usually given as units of activity per milligram of protein. One unit of activity is the amount of enzyme that produces one micromole of product per minute. The Michaelis constant, K_M, indicates the strength of ES binding when $k_{-1} \gg k_2$. The

bigger the value of K_M, the weaker the binding. Values of K_M vary between 10^{-2} and 10^{-7} M. K_M depends on pH and temperature.

Enzymes are catalysts that are very sensitive to many factors. The presence of other compounds can either increase or decrease their catalytic activity. The first case is in the presence of molecules called coenzymes[26]. Decrease of enzyme activity can proceed through three different kinetic pathways depending on type of inhibitor present in the system[26]. The first type is called competitive inhibition as both the substrate (S) and the inhibitor (I) compete for the same active site. Noncompetitive inhibition appears when the inhibitor does not bind to the active site but stops the enzyme from releasing the products. When the inhibitor binds not to the enzyme itself, but to the enzyme-substrate complex in order to create inactive ESI complex the inhibition is uncompetitive.

Enzyme activity dependence on the pH is also explained in terms of creation of active and inactive complexes by binding H^+[26]. The complexes exist in reversible equilibria:

$$EnH_2 \Leftrightarrow EnH^- + H^+ \Leftrightarrow En^{2-} + 2H^+ \tag{1.12}$$

For many enzymes, both EnH_2 and En^{2-} complexes are inactive, whereas EnH^- is the active one. From those dependencies, the activity of enzyme versus pH plot is usually a bell-shape curve specific for each enzyme.

Apart from the simple case with one active site, the enzyme can possess two or more active sites. In that case the mechanism could be sequential and proceed according to either an ordered or random path[27]. In an ordered mechanism first the substrates are bound and then products also released in an established sequence. In a random mechanism also binding of the substrates takes place before release of any product, but in both steps there is no order in which the substrate or product

undergoes reaction first. There is also a nonsequential mechanism possible called "ping-pong" when one of the products is released before the second substrate is bound.

In many cases, when enzymes possess multiple active centers, the Michaelis-Menten model is not valid. Several models such as the allosteric or the induced-fit model take into account additional effects such as cooperativity[27].

1.4 Nonlinearity in enzymatic reactions

Enzymes are essential catalysts in vast majority of metabolic processes in human body. Metabolic pathways are connected to each other by a complex network where many important reaction chains proceed in cycles. In such important biochemical cycles such as citric acid, glyoxylate or urea cycle all steps are enzyme-catalyzed[28]. It is obvious that feedback is present in those pathways because of nonlinear, periodical production of certain compounds. The probability that enzyme catalysis is the main source of feedback in those cycles is very high.

Many enzymatic reactions have been studied theoretically for decades from the perspective of being potential oscillators. The early models where oscillations were seen either involved a two enzyme system where the product of one reaction acted as an inhibitor for the other enzyme[29,30], or when substrate inhibition was coupled with product activation[31], or when in two-substrate systems one acts as inhibitor[32]. Newer detailed studies[33] showed that fluctuations in enzyme structure lead to violations of Michaelis-Menten kinetics and manifest in excess substrate inhibition effect. This effect is responsible for dynamic disorder driven bistability. Also oscillations caused by buffer and salt concentration were studied when enzyme reactions were performed in a charged membrane[34]. Theoretical models suggested oscillations occurred because of the pH-enzyme activity dependence[35] where pepsin

and chymotrypsin were suggested as potential enzymes for pH oscillators. Additionally potential pH oscillations in enzyme-catalyzed ester hydrolysis were studied by Ohmori and coworkers in an immobilized enzyme system[36], compartmentalized reactor[37] or a CSTR[38]. They studied trypsin, bromelain, ficin, chymotrypsin and papain catalyzed reactions, where only the last two gave oscillations in a reasonable range of experimental parameters.

The first and most intensively studied in vitro oscillating enzymatic system is glycolysis where allosteric phosphofructokinase is the main enzyme responsible for the oscillatory behavior. The detailed mechanism and ways of controlling the glycolytic system were studied from the oscillations in yeast cells[39-41], beef heart extracts[42-44] or rat skeletal muscle extracts[45,46] up to performing the reaction in a CSTR and obtaining simple and complex sustained oscillations in NADH[47]. Another well-studied example of an enzymatic oscillator is the oxidation of NADH catalyzed by horseradish peroxidase[48-50]. The oscillations in this system are between ferriperoxidase and oxyperoxidase. Also periodicity in the synthesis of cyclic adenosine monophosphate (cAMP) in *Dictyostelium discoideum* is attributed to two enzymes: adenyl cyclase and ATP pyrophosphohydrolase. The main mechanism responsible for oscillations here is the cooperative activation of the enzymes by products of different steps of the reaction, namely activation of adenyl cyclase by 5'AMP and of ATP phosphohydrolase by cAMP[48,51].

The first experimental attempts to design an enzymatic pH oscillator were made with use of papain[52,53], however regular oscillations could not be confirmed in further studies[54]. During the next years, a few attempts to construct enzymatic pH oscillators were made by modifying known feedback containing inorganic reactions[55-57]. The most significant step in designing an organic enzymatic pH

oscillator was shown in the glucose oxidase catalyzed reaction[58]. As this enzyme reacts according to the ping-pong mechanism, in the presence of different electron acceptors as substrates (such as glucose, molecular oxygen or ferricyanide) the system exhibits clocks, bistability and oscillations within a certain range of parameters. Further study showed also that this system exhibits interesting spatial behavior such as fronts and pulses[59].

1.5 Systematic design of pH oscillators

The growing interest of research on pH oscillators began in the mid80s. A discovery of the first halogen-free oscillator in sulfide ion − hydrogen peroxide reaction in a CSTR[60] initiated a new direction in the field of oscillatory reactions. pH changes became an important parameter and lead to discoveries of whole families of pH oscillators in the second half of 80s, such as: iodate-sulphite-ferrocyanide[61], hydrogen peroxide-thiosulphate-copper (II)[62], iodate-sulphite-thiourea[63], iodate-thiosulphate-sulphite[64], bromate − sulphite − ferrocyanide[65], hydrogen peroxide − sulphite − ferrocyanide[66], periodate − thiosulphate[67], or periodate-hydroxylamine[68]. Based on these systems and on theoretical models, a systematic approach to create new pH oscillators was proposed by Rabai, Orban and Epstein[69]. The strategy is firstly to find an autocatalytic reaction which produces H^+, so that it supports a clock behavior. Then it needs to be coupled with a hydrogen consuming reaction which will exhibit a pulse in a closed system, if the timescales of the rate constants of both reactions are similar. This coupled system performed in a CSTR should exhibit pH oscillations within a range of conditions given by a cross-shaped phase diagram. Using this strategy, a lot of new chemical oscillators have been created from the growing families of bromate[70-73], iodate[74] or sulphite[75-77] reactions. The growing interest in pH oscillators has moved into

synthesis of organic-based pH oscillators, such as the methylene-glycol-gluconolactone system[78,79]. The area of research on pH oscillations has also recently spread to polymer science[80,81], where the pH oscillation reaction coupled with a pH-sensitive polymer acts as a chemomechanical device, i.e. pump or actuator.

1.6 Outline of the thesis

The aim of the research discussed here was to construct a new enzymatic pH oscillator. One of the most promising enzymatic reactions that had not been investigated before in unbuffered conditions was the urea/urease reaction. As base is produced in this reaction, the initial pH was adjusted by sulphuric acid. The results of investigation of this reaction leading to clock behavior in a batch reactor and bistability in a CSTR are shown in Chapter 2. A simple model of this system mimicking the behavior in both setups is also introduced in Chapter 2. The urea/urease system was also investigated spatially, and led to pH fronts within a certain range of initial conditions which is the subject of Chapter 3. Also the model was expanded to include a spatial dimension and compared to the experimental results.

When the acid was changed to a weak, organic one, i.e. acetic acid, the behavior of the system changed: there was a variation in the shape of the pH-time plot in a closed system, but most significantly in a CSTR oscillations have been observed. The experimental results as well as introduction of different models to explain this behavior are described in Chapter 4.

The next step was to couple the reaction with an acid autocatalytic system. From a literature study and analysis of simple models it appeared that one of the most promising set of reactions to be coupled with the urea/urease system was

hydrolysis of esters and heterocycles. Kinetic analysis of the models and experimental investigation of several examples of hydrolysis of organic compounds, including aspirin, are shown in Chapter 5.

During the investigation of aspirin hydrolysis an intriguing spatial behavior of the crystals of aspirin has been observed and investigated: particle self-motion. The analysis of this phenomenon is the subject of Chapter 6.

Chapter 7 discusses future work connected to the results shown in this thesis and the possible applications of them.

1.7   References

(1)   Tyson, J. J.: *Biochemical Oscillators*; Springer-Verlag, New York, **2002**.

(2)   Scott, S. K.: *Oscillations, Waves and Chaos in Chemical Kinetics*; Oxford University Press: New York, **1994**.

(3)   Zhabotinsky, A. M.: *Chaos* **1991**, *1,* 379-386.

(4)   Agladze, K. I.; Dekepper, P.: *J. Phys. Chem.* **1992**, *96*, 5239-5242.

(5)   Neumann, B.; Nagyungvarai, Z.; Muller, S. C.: *Chem. Phys. Lett.* **1993**, *211*, 36-40.

(6)   Carballido-Landeira, J.; Vanag, V. K.; Epstein, I. R.: *PCCP Phys. Chem. Chem. Phys.* **2010**, *12*, 3656-3665.

(7)   Taylor, A. F.; Kapetanopoulos, P.; Whitaker, B. J.; Toth, R.; Bull, L.; Tinsley, M. R.: *Phys. Rev. Lett.* **2008**, *100,* 214101-1 - 214101-4.

(8)   Epstein IR; Pojman, J. A.: *An Introduction to Nonlinear Chemical Dynamics*; Oxford University Press: New York, 1998.

(9)   Noszticzius, Z.; Qi, O. Y.; McCormick, W. D.; Swinney, H. L.: *J. Am. Chem. Soc.* **1992**, *114*, 4290-4295.

(10)   Lente, G.; Bazsa, G.; Fabian, I.: *New J. Chem.* **2007**, *31*, 1707-1707.

(11)   Dekepper, P.; Epstein, I. R.; Kustin, K.: *J. Am. Chem. Soc.* **1981**, *103*, 2133-2134.

(12)   Epstein IR; Pojman, J. A.: *An Introduction to Nonlinear Chemical Dynamics*; Oxford University Press: New York, **1998**.

(13)   Heaney, P. J.; Davis, A. M.: *Science* **1995**, *269*, 1562-1565.

(14)   Vanag, V. K.; Epstein, I. R.: *Proc. Natl. Acad. Sci. U. S. A.* **2003**, *100*, 14635-14638.

(15)   Showalter, K.: *Nonlinear Sci. Today* **1994**, *4*, 1-10.

(16)   Bansagi, T.; Horvath, D.; Toth, A.: *J. Chem. Phys.* **2004**, *121*, 11912-11915.

(17)   Bockmann, M.; Muller, S. C.: *Phys. Rev. Lett.* **2000**, *85*, 2506-2509.

(18)   Tam, W. Y.; Horsthemke, W.; Noszticzius, Z.; Swinney, H. L.: *J. Chem. Phys.* **1988**, *88*, 3395-3396.

(19)   Davydov, V. A.; Manz, N.; Steinbock, O.; Zykov, V. S.; Muller, S. C.: *Phys. Rev. Lett.* **2000**, *85*, 868-871.

(20)   Toth, T.; Horvath, D.; Toth, A.: *J. Chem. Phys.* **2007**, *127*.

(21)   Pojman, J. A.; Epstein, I. R.; McManus, T. J.; Showalter, K.: *J. Phys. Chem.* **1991**, *95*, 1299-1306.

(22)   Pojman, J. A.; Nagy, I. P.; Epstein, I. R.: *J. Phys. Chem.* **1991**, *95*, 1306-1311.

(23)   Nagy, I. P.; Keresztessy, A.; Pojman, J. A.; Bazsa, G.; Noszticzius, Z.: *J. Phys. Chem.* **1994**, *98*, 6030-6037.

(24)   Pojman, J. A.; Komlosi, A.; Nagy, I. P.: *J. Phys. Chem.* **1996**, *100*, 16209-16212.

(25)   Turner, J. S.: *Phys. Fluids a-Fluid Dyn.* **1991**, *3*, 1218-1232.

(26)   Chang, R.: *Physical Chemistry with Applications to Biological Systems*; University Science Books, Willams College, **1981**.

(27)   Bisswagner, H.: *Enzyme Kinetics*; Weinhein: Wiley-VCH Verlag GmbH & Co. KGaA, **2008**.

(28)   Nelson DL; Lehninger AL; Cox MM: *Principles of Biochemistry*; New York: WH Freeman & Co., 2005.

(29)   Spangler, R. A.; Snell, F. M.: *Nature* **1961**, *191*, 457-458.

(30)   Spangler, R. A.; Snell, F. M.: *J. Theor. Biol.* **1967**, *16*, 381-405.

(31)   Selkov, E. E.: *Eur. J. Biochem.* **1968**, *4*, 79-86.

(32)   Seelig, F. F.: *Z. Naturfors. Sect. A-J. Phys. Sci.* **1976**, *31*, 731-738.

(33)   Chaudhury, S.; Igoshin, O. A.: *J. Phys. Chem. B* **2009**, *113*, 13421-13428.

(34)   Chay, T. R.; Zabusky, N. J.: *J. Biol. Phys.* **1983**, *11*, 27-31.

(35)   Shen, P. D.; Larter, R.: *Biophys. J.* **1994**, *67*, 1414-1428.

(36)   Ohmori, T.; Yang, R. Y. K.: *Biophys. Chem.* **1996**, *59*, 87-94.

(37)   Ohmori, T.; Nakaiwa, M.; Yamaguchi, T.; Kawamura, M.; Yang, R. Y. K.: *Biophys. Chem.* **1997**, *67*, 51-57.

(38)   Ohmori, T.; Yu, W. F.; Yamamoto, T.; Endo, A.; Nakaiwa, M.; Amemiya, T.; Yamaguchi, T.: *Chem. Phys. Lett.* **2005**, *407*, 48-52.

(39)   Chance, B.; Ghosh, A.; Estabrook, R. W.: *Proc. Natl. Ac. Sci. U S A* **1964**, *51*, 1244-1251.

(40)   Chance, B.; Ghosh, A.; Higgins, J. J.; Maitra, P. K.: *Ann. N.Y. Acad. Sci.* **1964**, *115*, 1010-1024.

(41)   Ghosh, A.; Chance, B.: *Biochem. Biophys. Res. Commun.* **1964**, *16*, 174-181.

(42)   Frenkel, R.: *Arch. Biochem. Biophys.* **1968**, *125*, 151-156.

(43)   Frenkel, R.: *Arch. Biochem. Biophys.* **1966**, *115*, 112-121.

(44)   Frenkel, R.: *Biochem. Biophys. Res. Commun.* **1965**, *21*, 497-502.

(45)   Tornheim, K.; Lowenstein, J. M.: *J. Biol. Chem.* **1975**, *250*, 6304-6314.

(46)   Tornheim, K.; Lowenste.Jm: *J. Biol. Chem.* **1974**, *249*, 3241-3247.

(47)   Nielsen, K.; Sorensen, P. G.; Hynne, F.; Busse, H. G.: *Biophys. Chem.* **1998**, *72*, 49-62.

(48)   Goldbeter, A.; Caplan, S. R.: *Ann. Rev. Biophys. Bioeng.* **1976**, *5*, 449-476.

(49)   Yamazaki, I.; Yokota, K.; Nakajima, R.: *Biochem. Biophys. Res. Commun.* **1965**, *21*, 582-586.

(50)   Kummer, U.; Hauser, M. J. B.; Wegmann, K.; Olsen, L. F.; Baier, G.: *J. Am. Chem. Soc.* **1997**, *119*, 2084-2087.

(51)   Rossoman.Ef; Sussman, M.: *Proc. Nat. Acad. Sci. U. S. A.* **1973**, *70*, 1254-1257.

(52)   Caplan, S. R.; Naparste.A; Zabusky, N. J.: *Nature* **1973**, *245*, 364-366.

(53)   Naparast.A; Thomas, D.; Caplan, S. R.: *Biochim. Biophys. Acta* **1973**, *323*, 643-646.

(54)   Ohmori, T.; Yang, R. Y. K.: *Biotechnol. Appl. Biochem.* **1994**, *20*, 67-78.

(55)   Vanag, V. K.: *J. Phys. Chem. A* **1998**, *102*, 601-605.

(56)   Hauser, M. J. B.; Strich, A.; Bakos, R.; Nagy-Ungvarai, Z.; Muller, S. C.: *Farad. Disc.* **2001**, *120*, 229-236.

(57)   Hauser, M. J. B.; Fricke, N.; Storb, U.; Muller, S. C.: *Zeit. Physik. Chem. Internat. J. Res. Phys. Chem. & Chem. Phys.* **2002**, *216*, 375-390.

(58)   Vanag, V. K.; Miguez, D. G.; Epstein, I. R.: *J. Chem. Phys.* **2006**, *125*, 194595-1 - 194595-11.

(59)   Miguez, D. G.; Vanag, V. K.; Epstein, I. R.: *Proc. Nat. Acad. Sci. U.S.A.* **2007**, *104*, 6992-6997.

(60) Orban, M.; Epstein, I. R.: *J. Am. Chem. Soc.* **1985**, *107*, 2302-2305.

(61) Edblom, E. C.; Orban, M.; Epstein, I. R.: *J. Am. Chem. Soc.* **1986**, *108*, 2826-2830.

(62) Orban, M.; Epstein, I. R.: *J. Am. Chem. Soc.* **1987**, *109*, 101-106.

(63) Rabai, G.; Nagy, Z. V.; Beck, M. T.: *React. Kinet. Catal. Lett.* **1987**, *33*, 23-29.

(64) Rabai, G.; Beck, M. T.: *J. Phys. Chem.* **1988**, *92*, 4831-4835.

(65) Edblom, E. C.; Luo, Y.; Orban, M.; Kustin, K.; Epstein, I. R.: *J. Phys. Chem.* **1989**, *93*, 2722-2727.

(66) Rabai, G.; Kustin, K.; Epstein, I. R.: *J. Am. Chem. Soc.* **1989**, *111*, 3870-3874.

(67) Rabai, G.; Beck, M. T.; Kustin, K.; Epstein, I. R.: *J. Phys. Chem.* **1989**, *93*, 2853-2858.

(68) Rabai, G.; Epstein, I. R.: *J. Phys. Chem.* **1989**, *93*, 7556-7559.

(69) Rabai, G.; Orban, M.; Epstein, I. R.: *Accounts Chem. Res.* **1990**, *23*, 258-263.

(70) Orban, M.; Epstein, I. R.: *J. Am. Chem. Soc.* **1992**, *114*, 1252-1256.

(71) Jonnalagadda, S. B.; Chinake, C. R.; Simoyi, R. H.: *J. Phys. Chem.* **1995**, *99*, 10231-10236.

(72) Rabai, G.; Hanazaki, I.: *J. Phys. Chem.* **1996**, *100*, 10615-10619.

(73) Okazaki, N.; Rabai, G.; Hanazaki, I.: *J. Phys. Chem. A* **1999**, *103*, 10915-10920.

(74) Mambo, E.; Simoyi, R. H.: *J. Phys. Chem.* **1993**, *97*, 13662-13667.

(75) Rabai, G.; Hanazaki, I.: *Chem. Commun.* **1999**, 1965-1966.

(76) Rabai, G.; Hanazaki, I.: *J. Phys. Chem.* **1996**, *100*, 15454-15459.

(77) Kovacs, K. M.; Rabai, G.: *J. Phys. Chem. A* **2001**, *105*, 9183-9187.

(78)   McIlwaine, R.; Kovacs, K.; Scott, S. K.; Taylor, A. F.: *Chem. Phys. Lett.* **2006**, *417*, 39-42.

(79)   Kovacs, K.; McIlwaine, R. E.; Scott, S. K.; Taylor, A. F.: *J. Phys. Chem. A* **2007**, *111*, 549-551.

(80)   Kim, S. J.; Kim, M. S.; Kim, S. I.; Spinks, G. M.; Kim, B. C.; Wallace, G. G.: *Chem. Mat.* **2006**, *18*, 5805-5809.

(81)   Topham, P. D.; Howse, J. R.; Fernyhough, C. M.; Ryan, A. J.: *Soft Matter* **2007**, *3*, 1506-1512.

2. Clocks and bistability in the urea/urease/sulphuric acid reaction

2.1 Introduction

The hydrolysis of urea catalyzed by the enzyme urease has the overall stoichiometry:

$$(NH_2)_2CO + H_2O \xrightarrow{\quad urease \quad} CO_2 + 2NH_3 \qquad (2.1)$$
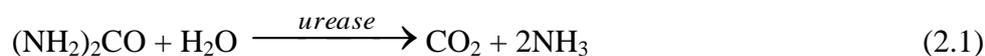
It is one of the most well-studied enzymatic systems. Ureases are widely spread throughout nature, they are responsible for nitrogen transport in plants[1] as well as for diseases such as urinary stone formation[2], or the presence of *Helicobacter Pylori* in the stomach[3]. Although the reaction has been studied from a molecular[4,5], kinetic[6,7] and biological perspectives[8,9], the system in such studies is always buffered so the autocatalytic character of this reaction has not been seen.

In this chapter it is shown that in unbuffered conditions, starting from low pH, the catalytic activity of the enzyme increases together with release of one of the products, ammonia, leading to nonlinear effects – a clock in batch and bistability in flow reactors. The kinetic model of the urea/urease reaction in unbuffered conditions is introduced and compared with the experimental results.

2.2 The urea/urease reaction

The first urease was found in putrid urine by Musculus, but detailed studies on this enzyme began with discovery of its presence in soybean by Takeuchi[10]. Currently a few dozen ureases are known from different sources such as bacteria[11,12], fungi[13,14] and plants[15,16]. Studies on the structure of urease show that depending on its source, the enzyme can be built by different sequences of genes but all types of urease possess two nickel active sites Ni_1 and Ni_2[10]. Ni_1 is surrounded by two histidine groups bound by N-atoms and lysine groups bound by an O-atom. Ni_2 is

surrounded also by an additional two histidine groups and aspartic acid bound by an

O-atom (Fig. 2.1).
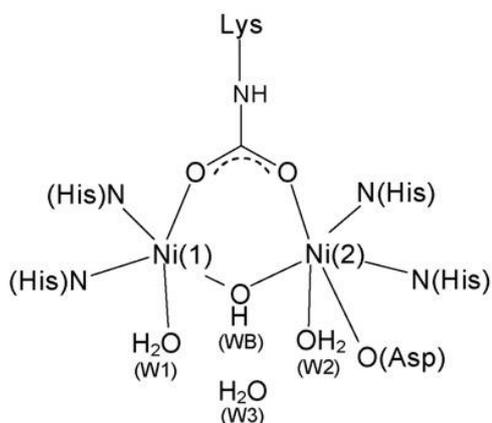
Figure 2.1 Structure of the active centre of urease, copied from (10)

The activity of urease depends on pH as variations in pH change the

conformation of proteins around binding site, resulting in a bell-shape function of

activity with respect to pH[17] (Fig.2.2).
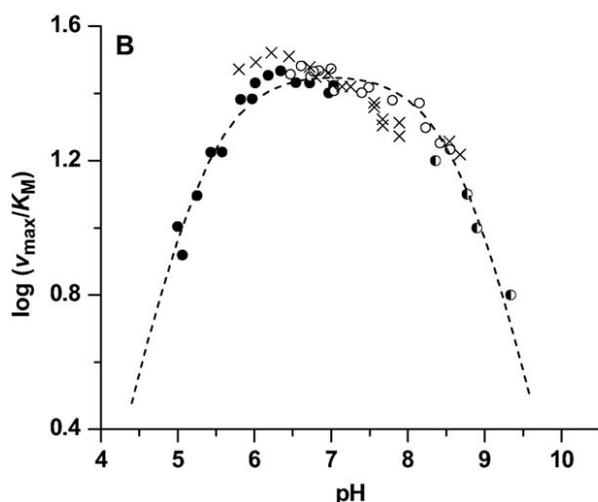
Figure 2.2 pH-rate activity of Jack bean urease, copied from (17)

Various compounds also have the potential to inhibit the activity of urease[10]. The

inhibitors are divided according to their inhibiting strength. The group of weak

inhibitors consists of the substrate urea, the product ammonium ions, and substrate

analogues[18]. Urease undergoes inactivation during the initial phase of activity with

weak inhibitors, then reactivates during course of the reaction. Thiols and

acetohydroxamic acid inhibit urease competitively with medium strength[19]. The

strongest urease inhibitors are esters and amides of phosphoric acid[2]. Heavy metal ions inhibit urease with strength changing as: $Hg^{2+} \approx Ag^{+} > Cu^{2+} > Ni^{2+} > Cd^{2+} > Zn^{2+} > Co^{2+} > Fe^{3+} > Pb^{2+} > Mn^{2+}$ [20]. Detailed studies of urease inhibition allow the control of the activity of the enzyme in bacteria in the body, as well as influencing the nitrogen cycles crucial in plants.

As urea is a highly stable molecule that resists decomposition, the reaction of its hydrolysis has not been observed without the presence of the enzyme[10]. The rate of reaction is 10^{14} faster than the noncatalyzed system[21,22]. Several models of the reaction mechanism have been proposed. In Fig. 2.3 two possible mechanisms are shown. The reaction mechanism starts from binding the oxygen from urea to the more electrophilic Ni_1 atom in the active site of urease. The next step is either to bind the nitrogen atom from one of the amino groups of urea or to create a second C-O bond with the Ni_2 site. This creates a tetrahedral geometry that allows ammonia and carbamate to be released. The nucleophilic attack of water is performed through bridging hydroxide that acts as an acid to facilitate leaving of NH_3 and the enzyme to return to its original structure.

The next sections of this chapter describe details of the experimental methods used to monitor the urea-urease reaction in unbuffered conditions. The results obtained in the batch system and continuous-flow stirred tank reactor (CSTR) are shown, followed by a presentation of the model and comparison of the experimental and theoretical findings, and finally the discussion and conclusions.
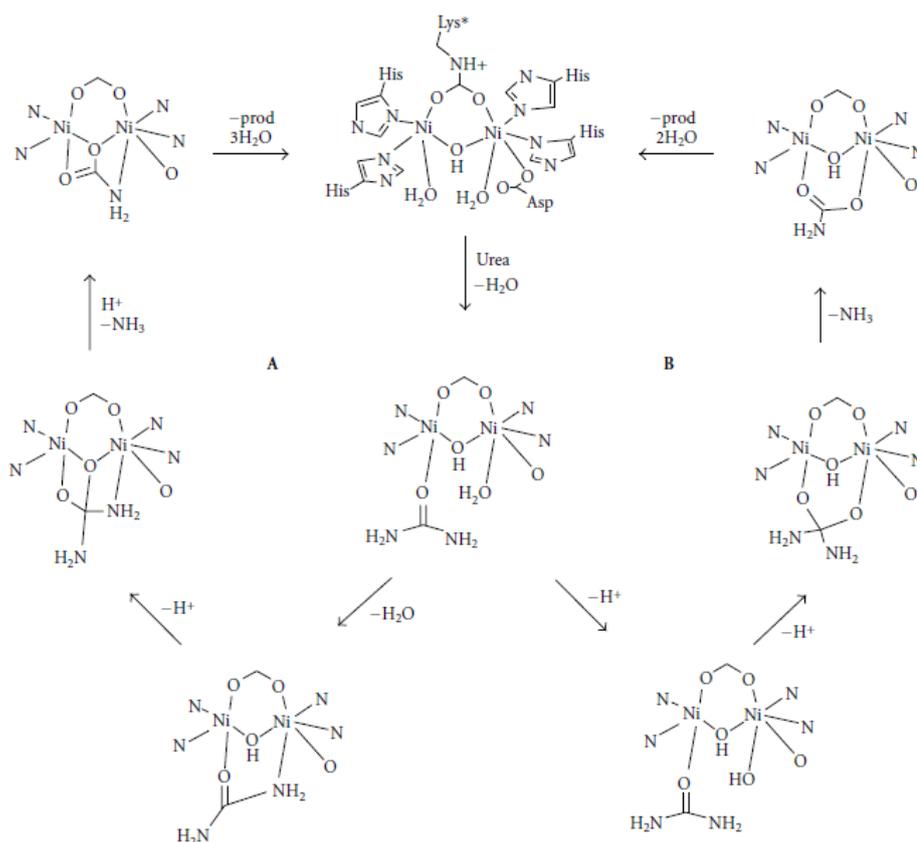
Figure 2.3 Two possible schematic mechanisms of the urea/urease reaction, copied from (25)

2.3 Experimental

This section describes the preparation of stock solutions of urea, urease and acid, followed by a description of the experimental procedure in closed and open systems.

2.3.1 Solutions

<u>Solution A: Urea</u>

A stock solution of $V = 500$ mL consists of 1.2×10^{-4} M H_2SO_4 from dilution of 0.5 M acid prepared from 98% sulphuric acid (AnalR BDH) and 0.03 M urea (National Diagnostics). As the molar mass of urea $M = 60.06$ g mol^{-1}, the mass added to the acid solution is $m = 0.45$ g.

Solution B: Urease

A stock solution of V = 250 mL consists of urease (type III Jack beans U1500-100KU Sigma Aldrich) dissolved in water. The example calculation of preparing urease solution is as follows: the average urease activity = 20990 units g^{-1} and urease activity that is needed in stock solution = 1.4 units mL^{-1}; the mass needed to be dissolved in 250 mL is m = 0.0165 g. Fresh urease solution is prepared every day as the activity of enzyme changes significantly with ageing over 24 hours.

2.3.2 Closed system procedure

The two stock solutions were mixed in equal amounts to give a total volume of 20 mL in the reactor. The clock reaction is performed in a cylindrical reactor with diameter d = 4.5 cm, stirred with a magnetic stirrer (IKA WERKE) of length l = 1.5 cm and stirring rate of 600 rpm. Reactor and reactant solutions are thermostated by Polystat CC3 that is coupled with the TLogger program (Labview). The readings of temperature are taken every 5 s. The pH measurements are taken by a HI 120 pH meter (Hanna) through HI 1131 electrode (Hanna) and captured with the HI 92000 program (Hanna). The readings of pH are taken every 10 s. The pH meter is calibrated with standard solutions of pH = 7.01 and pH = 4.01 (Acros Organics). Data points are saved as .xls files and are processed in Origin. pH versus time plots as well as d(pH)/dt versus time plots are constructed from which the peaks are extracted and clock times are determined. The plots showing induction period as a function of temperature and concentrations of urea, urease, sulphuric acid and acetic acid are plotted in Origin and the errors are calculated as standard deviations in Excel.

All of the experiments mentioned below were performed at 20 °C except where specified. Measurements of the temperature dependence were taken for

$[H_2SO_4]_0 = 1.2 \times 10^{-4}$ M, $[urea]_0 = 0.015$ M, $[urease]_0 = 0.7$ unit/mL with T = 5 °C, 10 °C, 20 °C and 30 °C. The initial concentrations were varied in separate experiments: 0.002 M $< [urea]_0 < 0.015$ M , 5.0×10^{-5} M $< [H_2SO_4]_0 < 2.5 \times 10^{-4}$ M, 0.4 unit/mL $< [urease]_0 < 1.4$ unit/mL. For each condition the experiments were repeated 6 times and mean induction time calculated.

2.3.3 Open system procedure

Solutions A and B were pumped by a Gilson pump in two separate channels into a closed reactor of diameter d = 3.5 cm and height h = 3.0 cm. The solution was pumped out by one outflow channel. The solution was stirred by a magnetic stirrer (IKA WERKE) with length of 1.5 cm and a stirring rate of 600 rpm. The pH measurements were taken as described in section 2.3.2.

Calibration:

The Gilson pump was calibrated every day before the experiments. The calibration procedure was as follows: the tubes were filled with water and the time to fill a 10 mL cylinder (with the tube that had highest effective pumping) was measured for a range of pump flow rates. The total volume pumped by all four channels was registered each time. The volumetric flow rate (VFR) was determined from:

$$VFR = \frac{V_{tot}}{t} \qquad (2.2)$$

where: V_{tot}– total volume, t – time (s), and flow rate (k_0) was determined from:

$$k_0 = \frac{VFR}{V_r} \qquad (2.3)$$

where: V_r– volume of the reactor

A calibration curve was plotted of flow rate dependence on pump rate.

2.4 Results

2.4.1 Closed system

The characteristic features of a clock reaction are the maximum reaction rate at non-zero time and the induction time. In this section, the dependence of these features on the initial chemical concentrations are investigated. The induction time is determined from the maximum slope of the pH time plot (Fig. 2.4 - Fig. 2.7) and the red lines on the induction time plots (Fig. 2.8) are intended to guide the eye. Typical clock reaction pH - time plots for different initial concentrations of urea, urease, acid and different temperatures are shown in Fig. 2.4, Fig. 2.5, Fig. 2.6 and Fig. 2.7 respectively. The clock time increases with decreasing urea (Fig. 2.4 and Fig. 2.8 (a)) and urease (Fig. 2.5 and Fig. 2.8 (b)) concentration as well as with temperature (Fig. 2.6 and Fig. 2.8 (c)). This is to be expected as the maximum rate is proportional to the urea and urease concentrations (as is shown later in the modelling section). The final pH decreases with lower initial urea and urease concentrations (shown in Fig. 2.4 and Fig. 2.5 respectively). For high urea and urease concentrations the pH goes to 8.5 whereas for low concentrations the final pH = 7.5. As shown in Fig. 2.6 temperature does not affect the final pH significantly. The clock time increases with increasing concentration of sulphuric acid (Fig. 2.7 and 2.8 (d)). There is no trend observed in final pH with initial concentration of the acid. It is possible to vary the clock times and final pH by changing the initial concentrations of any of the reactants. The system keeps its autocatalytic character in the whole range of investigated conditions.
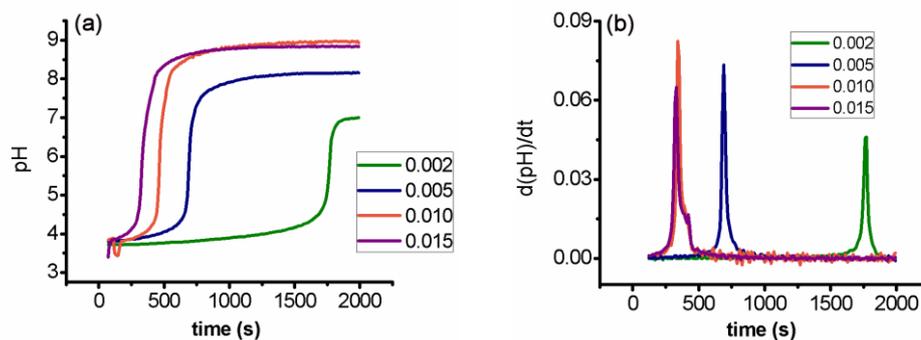
Figure 2.4 (a) pH and (b) d(pH)/dt changes as a function of time for different concentrations of urea [M]. $[H_2SO_4]_0 = 6.0 \times 10^{-4}$ M, $[urease]_0 = 0.7$ unit/mL
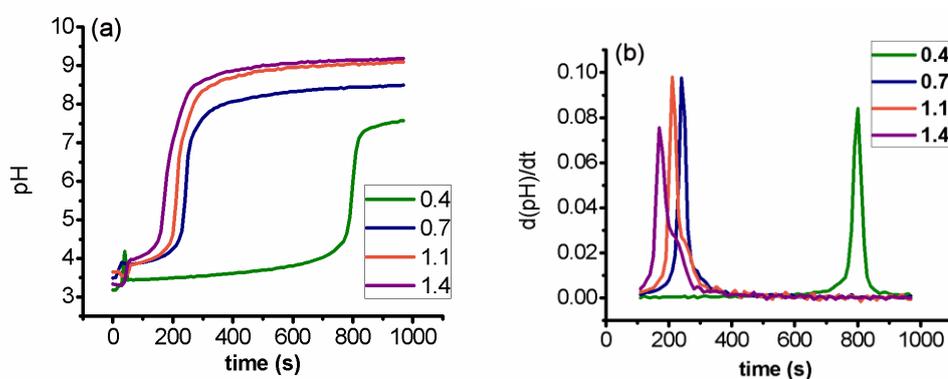
Figure 2.5 (a) pH and (b) d(pH)/dt changes as a function of time for different concentrations of urease [unit/mL]. $[H_2SO_4]_0 = 6.0 \times 10^{-4}$ M, $[urea]_0 = 0.015$M
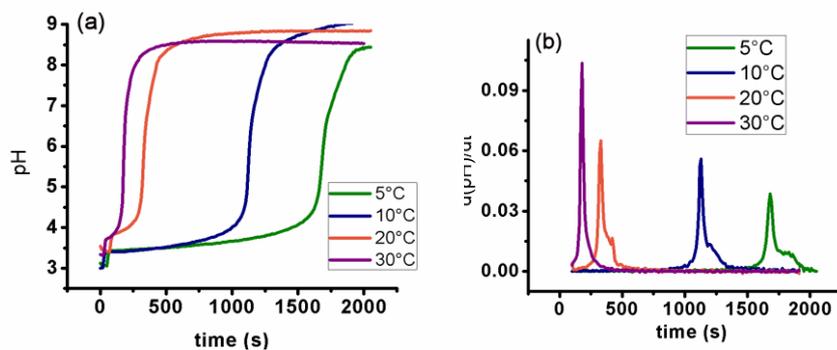
Figure 2.6 (a) pH and (b) d(pH)/dt changes as a function of time for different temperatures (°C), $[H_2SO_4]_0 = 6.0 \times 10^{-4}$ M, $[urease]_0 = 0.7$ unit/mL, $[urea]_0 = 0.015$ M
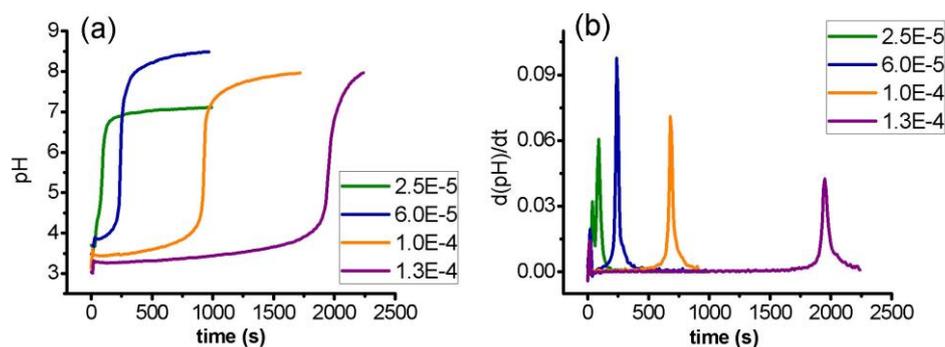
Figure 2.7 (a) pH and (b) d(pH)/dt changes as a function of time for different concentrations of sulphuric acid [M]. $[urease]_0 = 0.7$ unit/mL, $[urea]_0 = 0.015M$
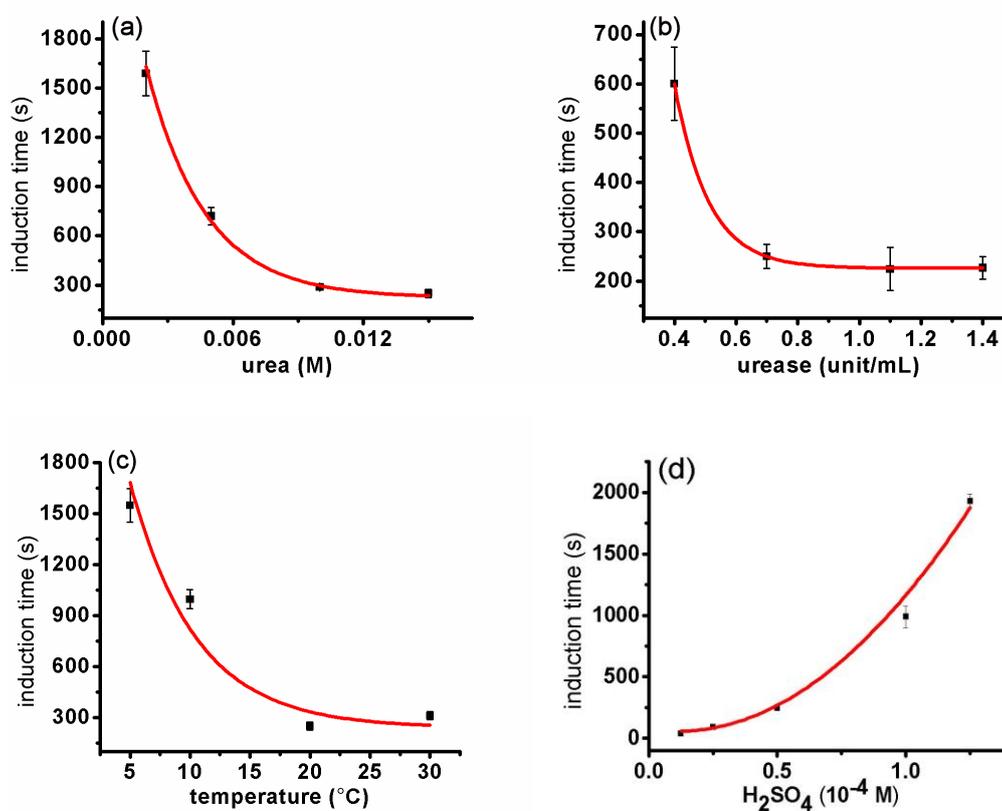
Figure 2.8 Induction time changes as a function of concentrations of (a) urea, (b) urease, (c) temperature, (d) sulphuric acid. Red lines are intended to guide the eye

Additionally a number of experiments in batch (open to the air or sealed) showed a much lower final pH and/or a drop of pH after the clock reaction, such as in the example shown in Fig. 2.9:
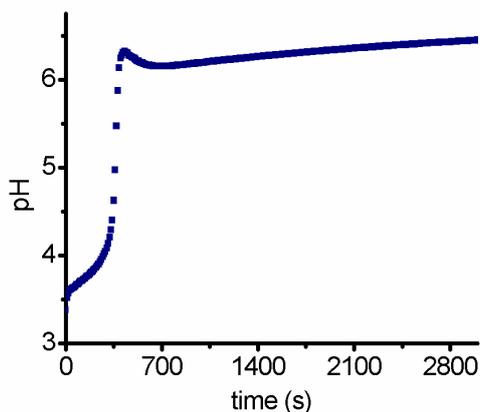
Figure 2.9 Example of a clock reaction with a drop of pH.

[sulphuric acid]$_0$ = 1 × 10^{-4} M,

[urea]$_0$ = 0.015 M,

[urease]$_0$ = 1 unit/mL

This occurred inconsistently, usually for lower concentrations of urease and smaller total reaction volumes. A preliminary investigation on the influence of the total volume on the final pH has been done. For the same set of initial concentrations a significant decrease in final pH with volume was observed as shown in Table 2.1.

Concentrations + volume (mL)	Average Final pH
[sulphuric acid]=7.5E-5 M, [urea]=0.015 M, [urease]=1.7 unit/mL	
20	7.42
10	6.87
5	6.32
[sulphuric acid]=1.50E-4 M, [urea]=0.030 M, [urease]=1.7 unit/mL	
20	7.81
10	7.67
5	7.32
[sulphuric acid]=2.25E-4 M, [urea]=0.030 M, [urease]=1.7 unit/mL	
20	8.6
10	7.65
5	7.62
[sulphuric acid]=3.0E-4 M, [urea]=0.030 M, [urease]=1.7 unit/mL	
20	8.61
10	8.02
5	7.39

Table 2.1 Comparison of final pH change with volume under different initial concentrations of urea and acid

2.4.2 Open system

While performing the reaction in a CSTR it was possible to observe a broad region of bistability as shown in Fig. 2.10. The region of bistability is between flow rates of 0.011 s^{-1} and 0.032 s^{-1}. The amplitude is between pH = 3.7 and pH = 8.3.
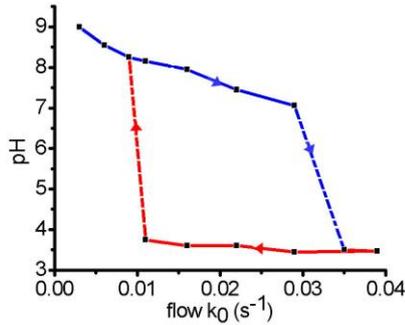
Figure 2.10 Example of bistability in the urea/urease/sulphuric acid system in a CSTR, [sulphuric acid]$_0$ = 1 × 10^{-4} M, [urea]$_0$ = 0.005 M, [urease]$_0$ = 1.4 unit mL^{-1}

Upon increasing the urea and decreasing the urease, the region of bistability shifts to higher flows keeping the same pH amplitude (Fig. 2.11).
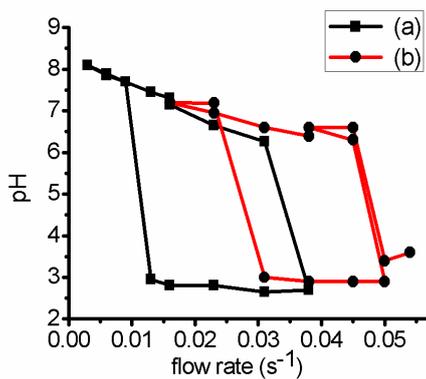
Figure 2.11 Ranges of bistability with (a) [sulphuric acid]$_0$ = 1 × 10^{-4} M, [urea]$_0$ = 0.005 M, [urease]$_0$ = 1.4 unit mL^{-1}, and (b) [sulphuric acid]$_0$ = 1 × 10^{-4} M, [urea]$_0$ = 0.010 M, [urease]$_0$ = 1.25 unit mL^{-1}

However, the region of bistability was not found to be reproducible. For the same initial concentrations of reactants, the region of bistability increases and shifts to higher flow rates in time within one continuous run (Fig. 2.12 a) but also can shrink and shift to lower flows, and the amplitude of the change of pH between branches decreases, when the pump is recalibrated and the solutions are freshly prepared (Fig. 2.12 b).
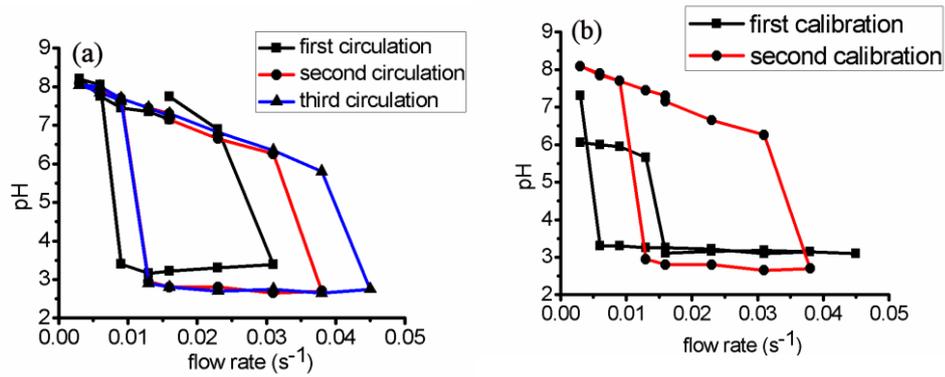
Figure 2.12 Shifts of bistability during (a) continuous change of flow rate in one experiment, and (b) recalibration of the pump in separate experiments. [sulphuric acid]$_0$ = 1 × 10^{-4} M, [urea]$_0$ = 0.005 M, [urease]$_0$ = 1.4 unit mL^{-1}

2.5 Modelling the urea/urease reaction

The proposed mechanism to model the reaction contains the enzyme-catalyzed hydrolysis of urea:

$$CO(NH_2)_2 + H_2O \xrightarrow{\text{urease}} 2NH_3 + CO_2 \tag{2.4}$$

and two hydrolysis equilibria:

$$CO_2 + H_2O \rightleftharpoons H^+ + HCO_3^- \qquad\qquad \text{pK} = 6.35 \tag{2.5}$$

$$HCO_3^- + H_2O \rightleftharpoons CO_3^{2-} + H_3O^+ \qquad\qquad \text{pK} = 10.25 \tag{2.6}$$

and two dissociation equilibria:

$$NH_4^+ \rightleftharpoons NH_3 + H^+ \qquad\qquad \text{pK} = 9.25 \tag{2.7}$$

$$H_2O \rightleftharpoons H^+ + OH^- \tag{2.8}$$

$$HA \rightleftharpoons A^- + H^+ \tag{2.9}$$
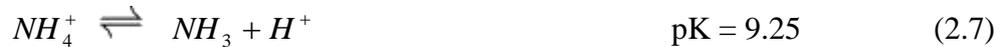
where HA is the weak acid. In this case HA = HSO_4^-, so the equilibrium becomes:

$$HSO_4^- \rightleftharpoons SO_4^{2-} + H^+$$

Assuming classic Michaelis-Menten kinetics and considering additionally uncompetitive substrate inhibition[24,25] and noncompetitive product inhibition[26] and adding a component that determines the pH-rate dependence[27] the rate of reaction (2.4) can be expressed as:

$$v = \frac{v_{max}[CO(NH_2)_2]}{\left(K_M + [CO(NH_2)_2](1 + \frac{[CO(NH_2)_2]}{K_S})\right)\left(1 + \frac{[NH_4^+]}{K_P}\right)\left(1 + \frac{K_{es2}}{[H^+]} + \frac{[H^+]}{K_{es1}}\right)} \quad (2.10)$$

where:

$$v_{max} = k_1[E]_0 \quad (2.11)$$

$[E]_0$ = the total amount of enzyme, K_S = equilibrium constant for uncompetitive substrate inhibition, K_P = equilibrium constant for noncompetitive product inhibition, K_{es1} = equilibrium constant for formation of active protonated form of the enzyme-substrate complex, K_{es2} = equilibrium constant for formation of inactive bi-protonated form.

The rate equations for all species are as follows:

$$\frac{d[CO(NH_2)_2]}{dt} = -v \quad (2.12)$$

$$\frac{d[NH_3]}{dt} = 2v + k_2[NH_4^+] - k_{-2}[NH_3][H^+] \quad (2.13)$$

$$\frac{d[NH_4^+]}{dt} = -k_2[NH_4^+] + k_{-2}[NH_3][H^+] \quad (2.14)$$

$$\frac{d[CO_2]}{dt} = v_1 - k_3[CO_2] + k_{-3}[HCO_3^-][H^+] \quad (2.15)$$

$$\frac{d[HCO_3^-]}{dt} = k_3[CO_2] - k_{-3}[HCO_3^-][H^+] - k_4[HCO_3^-] + k_{-4}[CO_3^{2-}][H^+] \quad (2.16)$$

$$\frac{d[CO_3^{2-}]}{dt} = k_4[HCO_3^-] - k_{-4}[CO_3^{2-}][H^+] \quad (2.17)$$

$$\frac{d[\text{H}^+]}{dt} = k_2[\text{NH}_4^+] - k_{-2}[\text{NH}_3][\text{H}^+] + k_3[\text{CO}_2] - k_{-3}[\text{HCO}_3^-][\text{H}^+] + k_4[\text{HCO}_3^-]$$ (2.18)
$$- k_{-4}[\text{CO}_3^{2-}][\text{H}^+] + k_5 - k_{-5}[\text{H}^+][\text{OH}^-] + k_6[HA] - k_{-6}[A^-][\text{H}^+]$$

$$\frac{d[\text{OH}^-]}{dt} = k_5 - k_{-5}[\text{OH}^-][\text{H}^+]$$ (2.19)

$$\frac{d[\text{HA}]}{dt} = -k_6[\text{HA}] + k_{-6}[A^-][\text{H}^+]$$ (2.20)

$$\frac{d[A^-]}{dt} = k_6[\text{HA}] - k_{-6}[A^-][\text{H}^+]$$ (2.21)

The rate constant values are taken from the literature and are given in Table 2.2:

Table 2.2 Values of rate constants (25°C) of reactions (2.7) - (2.12) [10,17,28,29]

	k_2	k_{-2}	k_3	k_{-3}	k_4	k_{-4}	k_5	k_{-5}	k_6	k_{-6}
Rate constants	(s^{-1})	($M^{-1}s^{-1}$)	(s^{-1})	($M^{-1}s^{-1}$)	(s^{-1})	($M^{-1}s^{-1}$)	(Ms^{-1})	($M^{-1}s^{-1}$)	(s^{-1})	($M^{-1}s^{-1}$)
	24	4.3×10^{10}	0.037	7.9×10^4	2.8	5×10^{10}	1×10^{-3}	1×10^{11}	1.2×10^9	1×10^{11}
	k_1	K_M	K_{es1}	K_{es2}	K_u	K_p				
Enzyme constants	($unit^{-1}$ ml M^{-1} s^{-1})	(M)								
	3.7×10^{-6}	3×10^{-3}	5×10^{-6}	2×10^{-9}	3	2×10^{-3}				

The equations were solved using XPPaut with the CVODE[30] integration method (Appendix II).

2.5.1 Model Results

In a closed system, the model gives good agreement with the experimental data, predicting the clock behaviour as shown in Fig. 2.13:

Figure 2.13 pH-time plots obtained experimentally (•) and in the model (—). Initial concentrations: $[urea]_0$= 0.015 M, $[urease]_0 = 0.7$ unit/mL, $[H_2SO_4]_0 = 1.0 \times 10^{-4}$ M, $[H^+]_0 = 1.0 \times 10^{-4}$ M, $[HSO_4^-]_0 = 1.0 \times 10^{-4}$ M
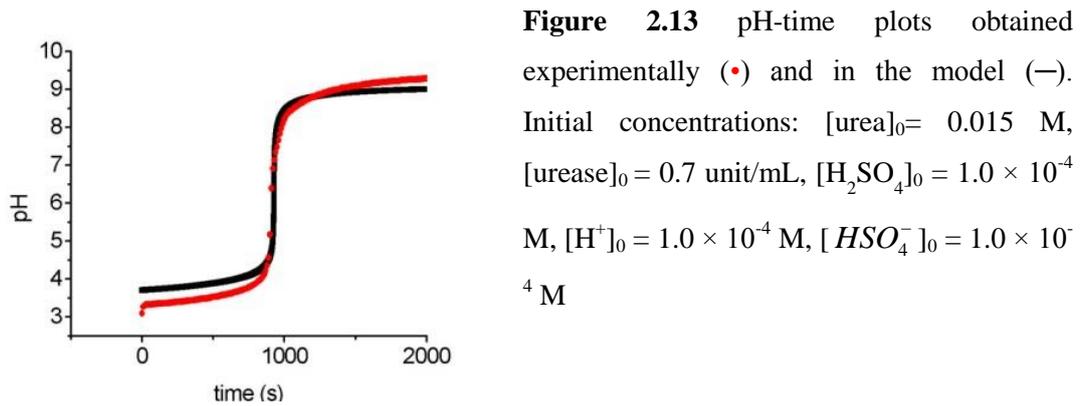
This curve is obtained by matching the enzyme parameters to best fit the experimental data, by trial and error, within the ranges given in the literature[10,17]. There is an acceleration in the rate of removal of urea accompanying the clock reaction in pH (Fig. 2.14), which is the first evidence of autocatalysis (Note: it is possible to obtain a pH clock without autocatalysis, see section 1.1). The changes of species in time predicted by the model are shown in Fig. 2.14. The model suggests that this reaction provides a promising possibility for designing a batch oscillator as the substrate, urea, is not fully consumed in the clock reaction, with only ca. 10% being consumed in the clock process.
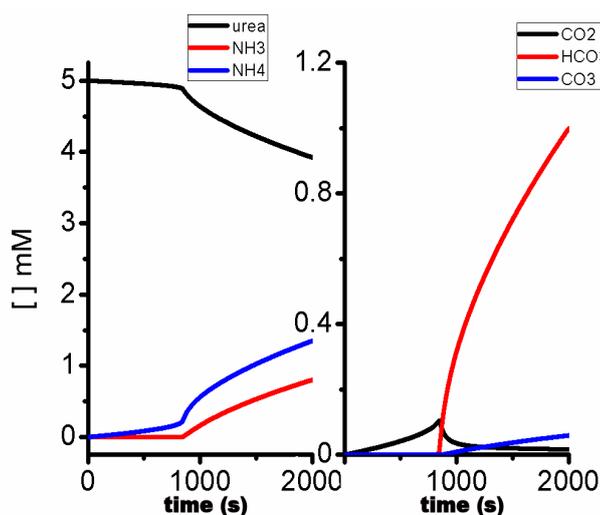
Figure 2.14 Modelled changes of ammonia, ammonium, urea, carbon dioxide, carbonate and bicarbonate in time. Initial concentrations: $[urea]_0$= 0.015 M, $[urease]_0 = 0.7$ unit/mL, $[H_2SO_4]_0 = 1.0 \times 10^{-4}$ M, $[H^+]_0 = 1.0 \times 10^{-4}$ M, $[HSO_4^-]_0 = 1.0 \times 10^{-4}$ M

The comparison of clock time dependencies on the concentrations of urea, urease, and sulphuric acid for experiments and the model are shown in Fig. 2.15. The model shows a decrease in induction time while increasing initial concentration of urea and urease as shown in the experiments. Also similar to the experimental results the induction time in the model increases with increasing initial concentration of the acid. The agreement between theory and experiment is qualitative not quantitative within a certain range of parameters, i.e. low urea and urease concentrations.
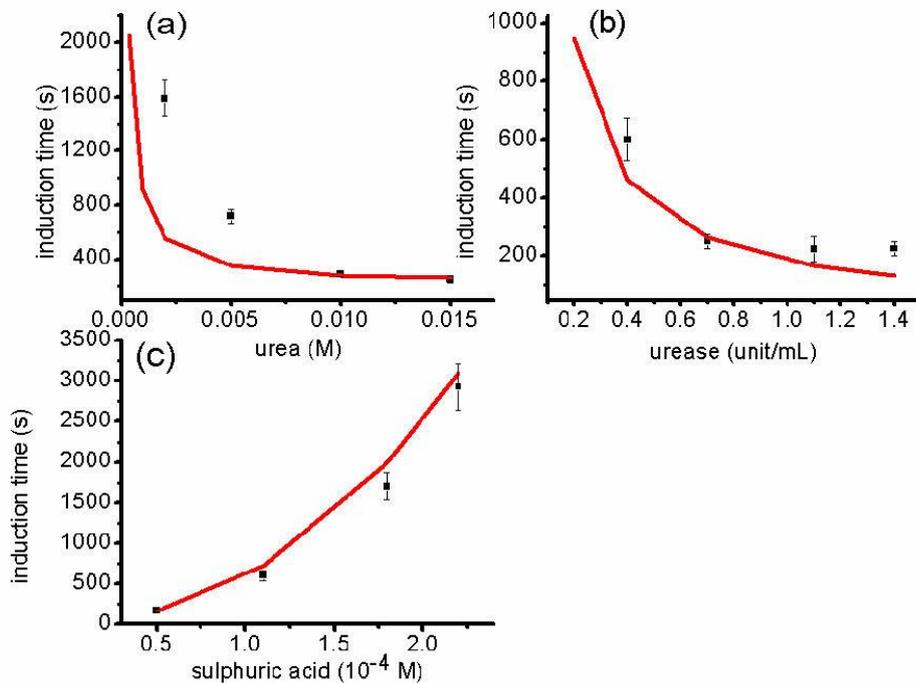
Figure 2.15 Model (line) and experimental (points) dependences of induction time on concentration of (a) urea, (b) urease, (c) sulphuric acid. Concentrations in (a) and (b): [urea]$_0$= 0.015 M, [urease]$_0$ = 0.7 unit/mL, [H$_2$SO$_4$]$_0$ = 6.0 × 10^{-5} M,, in (c): [urea]$_0$= 0.005 M, [urease]$_0$= 1.4 unit/mL

If the flow component given by equation:

$$\frac{d[X]}{dt} = k_0(X_0 - X) \tag{2.22}$$

is added to equations (2.12) - (2.21), bistability is predicted in a range of flow rates from 0.018 s^{-1} to 0.048 s^{-1} which is similar to the experimental results shown in Fig. 2.10.
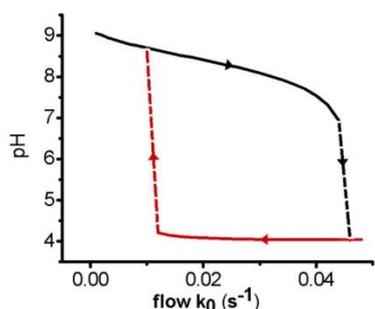
Figure 2.16 Bistability predicted in the model for an open reactor, [urea]$_0$= 0.005 M, [urease]$_0$= 1.4 unit/mL, [H$_2$SO$_4$]$_0$ = 6.0×10^{-5} M

Regions of bistability, thermodynamic (only high pH) and flow (only low pH) states are predicted in the model and depend on the concentrations of all reactants as shown in Fig. 2.17. For higher urea and urease concentrations, the region of bistability is broader. The thermodynamic state appears only at high urease and low acid concentrations in a narrow range of flow rates.
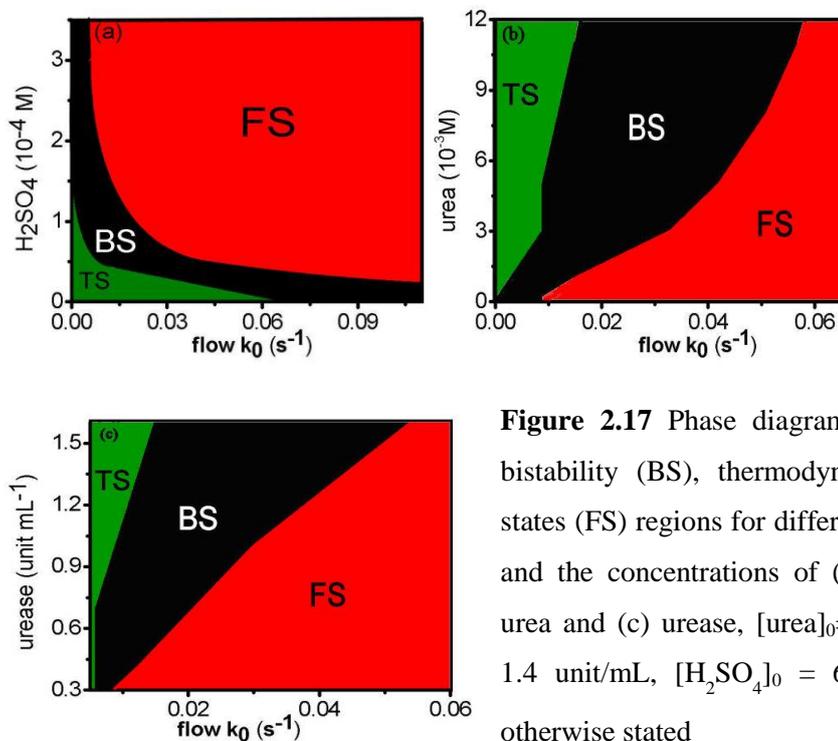
Figure 2.17 Phase diagram showing regions of bistability (BS), thermodynamic (TS) and flow states (FS) regions for different values of flow rate and the concentrations of (a) sulphuric acid, (b) urea and (c) urease, [urea]$_0$= 0.015 M, [urease]$_0$= 1.4 unit/mL, [H$_2$SO$_4$]$_0$ = 6.0×10^{-5} M, unless otherwise stated

2.6 Discussion

The results in this chapter show the first experimental example of base autocatalysis in an enzymatic reaction. In a batch reactor a clock reaction is observed giving a significant change of pH from pH = 3.5 to pH = 8.5. This is the first evidence that positive feedback is present in the system. The feedback arises from the pH dependence of enzyme activity[17] (as shown in Fig. 2.2) coupled with the production of base (NH_3) so that sudden acceleration of the reaction is seen when the system reaches the pH when the activity of enzyme is at its maximum.

In the urea/urease reaction, clock behaviour is shown for all urea, urease and sulphuric acid concentrations as opposed to the glucose oxidase enzymatic system where the autocatalytic effect decreases with decreasing concentration of the substrate, namely $[Fe(CN)_6]_0^{3-}$[31]. The urea/urease reaction can be thought of as the simplest example of a pH autocatalytic enzymatic reaction as a Michaelis-Menten model gives good qualitative agreement with experiments in terms of induction time dependencies on the initial concentrations of urea, urease, and sulphuric acid. This is contrary to the glucose oxidase[31] enzyme reaction where a complex ping-pong mechanism is needed to explain the nonlinear behaviour. At very low concentrations of urea and high concentrations of acid there is limited quantitative agreement. This may be attributed to the fact that at low concentrations of reactants the kinetics of the urea/urease reaction is governed not by Michelis-Menten kinetics anymore as has been observed in previous studies[32].

The rate constants $k_2 - k_{-6}$ used in the model are well established[28,29]. The rate constants k_1, K_M, K_{es1}, K_{es2}, K_u and K_p have been varied in this work, but the ranges of those parameters are taken from Krajewska's papers[10,17], however they were adjusted by trial and error. One way to improve the agreement between the model

and experiments is to use packages such as Zita using nonlinear parameter estimation[33]. This will be the subject of further investigation.

There are several other processes not included in the model that would potentially improve the agreement between theory and experiments. First of all gaseous CO_2 production may play an important role in the system, so it will be worth considering the CO_2 liquid-gas equilibrium and the H_2CO_3 and HCO_3^- formation processes[34] in future modelling. Also transfer of ammonia to the gas phase may occur under certain conditions, changing the final pH and influencing clock times. Also taking into account the temperature dependencies of enzyme activity and rate constants may improve the quantitative agreement between the model and experiments.

For low urease concentrations it is probable that non-mass action kinetic effects should be taken into account i.e. stochastic models[35] will be more appropriate. The first evidences of this type of kinetics taking place are the decrease of final pH with total volume of solution.

The decrease of induction time with increasing temperature comes first of all from the Arrhenius dependence[27]:

$$k = A\exp(-\frac{E_a}{RT})$$
(2.23)

where: k – reaction rate, A – pre-exponential factor, E_a – activation energy, R – gas constant, T – absolute temperature. Thus k_1 is expected to increase with increasing temperature. Secondly the fact that the activity of urease increases significantly from 10 °C to 70 °C, with a maximum at 70 °C that is followed by a decrease at higher temperatures[36] plays an additional role in the kinetics of the urea/urease system. As shown in Fig. 2.6 temperature does not affect the final pH significantly.

The second evidence for the autocatalytic character of the system is the experimental observation of bistability in CSTR. Bistability is also predicted in the model and regions of bistability, thermodynamic and flow states are mapped depending on initial concentrations of urea, urease and sulphuric acid. However the range of bistability and the amplitude were found to be sensitive to small changes, or fluctuations, in the inflow of reactants and temperature and thus the reproducibility of the data was poor. For these reasons, the complete regions of bistability, thermodynamic and flow states were not mapped experimentally.

2.7 Conclusions

The pH autocatalytic reaction of enzyme catalysed hydrolysis of urea was studied under nonbuffered conditions, showing the first experimental observations of a pH clock from low to high pH in this system in a batch reactor. It was possible to obtain a wide range of clock times, from several to two thousand seconds, when changing the initial concentrations of the reactants. In a CSTR, the urea/urease system showed a wide range of bistability which proves the validity of the model in this region of phase diagram. Regions of bistability, thermodynamic and flow states in phase diagrams of the flow rate and concentrations of urea, urease, and sulphuric acid were predicted in the model.

2.8 References

(1)   Wang, W. H.; Kohler, B.; Cao, F. Q.; Liu, L. H.: *Plant Sci.* **2008**, *175*, 467-477.

(2)   Krajewska, B.: *J. Mol. Cat. B Enz.* **2009**, *59*, 9-21.

(3)   Qin, Y.; Cabral, J. M. S.: *Biocatal. Biotransform.* **2002**, *20*, 1-14.

(4)   Estiu, L. G.; Merz, K. M.: *Abstr. Papers Am. Chem. Soc.* **2004**, *227*, U1006-U1006.

(5)   Estiu, G.; Metz, K. M.: *J. Am. Chem. Soc.* **2004**, *126*, 6932-6944.

(6)   Fidaleo, M.; Lavecchia, R.: *Chem. Biochem. Eng. Q.* **2003**, *17*, 311-318.

(7)   Krajewska, B.; Chudy, M.; Drozdek, M.; Brzozka, Z.: *Electroanal.* **2003**, *15*, 460-466.

(8)   Stingl, K.; Uhlemann, E. M.; Schmid, R.; Altendorf, K.; Bakker, E. P.: *J. Bacteriol.* **2002**, *184*, 3053-3060.

(9)   Scott, D. R.; Marcus, E. A.; Weeks, D. L.; Sachs, G.: *Gastroenterol.* **2002**, *123*, 187-195.

(10)   Krajewska, B.: *J. Mol. Cat. B-Enz.* **2009**, *59*, 9-21.

(11)   Schneider, J.; Kaltwasser, H.: *Arch. Microbiol.* **1984**, *139*, 355-360.

(12)   Todd, M. J.; Hausinger, R. P.: *J. Biol. Chem.* **1987**, *262*, 5963-5967.

(13)   Smith, P. T.; King, A. D.; Goodman, N.: *J. Gen. Microbiol.* **1993**, *139*, 957-962.

(14)   Mirbod, F.; Schaller, R. A.; Cole, G. T.: *Med. Mycol.* **2002**, *40*, 35-44.

(15)   Norris, R.; Brocklehurst, K.: *Biochem. J.* **1976**, *159*, 245-257.

(16)   Follmer, C.; Real-Guerra, R.; Wasserman, G. E.; Olivera-Severo, D.; Carlini, C. R.: *Eur. J. Biochem.* **2004**, *271*, 1357-1363.

(17)   Krajewska, B.; Ciurli, S.: *Plant Physiol. Biochem.* **2005**, *43*, 651-658.

(18)   Blakeley, R. L.; Hinds, J. A.; Kunze, H. E.; Webb, E. C.; Zerner, B.: *Biochem.* **1969**, *8*, 1991-&.

(19)   Todd, M. J.; Hausinger, R. P.: *J. Biol. Chem.* **1989**, *264*, 15835-15842.

(20)   Zaborska, W.; Krajewska, B.; Olech, Z.: *J. Enz. Inhibit. Med. Chem.* **2004**, *19*, 65-69.

(21)   Karplus, P. A.; Pearson, M. A.; Hausinger, R. P.: *Acc. Chem. Res.* **1997**, *30*, 330-337.

(22)   Blakeley, R. L.; Zerner, B.: *J. Mol. Catal.* **1984**, *23*, 263-292.

(23)   Carlsson, H.; Nordlander, E.: *Bioinorg. Chem. Appl.*, **2010,** *8*, 364891-364899.

(24)   Moynihan, H. J.; Lee, C. K.; Clark, W.; Wang, N. H. L.: *Biotechnol. Bioeng.* **1989**, *34*, 951-963.

(25)   Huang, T. C.; Chen, D. H.: *J. Chem. Technol. Biotechnol.* **1991**, *52*, 433-444.

(26)   Tanaka, T.; Kawase, M.; Tani, S.: *Biorg. Med. Chem.* **2004**, *12*, 501-505.

(27)   Chang, R.: *Physical Chemistry with Applications to Biological Systems*; University Science Books, Willams College, **1981**.

(28)   Wang, X. G.; Conway, W.; Burns, R.; McCann, N.; Maeder, M.: *J. Phys. Chem. A* **2010**, *114*, 1734-1740.

(29)   Eigen, M.: *Angew. Chem.-Int. Edit.* **1964**, *3*, 1-72.

(30)   Ermentrout, G. B.: *Simulating, Analyzing and Animating Dynamical Systems: A Guide to XPPAUT for Researchers and Students*; SIAM, **2002**.

(31)   Vanag, V. K.; Miguez, D. G.; Epstein, I. R.: *Journal of Chemical Physics* **2006**, *125*, 194595-1 - 194595-11.

(32)   Kistiakowsky, G. B.; Rosenberg, A. J.: *J. Am. Chem. Soc.* **1952**, *74*, 5020-5025.

(33)   Attila, J.: ZiTa, a Comprehensive Program Package for Fitting Parameters of Chemical Reaction Mechanism. 5.0 ed.: Szeged, **1989-1998**.

(34)   Wang, X. G.; Conway, W.; Burns, R.; McCann, N.; Maeder, M.: *J. Phys. Chem. A* **2009**, *114*, 1734-1740.

(35)   Goutsias, J.: *Biophys. J.* **2007**, *92*, 2350-2365.

(36)   Sahrawat, K. L.: *Plant and Soil* **1984**, *78*, 401-408.

3. Fronts in the urea/urease/sulphuric acid system

3.1 Introduction

Investigation of the spatial behavior of the urea/urease/sulphuric acid reaction in thin layers is presented for a range of concentrations of reactants. For very high urease concentrations two types of propagating pH fronts were obtained: spontaneous with short clock times and initiated by product solution with long clock times. Under much lower concentrations of the enzyme, a clock reaction was obtained in a batch reactor, but no front propagation was observed. The spatial behavior was modelled by expansion of the model presented in Chapter 2 with diffusion included. Both in the experiment and simulations, correlations between the concentrations of reactants, clock times and average front speed were found.

3.2 Experimental

Solutions were prepared as discussed in Chapter 2. In order to visualize the fronts, 0.005 g of cresol red (Fisher Scientific Ltd.) was added to 250 mL of both reactant solutions. For each set of concentrations, before performing an experiment in a spatial reactor, the pH clock time was determined in a batch reactor (shown schematically in Fig. 3.1 a). The total volume of solutions in the batch reactor was 20 mL.

The fronts were observed in a reactor that consists of the lid of a Petri dish with diameter $d = 5$ cm covered by its base so that the reaction was sealed from the atmosphere (Fig. 3.1 b). The Petri dish was placed in a cell thermostated by Polystat CC3. The standard temperature was 20 ºC. In a batch reactor, 20 mL of solution was stirred for 30 s with a magnetic stirrer (IKA WERKE) of length $l = 1$ cm and stirring rate of 600 rpm before 1.5 mL was extracted with a pipette and added to the Petri dish creating a layer of depth $h = 0.8$ mm. The pictures of the fronts were taken every 5 s by a CCD camera coupled with the MATLAB program (The MathWorks).
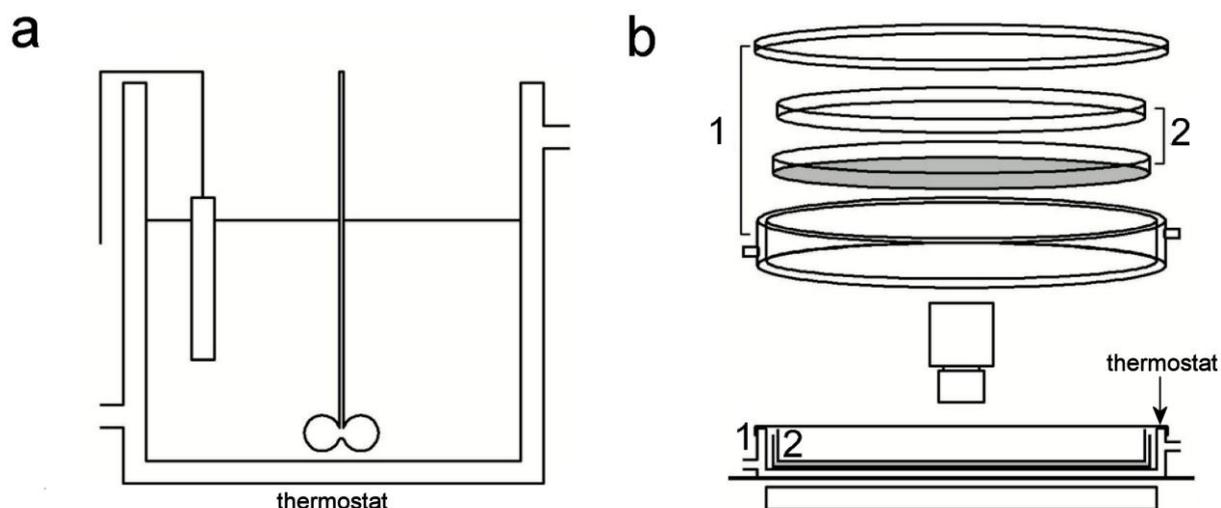
Figure 3.1 Schematic representation of the experimental set-up (a) the well-stirred batch reactor apparatus with pH probe and stirrer, (b) spatial apparatus with camera , where 1 indicates the outer thermostated glass dish, and 2 indicates the inner Petri dish containing the reaction solution

When the clock time was less than 1000 s, the fronts were left to self-initiate. When the clock time was above 1000 s, the front was initiated by a drop of product solution in the middle of Petri Dish through a hole with diameter d = 1 mm.

The front profiles were analyzed by code written in MATLAB (Appendix III) that is illustrated in section 3.3. For each front, the average speed from propagation in different directions was determined (excluding erroneous data, see Fig. 3.6). The errors in front speed are calculated as standard deviations for each set of conditions. The standard deviation in front speed was determined in a single experiment and then over different experiments. The experiments were repeated at least 5 times.

3.3 Results

Depending on the initial concentrations and hence the clock time, several different types of spatial behaviour were seen. The first case is when the clock time is around a few thousands seconds and the front only propagates after initiation with

product solution in the centre of the dish or from the edges (Fig. 3.1 a-c). In the

second case the clock time is slightly less than 1000 s and self-initiation starts to

appear in several places in the solution (Fig. 3.1 d – f). In the last case when the

clock time is much shorter than 1000 s, fast spontaneous self-initiation in the whole

of the reactor is observed with many starting points (Fig. 3.1 g – i).
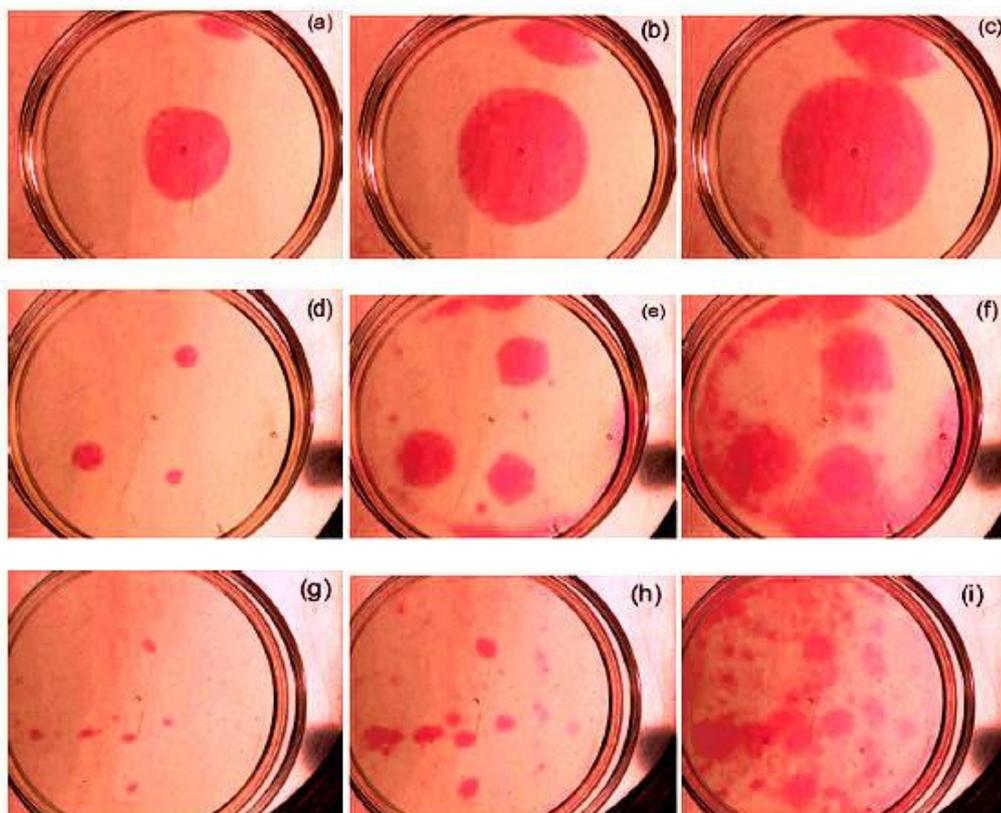
Figure 3.2 Illustration of different types of behaviour depending on initial concentrations of reactants and clock times. (a) – (c) [sulphuric acid] $_0$ = 4.05 × 10^{-4} M, [urea] $_0$ = 0.009 M, [urease]$_0$ = 17 unit mL^{-1}. Clock time = 3000 s. (d) – (f) [sulphuric acid] $_0$ = 4.05 × 10^{-4} M, [urea] $_0$ = 0.03 M, [urease] $_0$ = 17 unit mL^{-1}. Clock time = 900 s. (g) – (i) [sulphuric acid] $_0$ = 4.05 × 10^{-4} M, [urea] $_0$ = 0.03 M, [urease] $_0$ = 24 unit mL^{-1}. Clock time = 300 s

For each of the fronts it was possible to extract space-time plots (as shown in

the example in Fig. 3.3 a) and intensity profiles in space (Fig. 3.3 b). This example

shows that the front propagated with a constant speed and concentration profile.

However the front speed was found to differ depending on the direction of

propagation in space. This was sometimes due to imperfect initiation of the front. In order to reduce the error in calculating the front speed for a particular concentration, each of the fronts has been analysed in 16 different directions simultaneously as shown for different cases in Figs 3.4, 3.6, 3.7.
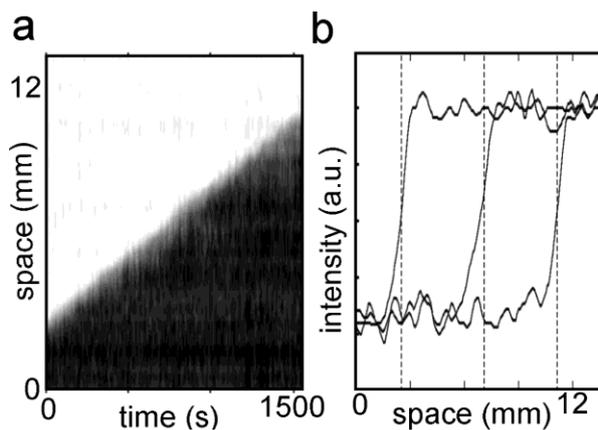
Figure 3.3 (a) Typical space – time plot, and (b) intensity profiles in space. [sulphuric acid]$_0$= 4.05 × 10^{-4} M, [urea]$_0$ = 0.03 M, [urease]$_0$ = 17 unit mL^{-1}

For long clock times (> 1000 s), the front can be analyzed using many time points when the reaction is far from completion. In spite of a slight variation of front speed in a few cases (for example Fig. 3.4 b5, b8 or b10), the front position changes linearly in time giving a similar range of front speed in all directions (in these conditions 0.34 – 0.39 mm min^{-1}).
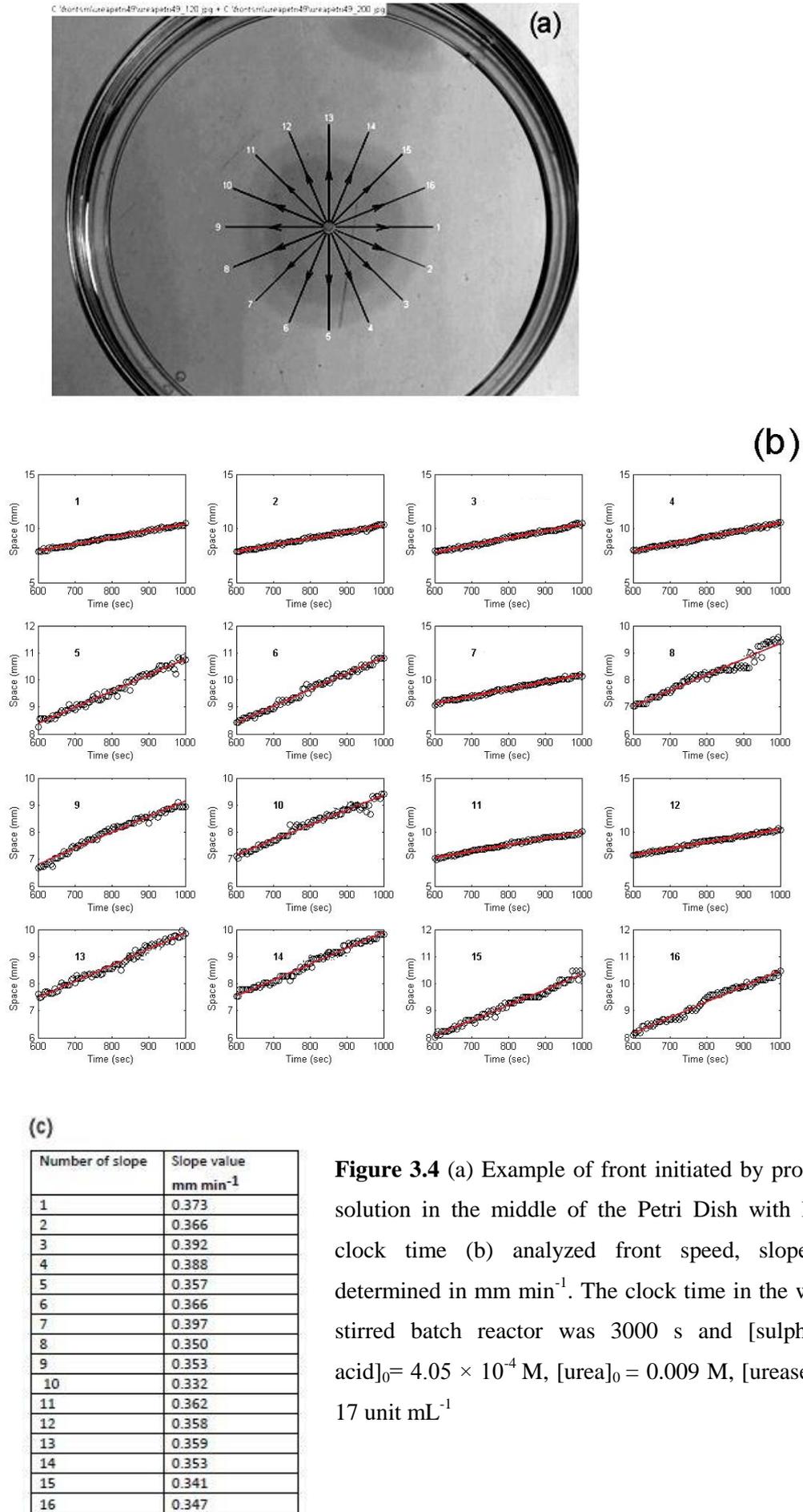
Figure 3.4 (a) Example of front initiated by product solution in the middle of the Petri Dish with long clock time (b) analyzed front speed, slope is determined in mm min^{-1}. The clock time in the well-stirred batch reactor was 3000 s and [sulphuric acid]$_0$= 4.05 × 10^{-4} M, [urea]$_0$ = 0.009 M, [urease]$_0$ = 17 unit mL^{-1}

Number of slope	Slope value mm min^{-1}
1	0.373
2	0.366
3	0.392
4	0.388
5	0.357
6	0.366
7	0.397
8	0.350
9	0.353
10	0.332
11	0.362
12	0.358
13	0.359
14	0.353
15	0.341
16	0.347

For several examples of experiments with longer clock times it was possible to calculate the front speed in three different periods of front propagation: $50 - 500$ s, $500 - 1000$ s and $1000 - 1500$ s as shown in Fig. 3.5. There is a trend visible that the front accelerates towards the end of the reaction. The change of front speed can be up to 16% (seen in the example with clock time = 1700 s), though no definite quantitative correlation between change of front speed and clock time was found.
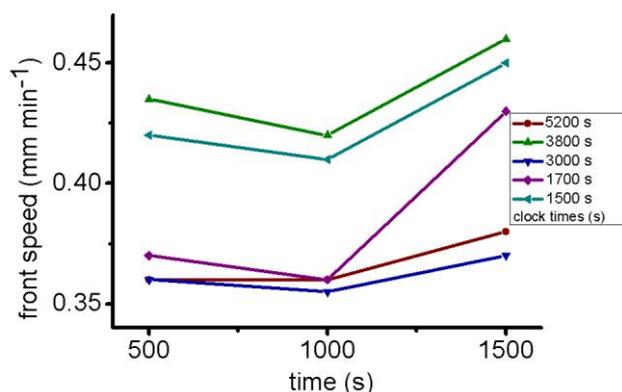
Figure 3.5 Examples of change of front speed during the course of the reaction for reactions with different clock times

In the second case of intermediate clock times ($300 - 1000$ s), it is also possible to analyze the front position with a reasonable number of time points between self-initiation and the clock time. The number of self-initiated spots is small enough so that they do not merge and it is possible to analyze them separately. The space-time plots follow the linear dependence in most cases (with a bigger variation in Fig. 3.3 b1, b12 and b16), though the range of front speeds varies more in different directions (from 0.50 to 0.63 mm min^{-1}).

73
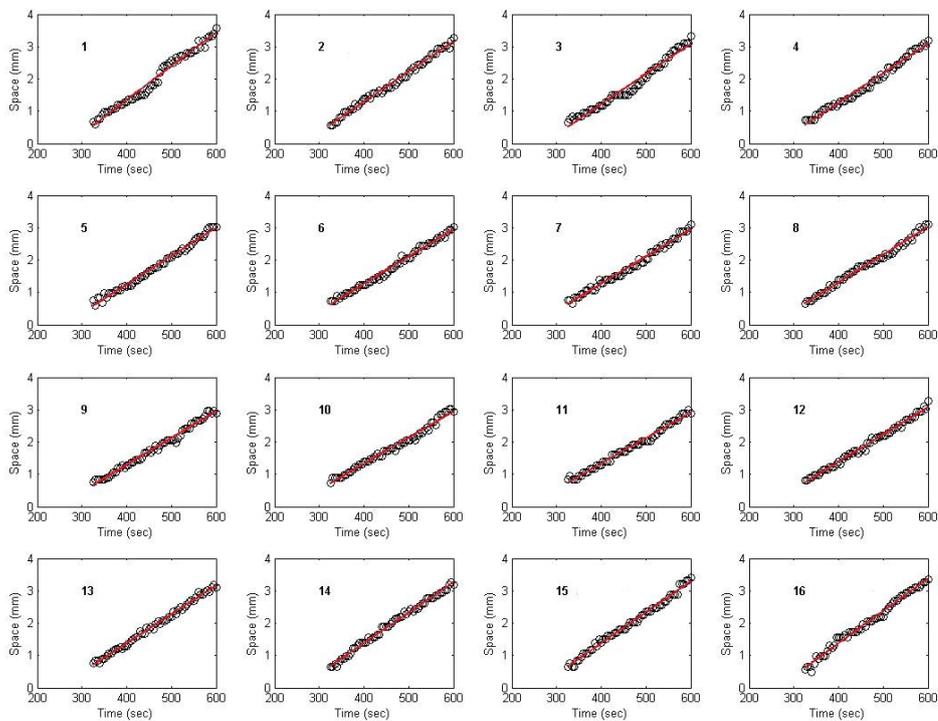
(c)

Number of slope	Slope value mm min^{-1}
1	0.627
2	0.559
3	0.561
4	0.548
5	0.527
6	0.508
7	0.503
8	0.517
9	0.498
10	0.484
11	0.473
12	0.509
13	0.536
14	0.564
15	0.574
16	0.599

Figure 3.6 (a) Example of fronts initiated spontaneously with intermediate clock time, (b) analyzed front speed with slope given in mm min^{-1}. The clock time in a well-stirred batch reactor was 900 s and [sulphuric acid]$_0$ = 4.05 × 10^{-4} M, [urea]$_0$ = 0.03 M, [urease]$_0$ = 17 unit mL^{-1}

Under conditions that result in very short clock times (< 300 s), spontaneous self-initiation begins rapidly in the whole area of the reactor. The front speed increases significantly (up to an average of 1.0 mm min^{-1}) as under these conditions it is only possible to do the calculations near the clock time. The values of the front speed vary in different directions (from 0.69 to 1.34 mm min^{-1}) and the space-time plots show deviation from linearity. There are much less time points taken than in the first two cases, as well as a much bigger density of self-initiated fronts that interact with each other and merge.
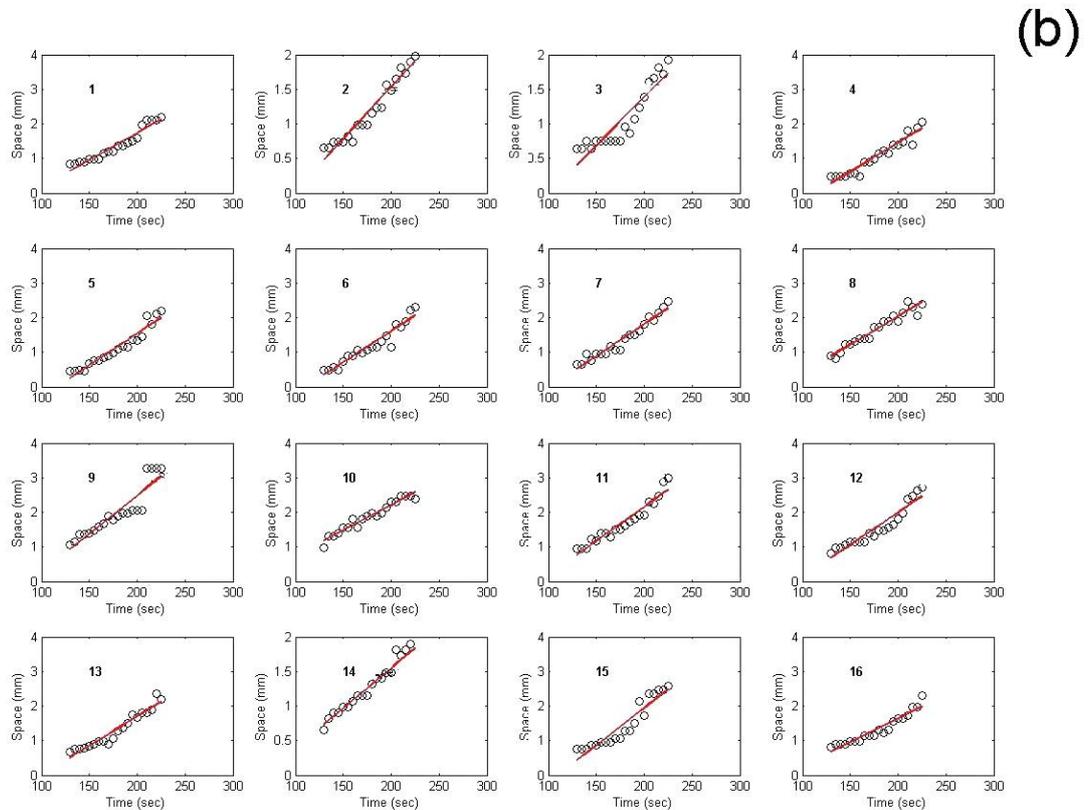
Number of slope	Slope value mm min^{-1}
1	0.937
2	0.892
3	0.835
4	0.999
5	1.102
6	1.082
7	1.108
8	0.984
9	1.836
10	0.878
11	1.185
12	1.125
13	1.023
14	0.694
15	1.297
16	0.829

Figure 3.7 (a) Example of front initiated spontaneously with short clock time (b) analyzed front speed in mm min^{-1}. The clock time in well-stirred batch reactor was 300 s. [sulphuric acid]$_0$ = 4.05 × 10^{-4} M, [urea]$_0$ = 0.03 M, [urease]$_0$ = 24 unit mL^{-1}

Another type of spatial behaviour is observed when the concentration of the enzyme is a few magnitudes lower. By manipulation of acid concentration it is still possible to obtain short clock times in a batch reactor (in a range of 300 - 500 s), with final pH > 8.0, but neither front propagation or conversion to high pH is seen in a Petri dish (as shown in Fig. 3.8). Intensity profiles and the space-time plot (Fig. 3.9) show that there is propagation only at the beginning due to diffusion of the product solution from the initiation site. Then the front does not move, giving a noisy signal after 4000 s when it becomes completely diffuse.
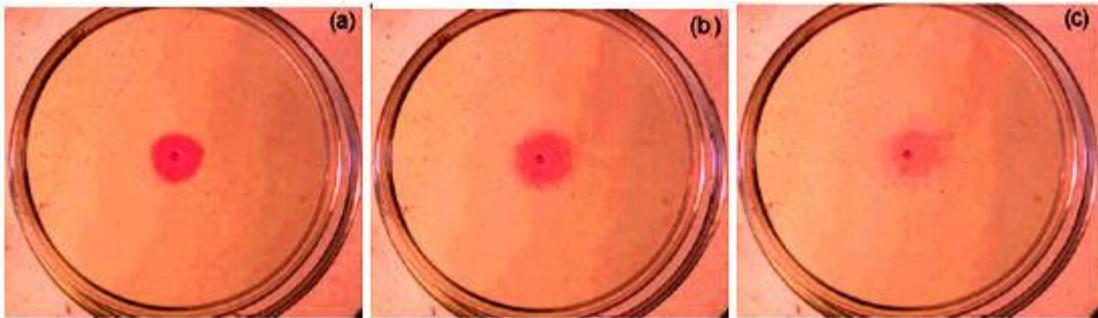
Figure 3.8 Example of lack of front propagation in lower urease conditions in spite of short clock time in the well-stirred reactor (350 s). [sulphuric acid]$_0$ = 1.6 × 10^{-4} M, [urea]$_0$ = 0.03 M, [urease]$_0$ = 3.4 unit mL^{-1}. (a) 520 s, (b) 3220 s, (c) 6000 s
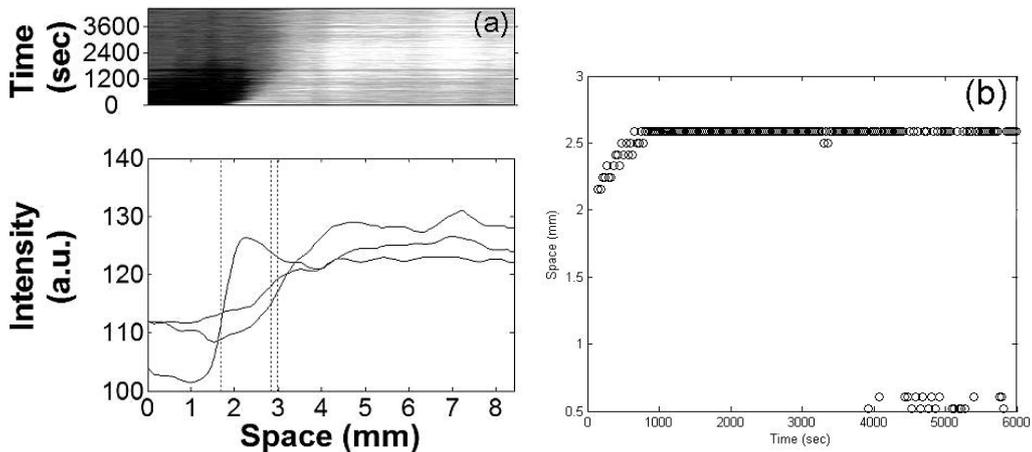
Figure 3.9 (a) Intensity profiles and (b) Space-time plot for experimental conditions in Fig. 3.8

The dependence of the front speed on initial concentrations of reactants is shown in Fig. 3.10. The front speed increases significantly with urease concentration and decreases with acid concentration. The concentration of urea does not have as significant an influence on the front speed as the other reactants. For higher front speeds, the error is larger. This may be due to the fact that when self-initiation is observed there is less time between front initiation and clock time of the whole solution, so there are less data points to be analysed. The analysis of the front speed is affected by merging of the fronts that makes the number of possible time points even smaller and the data is noisier closer to the clock time.
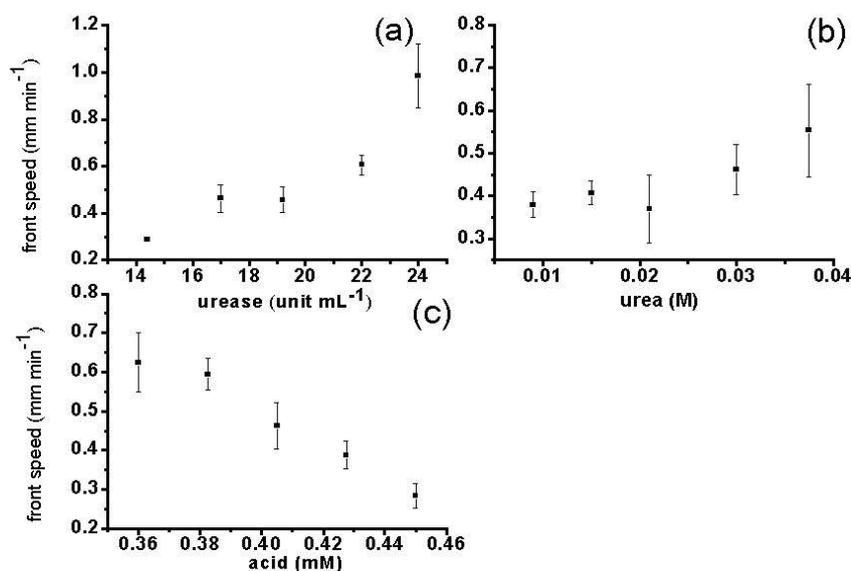
Figure 3.10 Changes of front speed with initial concentrations of (a) urease, (b) urea and (c) acid where error bars are standard deviations. The standard concentrations were: [sulphuric acid]$_0$ = 4.05 × 10^{-4} M, [urea]$_0$ = 0.03 M, [urease]$_0$ = 17 unit mL^{-1}

As, in general, the front speed relates to the chemical timescale of the reaction according to the equation[1,2]:

$$c = A\sqrt{(Dk')}$$

(3.1)

where: c – front speed, A – constant, D – diffusion coefficient, k' – pseudo-first rate order rate constant, the dependence of front speed on clock time (related to 1/k') is fitted according to the power law: $y = ax^b$ (as shown in Fig. 3.11). The value of the coefficient b = –0.35 is still far from the expected value of –0.5 which may be due to lack of experimental data points or poor quantitative reproducibility. The trend of the power-law dependence given in eq. 3.1 is observed and it shows that for long clock times the front speed does not change as significantly as for short clock times.
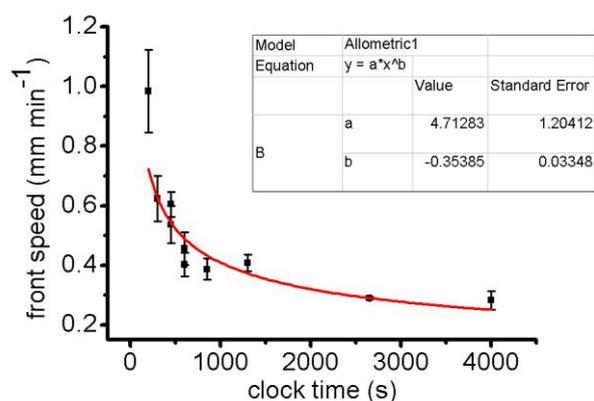
Figure 3.11 The dependence of front speed on clock time

The effect of temperature on the front speed has been investigated and is shown in Fig. 3.12. The influence of temperature is not as significant in the range between 17 ºC and 23 ºC, but below 14 ºC the system hardly exhibits any self-initiation, the front speed becomes much lower with a bigger variation.
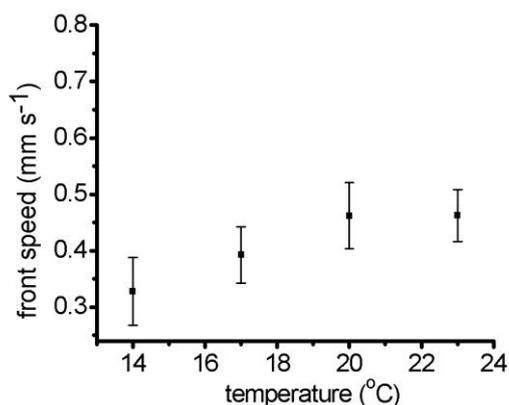
Figure 3.12 The dependence of front speed on temperature. [sulphuric acid]$_0$ = 4.05×10^{-4} M, [urea]$_0$ = 0.03 M, [urease]$_0$ = 17 unit mL^{-1}

3.4 Modelling

The model of spatial behaviour of the urea/urease reaction was developed from the batch model described in section 2.5. The same set of reactions was taken into account as described by equations 2.7 − 2.12, for each of the variable, C_i, a differential equation with both reaction, $f(C_i)$, and diffusion, $D_i \frac{\partial^2 C_i}{\partial x^2}$, terms was applied:

$$\frac{\partial C_i}{\partial t} = f(C_i) + D_i \frac{\partial^2 C_i}{\partial x^2} \qquad (3.2)$$

where D_i is the diffusion coefficient of C_i, and x represents space. For one spatial dimension the partial differential equations were solved using CVODE for time and 2nd order central difference approximation for space in XPPAUT. The code used is attached in the Appendix II. The spatial step size was r = 0.2 mm, and number of grid points was N = 190 so the total length of the domain was 38 mm. The rate constants are identical to the ones given in Table 2.2 apart from k_1 that was lowered to 2.2 × 10^{-6} unit^{-1} mL mol^{-1} s^{-1} to better match the experimental results. The diffusion coefficients were taken as[4] D_H = 5 × 10^{-3} mm^2 s^{-1} for H$^+$, D_{OH} = 2 × 10^{-3} mm^2 s^{-1} for OH$^-$, and for the rest of the species as D_x = 1 × 10^{-3} mm^2 s^{-1}. The first two grid points concentrations (X[1..2]) were set as the reacted solution in order to initiate a front. The rest of the grid points (X[3..190]) were set with the initial concentrations. No flux boundary conditions were used: X[0] = X[1] and X[190] = X[191].

3.4.1 Results

An example of modelled spatiotemporal changes of pH (a), urea (b), NH_3 (c) and CO_2 (d) for conditions giving a clock time = 1400 s are shown in Fig. 3.13. As expected from simulations in a batch reactor (Fig. 2.14), the concentration of urea

decreases in time as the pH increases. The concentration of ammonia increases in time, whereas CO_2 reaches its maximal concentration at the border of reacted and unreacted solution, then decreases back to 0, so there is a pulse of CO_2 propagating through the reaction mixture.
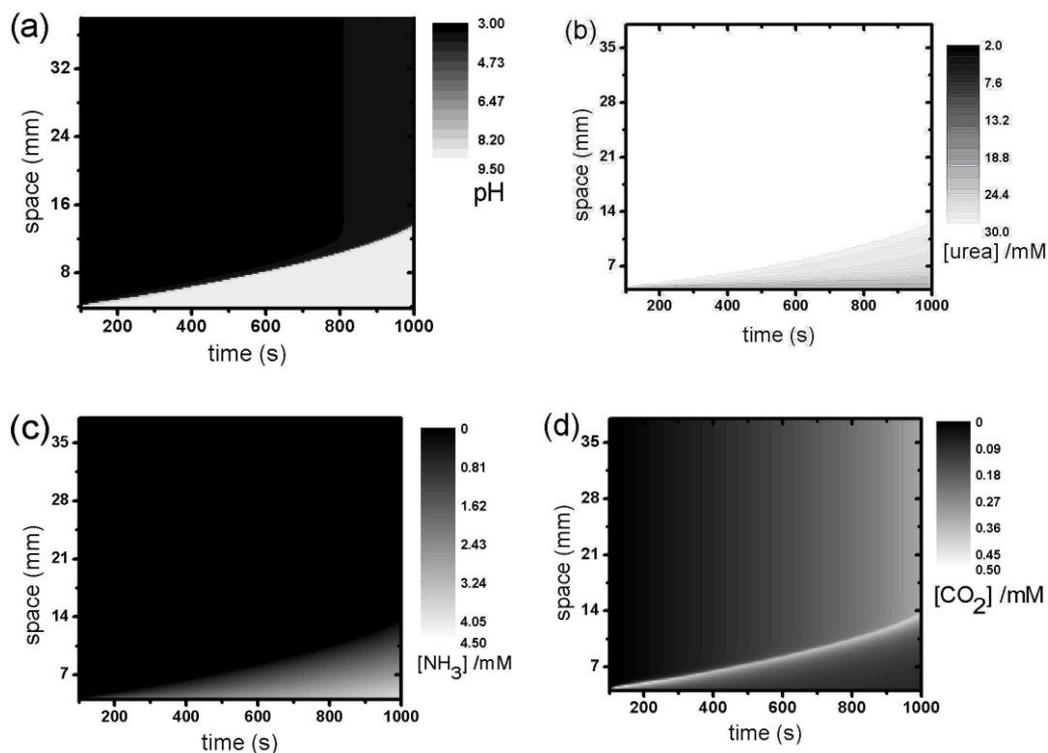
Figure 3.13 Illustration of modelled spatiotemporal changes of pH (a), urea (b), NH_3 (c) and CO_2 (d). [sulphuric acid]$_0$ = 4.05 × 10^{-4} M, [urea]$_0$ = 0.03 M, [urease]$_0$ = 18 unit mL^{-1}. Clock time = 1400 s

As in the experiments, it was possible to extract pH-space profiles at different time points, showing the change of pH is sharp as the front propagates:
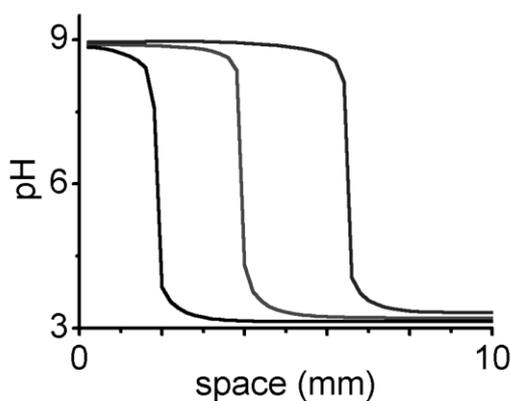
Figure 3.14 Modelled pH-space profiles at 200, 500, and 800 s with [sulphuric acid]$_0$ = 4.05 × 10^{-4} M, [urea]$_0$ = 0.03 M, [urease]$_0$ = 14 unit mL^{-1}

A front position *vs.* time plot is shown in Fig. 3.15 (a), where two regions of front speed are distinguished: the initial propagation and the later one. The distinction is made in order to show the acceleration of front speed with propagation of the front. To show this tendency for a wider range of conditions, an analogous plot has been made in Fig. 3.15 (b) for initial concentrations giving shorter clock time (800 s).
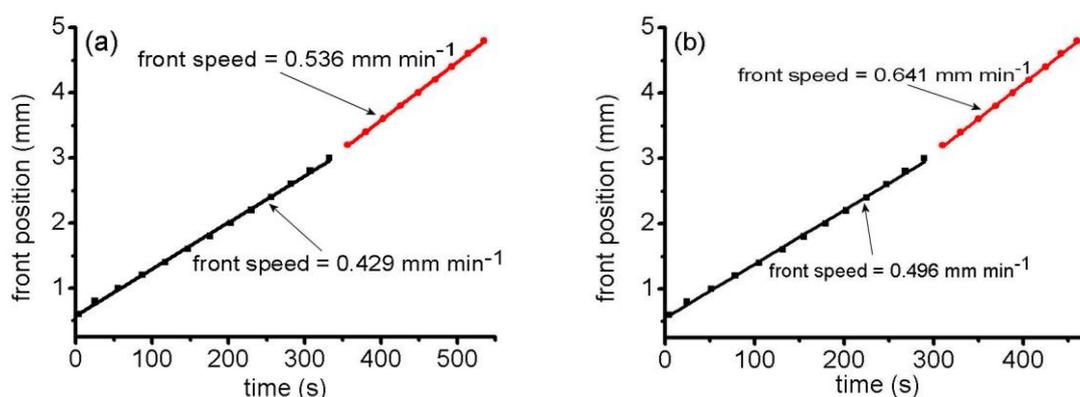
Figure 3.15 Front position *vs.* time plots for (a) [sulphuric acid]$_0$ = 4.05 × 10^{-4} M, [urea]$_0$ = 0.03 M, [urease]$_0$ = 18 unit mL^{-1}, clock time = 1400 s; (b) [sulphuric acid]$_0$ = 4.05 × 10^{-4} M, [urea]$_0$ = 0.03 M, [urease]$_0$ = 24 unit mL^{-1}, clock time = 800 s

It is clearly visible that closer to the clock time, the slope is bigger. The difference in front speed between faster and slower clock reactions increases in time. Therefore in order to compare the experimental results of front speed under different initial concentrations of urea, urease and acid with the simulations, for each of the conditions an upper and lower value of wave speed was calculated. The border between the front position for the upper and lower speed was taken for simplicity to be 3 mm from the initiation site. The comparison of experimental results with the model is shown in Fig. 3.16. Both the upper and lower calculated values of front speeds confirm the trends obtained in experiments: the front is faster for higher urea and urease concentrations; the front is slower for higher acid. The modelled variation of front speed is within a smaller range when changing the concentration of urea,

than changing urease or acid. With conditions giving shorter clock times (low acid, high urea and urease) the experimental data fits better with the upper front speed calculated from the later period of propagation. With longer clock times (low urea and urease, higher acid) the experimental data are closer to the lower front speed calculated from the earlier period of propagation (far from clocking). The model is far from agreement for very high urease (24 unit mL^{-1}) and high acid (0.45 mM).
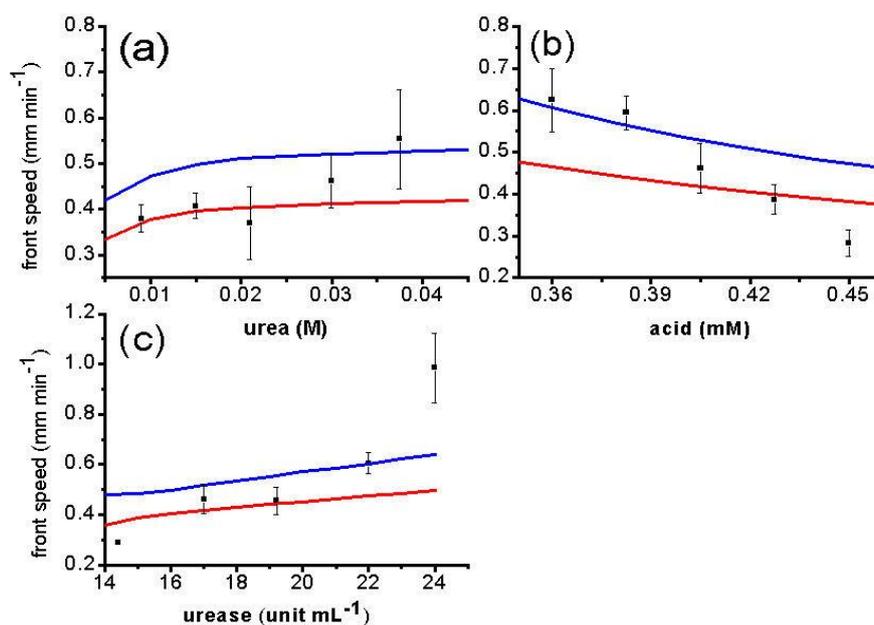
Figure 3.16 Comparison of simulated upper and lower front speed values (lines) with experiments for different initial concentrations of (a) urease, (b) urea and (c) acid. Standard concentrations were: [sulphuric acid]$_0$ = 4.05 × 10^{-4} M, [urea]$_0$ = 0.03 M, [urease]$_0$ = 17 unit mL^{-1}

The model also shows the impact of diffusion of different species on the front propagation. The analysis of single diffusion of H$^+$, OH$^-$, NH$_3$ and HCO_3^- (diffusion of all the other species are set to 0) shows that there is no front propagation if only OH$^-$ diffuses (Fig. 3.17 b), however the front propagation still proceeds if only H$^+$, NH$_3$ or HCO_3^- diffuse independently (Fig. 3.17 a, c and d). This may be a

consequence of the way the model is written, i.e. we do not explicitly include reaction of OH^- with other species except H^+. This means that NH_3 acts as autocatalyst.
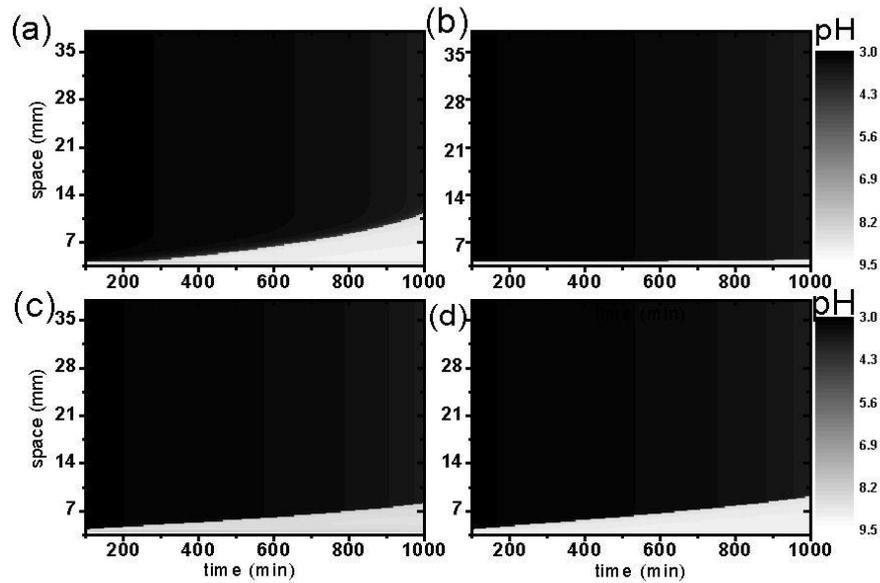
Figure 3.17 Dependence of the front propagation on diffusion of (a) H^+, (b) OH^- ,(c) HCO_3^- and (d) NH_3 alone ($D_{other} = 0$)

When the enzyme concentration is lowered down to 3.4 units mL^{-1}, the model still exhibits front propagation as shown in pH spatiotemporal profile in Fig. 3.18 (a) and in the front speed plot in Fig. 3.18 (b). The analysis of the front speed shows the same tendency as under high enzyme conditions – closer to the clock time, the front is faster.
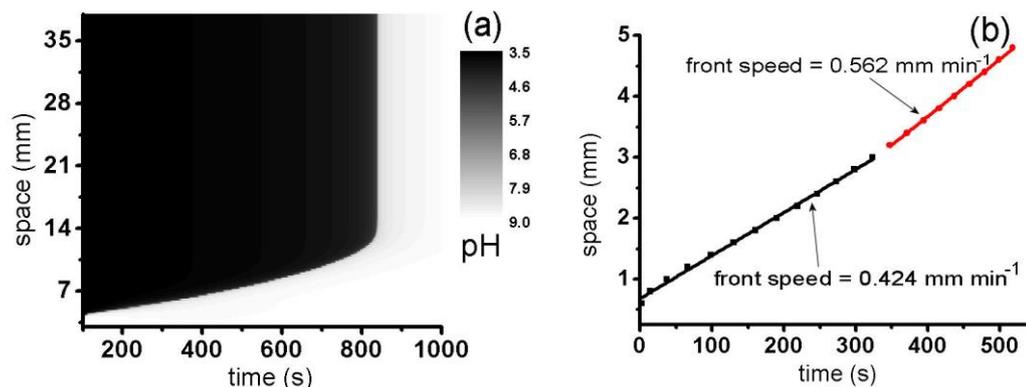
Figure 3.18 (a) Spatiotemporal changes of pH, and (b) front position vs time plot for low enzyme concentration. [sulphuric acid]$_0$ = 1.6 × 10^{-4} M, [urea]$_0$ = 0.03 M, [urease]$_0$ = 3.4 unit mL^{-1}

3.5 Discussion

The results in this chapter show that the urea/urease system exhibits pH front propagation within a certain range of initial conditions. In comparison to the other examples of enzyme catalyzed reactions undergoing front or wave propagation *in vitro*[3,4] it may be the simplest and the easiest enzymatic front system to characterize. It is the simplest system as the mechanism that contains five acid-base equilibria (2.8 – 2.12) of the products and the main enzyme-catalysed decomposition of urea (2.7) with addition of diffusion terms predicts the front propagation. The model shows reasonable quantitative agreement with the experimental data in a range of enzyme concentrations (from 17 to 22 unit mL^{-1}), in lower acid concentrations (from 0.36 to 0.43 mM) and in a wide range of urea concentrations (from 0.015 to 0.037 M), providing that the front speed is modelled for earlier and later periods of front propagation to account for acceleration as the reaction proceeds. There is experimental evidence that the front accelerates as the reaction proceeds (Fig. 3.5 and Fig. 3.7). However, due to experimental limitations, such as merging of fronts or late times of appearance of self-initiated fronts, it was not possible to calculate the

front speed for earlier and later periods of propagation for all sets of concentrations. Even for longer clock times the front speed does not change in a reproducible way in time (as shown in Fig. 3.5).

According to the current model the key species required for front propagation are: H^+ or HCO_3^-, or NH_3 but not OH^-. This fact means that the weaker bases, such as HCO_3^- or NH_3 given in the model are the species responsible for the autocatalytic character of the system. The front speed is in the range $0.2 – 1$ mm min^{-1}. In most of the known pH front systems such as bromate/sulphite[5] or chlorite/tetrathionate[6] reaction the front speed is $10 – 20$ times bigger than in the urea/urease, namely $1 – 20$ mm min^{-1}. This may be attributed to the fact that these systems contain an acid autocatalytic step, and the diffusion of acid is 2.5 times faster than OH^- and 5 times faster than NH_3. The only known example of a base-driven front is the (ethylenediaminetetraacetato)cobalt(II)/hydrogen peroxide system[7] where the planar wave speed was found to be around 0.48 mm min^{-1}. This system is not the best reference as fronts become unstable which leads to fingering in long term measurements, hence the fact that the front speed is 17 times bigger at this stage may be because of convection rather than reaction-diffusion.

Further experimental characterisation of the system showed when front propagation did not occur: for temperatures lower than 17 ºC and five times lower enzyme concentrations, in spite of a reasonable clock time in the well-stirred batch reactor under these conditions (400 s). The model still shows the regular propagation of a front at low enzyme concentration, which gives information about the limit of its validity. Other experimental data also suggests there is a limit of this model at low enzyme i.e. the results in a well-stirred system in Table 2.1 where there is a trend showing a significant decrease in final pH with the volume of the solution. Also

occasionally there were situations when no clock was observed in the batch reactor, but only a very slow increase of pH over few thousands seconds, even with conditions that usually provide an intermediate clock time and final pH = 9. An approach to consider is that under much lower enzyme concentration the urea/urease reaction undergoes non-mass action kinetics[8] or is highly sensitive to mixing effects (as many other autocatalytic reactions are[9]). Although usually non-mass action kinetics starts to play a role at a much smaller scale than a few mL, it still may be pronounced in this system because of the small amounts of enzyme used in these experiments, which is not necessarily seen on an industrial scale when the activity is calibrated. So for low enzyme concentrations in two separate experimental set-ups (batch reactor in chapter 2 and spatial here) the model introduced in the section 2.4 does not describe the behaviour observed and new approaches need to be considered[10].

In contrast to the previously introduced enzymatic systems that exhibit fronts, the urea/urease reaction is easy to characterise and the dependencies of spatial behaviour on the parameters such as initial concentrations and temperature of the reactants have been determined. Although under certain conditions (such as high enzyme or low acid) the errors in calculated front speed are high, the ranges of concentrations giving self-initiation, initiated front propagation and no propagation are known.

3.6 Conclusions

A spatial investigation of the urea/urease/sulphuric acid reaction in a thin layer has been made. The system exhibits propagating pH fronts in a wide range of conditions. Three different types of spatial behaviour have been observed depending on initial concentrations of reactants: self-initiation of fronts, initiated front and no

propagation. The fronts are reproducible providing the enzyme is above critical level. Front propagation has been predicted in a model that gives a reasonable agreement with the experimental data.

3.7 References

(1)   Scott, S. K.: *Oscillations, Waves and Chaos in Chemical Kinetics*; Oxford University Press: New York, 1994.

(2)   Scott, S. K.; Showalter, K.: *J. Phys. Chem.* **1992**, *96*, 8702-8711.

(3)   Miguez, D. G.; Vanag, V. K.; Epstein, I. R.: *Proc. Nat. Acad. Sci. U. S. A.* **2007**, *104*, 6992-6997.

(4)   Bodo, G.; Branca, R. M. M.; Toth, A.; Horvath, D.; Bagyinka, C.: *Biophys. J.* **2009**, *96*, 4976-4983.

(5)   Keresztessy, A.; Nagy, I. P.; Bazsa, G.; Pojman, J. A.: *J. Phys. Chem.* **1995**, *99*, 5379-5384.

(6)   Horvath, D.; Toth, A.: *J. Chem. Phys.* **1998**, *108*, 1447-1451.

(7)   Evans, R.; Timmel, C. R.; Hore, P. J.; Britton, M. M.: *Chem. Phys. Lett.* **2004**, *397*, 67-72.

(8)   Berry, H.: *Biophys. J.* **2002**, *83*, 1891-1901.

(9)   Epstein, I. R.: *Nature* **1995**, *374*, 321-327.

(10)   Wilkinson, D. J.: *Nat. Rev. Genet.* **2009**, *10*, 122-133.

4. Clocks and oscillations in the urea/urease/acetic acid reaction

4.1 Introduction

Further investigation of the properties of the urea/urease/acid reaction introduced in the previous chapters was made by changing the acid from a strong to a weak one: acetic acid. The system was studied in unbuffered conditions in a closed reactor and exhibited clocks with a different profile than when using sulphuric acid. In a CSTR, instead of bistability large amplitude oscillations were observed and studied under different ranges of parameters.

The full kinetic model introduced in chapter 2 was adapted by using the rate constants for acetic acid, though as it does not mimic the experimental results in a CSTR, different factors affecting the kinetics of the system, such as signal to noise, were investigated.

4.2 Experimental

Solutions were prepared as discussed in Chapter 2 with acetic acid replacing sulphuric acid in Solution A. The same batch reactor and CSTR procedure was followed. The behaviour of the system was recorded from pH measurements in the CSTR changing the pumping rate from settings 8 to 35 (which is close to maximum pump setting). The changes of pH at a certain pump rate have been measured for around 50 minutes. The flow rate was calibrated from the pump rate every day before the experiments were performed. Stock solutions undergo slow hydrolysis so have to be freshly prepared at least daily. 1 L stock solutions were prepared, fresh reactant solutions were supplied when needed. Initial concentrations of urea, urease and acetic acid were varied, urea from 0.01 to 0.03 M, urease from 1.25 unit/mL to 2.50 unit/mL, acetic acid from 2.92×10^{-4} M to 8.77×10^{-4} M. The temperature during

measurements was 16 °C. Experiments always started from the high pH product solution.

4.3 Results

4.3.1 Closed system

Reactions with acetic acid performed in a closed reactor exhibited acceleration in the production of OH$^-$ but with a less sharp pH change in time, compared to sulphuric acid, as shown in Fig.4.1. Clock reactions are observed in all ranges of initial concentrations of acetic acid: from [acetic acid]$_0$ = 2.92 × 10^{-4} M giving clock time = 250 s, to [acetic acid]$_0$ = 1.17 × 10^{-3} M giving clock time = 1500 s as shown in Fig. 4.2. In this range of concentrations of acetic acid the induction time increases almost linearly with concentration of the acid (Fig. 4.2 c).
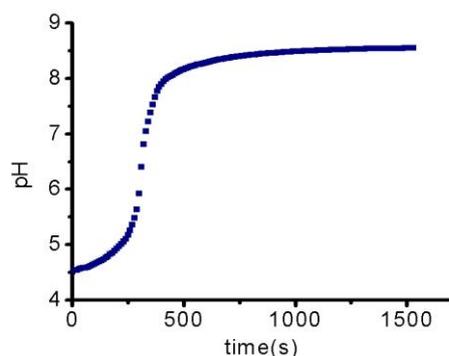
Figure 4.1 Example of a clock reaction in urea/urease/acetic acid system, [urease]$_0$ = 1.3 unit/mL, [urea]$_0$ = 0.005 M, [acetic acid]$_0$ = 5.85 × 10^{-4} M
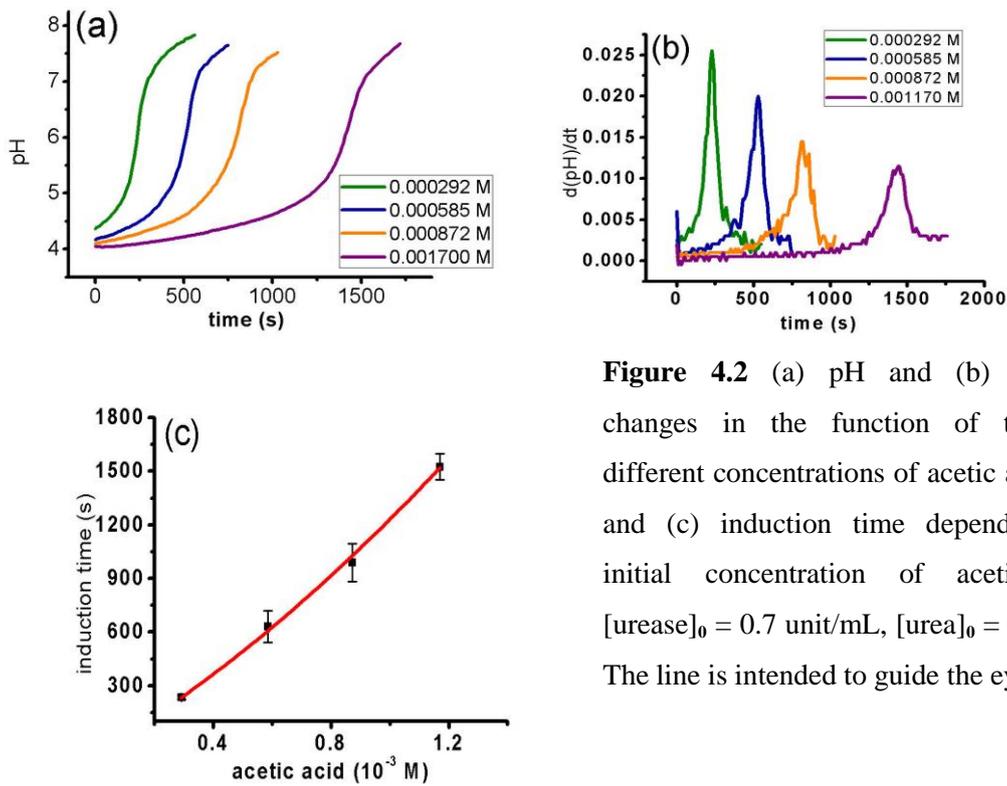
Figure 4.2 (a) pH and (b) d(pH)/dt changes in the function of time for different concentrations of acetic acid [M], and (c) induction time dependence on initial concentration of acetic acid. $[urease]_0 = 0.7$ unit/mL, $[urea]_0 = 0.005$ M. The line is intended to guide the eye

4.3.2 Open system

4.3.2.1 Oscillations

While performing the urea/urease/acetic acid reaction in a CSTR with a decrease of the pump rate for typical initial concentrations of reactants: $[urea]_0 = 0.01$ M, $[urease]_0 = 1.25$ unit/mL, $[acetic\ acid]_0 = 5.85 \times 10^{-4}$ M, a trend in the stability of the pH was seen. At the highest flow rate the pH decreases quickly to a low value and is stable under these conditions (Fig. 4.3 a). Then after a decrease of the flow rate, large amplitude changes of pH appear (from pH = 3.5 to 6.5) with a period of approximate 10 minutes and a systematic increase in the stability of the high pH in time and destabilisation of the low pH is observed (Fig. 4.3 b). When lowering the flow rate further, there is an increase in the period of the oscillations and further stability of the high pH state is noticed (Fig.4.3 c) until final stabilization

of the high pH steady state occurs as shown in Fig. 4.3 d-f. The high pH steady state is attained by a sudden increase and then slow decrease in pH. A lower pump rate gives a higher final pH.
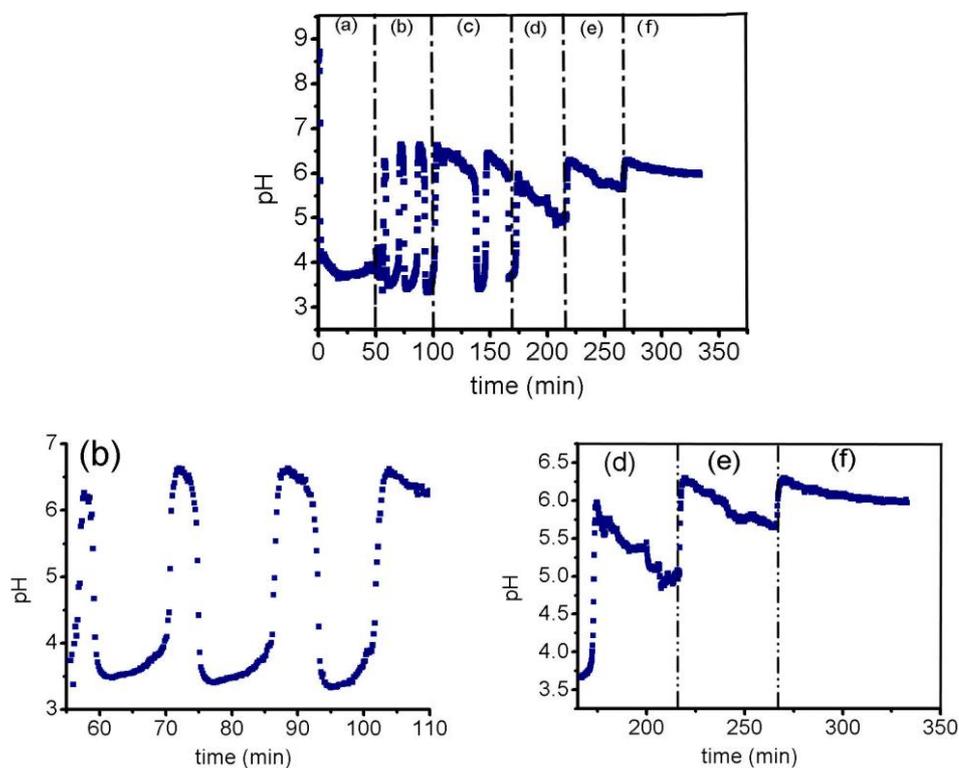
Figure 4.3 pH changes in time with decreases in the flow rate (a) 0.058 s^{-1}, (b) 0.052 s^{-1}, (c) 0.044 s^{-1}, (d) 0.037 s^{-1}, (e) 0.030 s^{-1}, (f) 0.021 s^{-1}, with [urea]$_0$ = 0.01 M, [urease]$_0$ = 1.25 unit/mL, [acetic acid]$_0$ = 5.85×10^{-4} M

Starting at a low flow rate, firstly the system drops from the high pH of the product solution to pH ~ 4.5 and then after some time it suddenly goes back to a higher pH (~ 7.5) as showed in Fig. 4.4 a. When increasing the flow rate, the system loses its stability in pH at a slightly higher flow rate than when decreasing the flow (0.024 s^{-1}, Fig. 4.4 b). The pH changes are shifted in this case compared to when decreasing the flow (from pH = 4.5 to 7.5), and the period of a single oscillation is longer ~25 min. In Figs. 4.4 b – d, a very similar trend is seen during 50 minutes of the measurement: a short pulse, followed by longer stability of the high pH state (20

minutes in Fig. 4.4 d). A further increase of the flow (Fig. 4.4 e) does not make the system stabilize in pH, but shifts the region of pH to lower values (from 3.7 to 6.5) with two pulses of smaller amplitude.
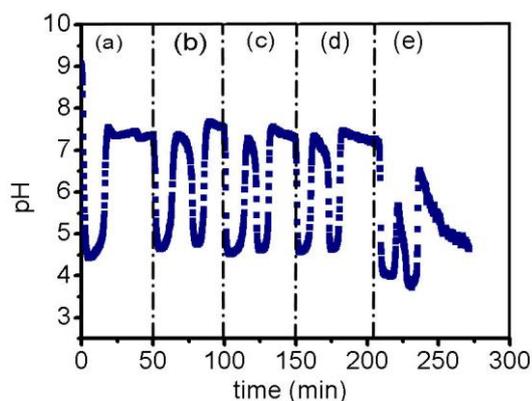
Figure 4.4 pH changes in time with increases in the flow rate (a) 0.017 s^{-1}, (b) 0.024 s^{-1}, (c) 0.033 s^{-1}, (d) 0.042 s^{-1}, (e) 0.052 s^{-1} , with $[urea]_0 = 0.01$ M, $[urease]_0 = 1.25$ unit/mL, $[acetic\ acid]_0 = 5.85 \times 10^{-4}$ M

In order to compare the behaviour of the system when increasing or decreasing the flow rate, a bifurcation diagram was constructed (Fig. 4.5). When there were no high amplitude oscillations, the final pH was taken. When an instability appeared, the maximum and minimum of the highest amplitude oscillation was taken. It is clearly seen that when increasing the flow, the region of oscillations begins at much lower flow rates, and when decreasing the flow the system stabilizes pH at $k_0 = 0.037$ s^{-1}. The pH oscillations are shifted to lower values when decreasing the flow compared to when increasing the flow.
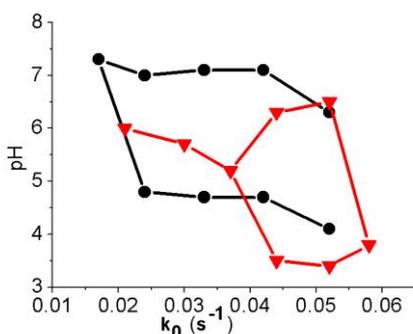
Figure 4.5 pH bifurcation diagram in the flow reactor: red line (triangles) - decreasing the flow rate, black line (circles) – increasing the flow rate, with $[urea]_0 = 0.01$ M, $[urease]_0 = 1.25$ unit/mL, $[acetic\ acid]_0 = 5.85 \times 10^{-3}$ M

4.3.2.2 Different concentrations of reactants

The range of flow rates where the high or low pH is stable or where oscillations appear has been investigated for different reactants concentrations. Values of the flow rates where high amplitude oscillations were recorded are shifted, but oscillations are still repeatedly seen in the majority of conditions. For example, for a higher acid concentration, [acetic acid]$_0$ = 8.77×10^{-4} M, when decreasing the flow, the low pH is stable up to k_0 = 0.025 s^{-1} where oscillations are seen, as shown in Fig.4.6. The presence of regular micro-oscillations (probably caused by pumping) is clearly visible (Fig. 4.6 c). This experiment shows that both the low and high pH can be stable in a long timescale and the large-amplitude spikes appear only under a specific flow rate. Under these conditions both the period and amplitude of the oscillations increase in time (Fig. 4.6 d). At the beginning the amplitude is only 1.8 pH units growing to 3.5 pH units 25 minutes later. The period between the maximum of the first and second spike is 16 minutes, and between the second and third spike is 34 minutes. The small amplitude oscillations are visible in the low pH state even when the reaction is oscillating (Fig. 4.6 d).
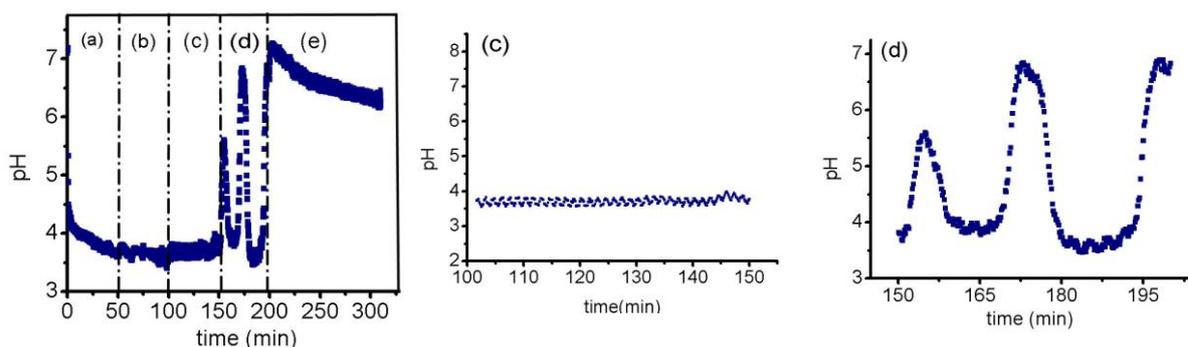
Figure 4.6 pH changes in time with decreases in the flow rate (a) 0.052 s^{-1}, (b) 0.042 s^{-1}, (c) 0.033 s^{-1}, (d) 0.025 s^{-1}, (e) 0.017 s^{-1} , [urea]$_0$ = 0.01 M, [urease]$_0$ = 1.25 unit/mL, [acetic acid]$_0$ = 8.77×10^{-4} M

A similar tendency was observed for higher urease concentrations (1.87 unit/mL) with again increasing stability of the high pH state under certain flow rates (Fig. 4.7). Instabilities appear at lower flows compared to with higher acid and there is a broader region of flow rates showing a stable high pH. The period of oscillations increases from 8 to 20 minutes, the amplitude from 1 to 2.5 pH units as shown in Fig. 4.7 b.
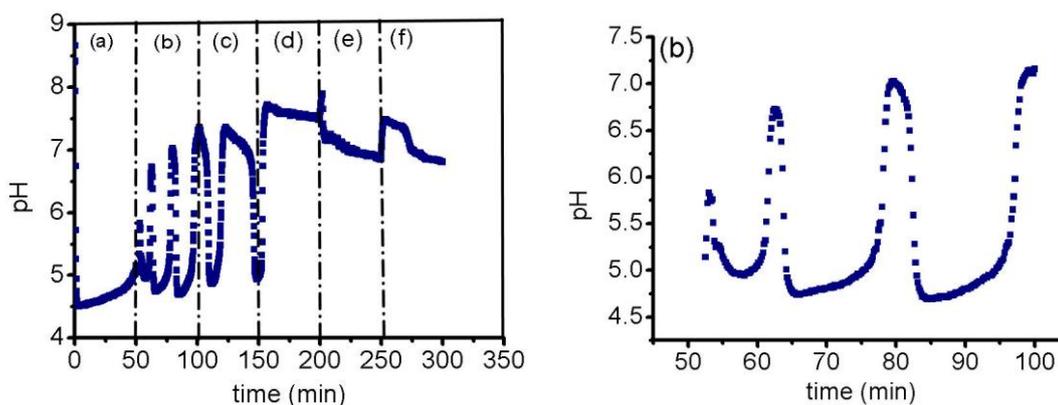
Figure 4.7 pH changes in time with decreases in the flow rate (a) 0.044 s^{-1}, (b) 0.038 s^{-1}, (c) 0.032 s^{-1}, (d) 0.026 s^{-1}, (e) 0.020 s^{-1}, (f) 0.013 s^{-1}, $[\text{urea}]_0 = 0.01$ M, $[\text{urease}]_0 = 1.87$ unit/mL, $[\text{acetic acid}]_0 = 5.85 \times 10^{-4}$ M

4.3.2.3 Step changes of the flow rate

In order to determine whether there is hysteresis in the oscillatory region, an experiment was performed where the flow was decreased to the oscillatory region then to the high pH steady state and back in large steps (Fig. 4.8). Oscillations occur at the same flow rate (0.039 s^{-1}), however they differ qualitatively. When preceded by the low pH state, the oscillations are sharp in shape, having low pH periods in between ($30 - 60$ mins in Fig. 4.8). When the oscillations are preceded by the high pH state they can be either sharp after a long "induction period" ($110 - 140$ mins) or broad ($240 - 270$ mins). Also it appeared that when preceded by lower flows with

oscillatory behaviour, broad oscillations between high and low pH were observed at

$k_0 = 0.044$ s^{-1} rather than a low pH steady state (140 – 170 mins).
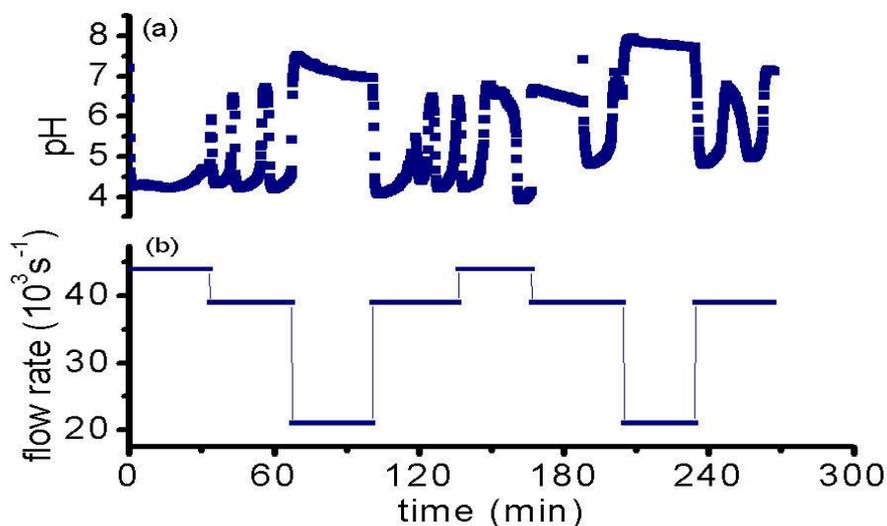
Figure 4.8 pH change in time for step changes of flow rates, with $[urea]_0 = 0.01$M, $[urease]_0 = 1.87$ unit/mL, $[acetic\ acid]_0 = 5.85 \times 10^{-4}$ M

4.3.2.4 Temperature effects

Performing the reaction under different temperatures (8 °C difference) showed the same tendency in behavior of the system:
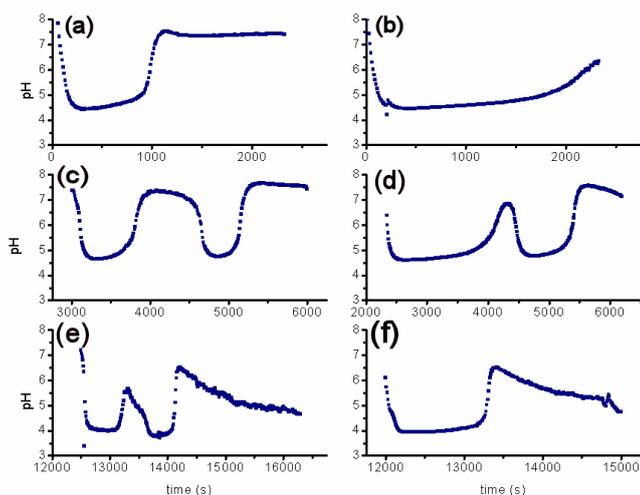
Figure 4.9 Comparison of behavior of the system under 23 °C (Figs. a, c and e) and 15 °C (Figs b, d and f). $[urea]_0 = 0.01$M, $[urease]_0 = 1.25$ unit/mL, $[acetic\ acid]_0 = 2.92 \times 10^{-4}$ M. Flow rates: (a) and (b) $= 0.014$ s^{-1}, (c) and (d) $= 0.018$ s^{-1}, (e) and (f) 0.045 s^{-1}

As showed in Figs 4.9 a and b, the system in both cases goes to a low pH at the beginning and then goes back to a high pH, however at 23 ºC it takes around 1000 s to return to the high pH and at 15 ºC from 1800 s the pH slowly increases. The oscillations appear under the same flow rate yet at a lower temperature it takes twice the time (23 ºC – 750 s, 16 ºC – 1500 s) and additionally the high pH state is stable faster at 23 ºC and for a longer period of time (Fig. 4.9 c). At $k_0 = 0.045$ s^{-1} it is possible to see similar behaviour in a longer timescale: the system goes to high pH for very short time and then slowly returns to the low pH state (Figs 4.9 e – f), however at 23 ºC an additional instability is noticed at the beginning (after 500 s) that is not present at 15 ºC.

4.3.2.5 Bifurcation and phase diagrams

For each set of concentrations bifurcation diagrams were constructed in an analogous way to Fig. 4.5:
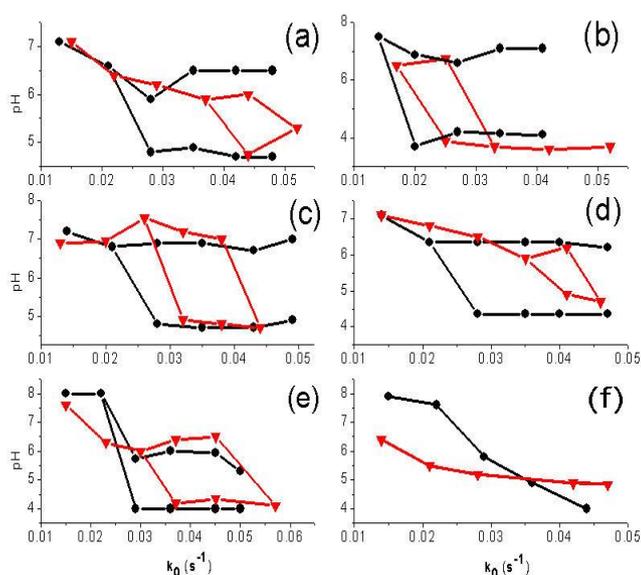
Figure 4.10 Bifurcation diagrams in the flow reactor for different sets of inflow concentrations. The standard concentrations are the same as in Fig. 4.5: $[urea]_0 = 0.01$ M, $[urease]_0 = 1.25$ unit/mL, $[acetic\ acid]_0 = 5.85\times10^{-4}$ M, with one varied reactant: (a) $[acetic\ acid]_0 = 2.92\times10^{-4}$ M, (b) $[acetic\ acid]_0 = 8.77\times10^{-4}$ M, (c) $[urease]_0 = 1.87$ unit/mL, (d) $[urease]_0 = 2.50$ unit/mL, (e) $[urea]_0 = 0.02$ M, (f) $[urea]_0 = 0.03$ M, where red line (triangles) – decreases in flow, black line (circles) – increases in flow

The oscillations usually keep their amplitude and increase in period while increasing the flow rate in the whole range of flows for all conditions investigated. For high acid (Fig. 4.10 b), high urea (Fig. 4.10 e) and urease concentrations (Fig. 4.10 c) the amplitude of oscillations overlaps while increasing and decreasing flow. The amplitude becomes much smaller while decreasing flow for low acid (Fig. 4.10 a) and high urease concentrations (Fig. 4.10 d). The oscillatory region while decreasing the flow is smaller for high urease (Figs 4.10 d and 4.11 b) and low acid (Figs 4.10 a and 4.11 c) concentrations. The oscillations disappear completely for high urea concentrations for both increasing and decreasing the flow (Figs 4.10 f, 4.11 a and 4.11 d). Under these conditions the system shifts to steady states, there was no bistability noticed in this region of phase diagram. The flow state is mostly seen only under $k_0 > 0.045$ s^{-1}, apart from high acid where it is stable already at $k_0 = 0.034$ s^{-1} (Fig. 4.10 b).

Using the experimental data it was also possible to construct very basic phase diagrams in order to better illustrate the trends of behaviour of this system in certain ranges of experimental conditions. For the majority of conditions the same tendency is observed: with increasing the flow rate, the system becomes oscillatory from a high pH steady state (apart from high urea where no oscillations are seen). With decreasing the flow rate the system starts from a low pH steady state, transits through the oscillatory region and reaches the high pH steady state. With decreasing the flow rate the thermodynamic state is stable for a large range of flows for low acid (Fig. 4.10 a) and all ranges of urea and urease. While increasing the flow in most of the conditions the thermodynamic state is only stable at $k_0 = 0.018$ s^{-1} and also $k_0 = 0.022$ s^{-1} in medium and high acid.
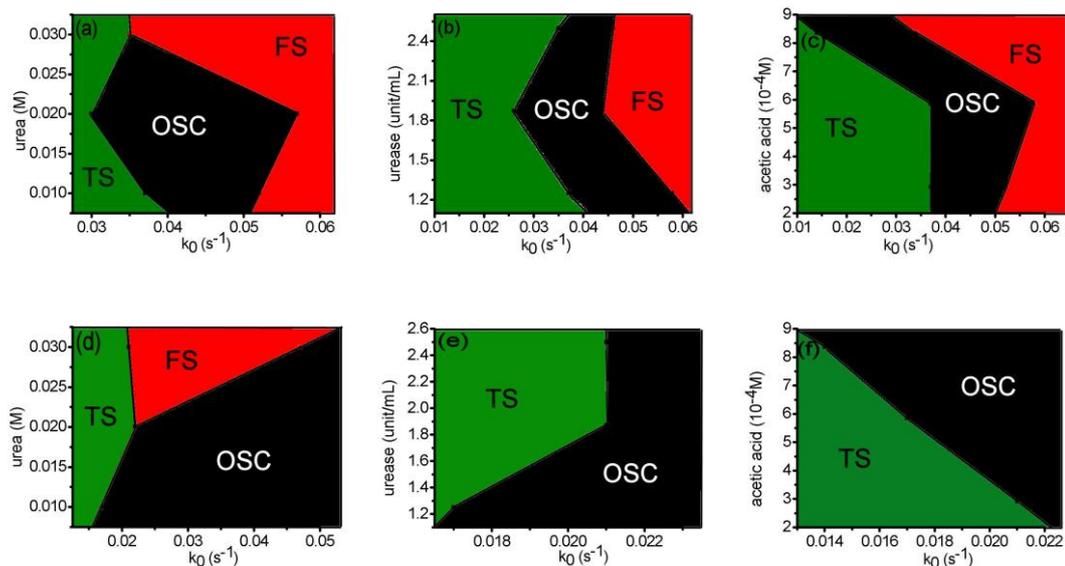
Figure 4.11 Experimental phase diagrams for different concentrations of urea, urease and acetic acid while decreasing the flow (a-c) and increasing flow (d-f) in time. TS = thermodynamic state; OSC = oscillations; FS = flow state

4.4 Modelling

The model consists of the same set equations as applied to the urea/urease/sulphuric acid system, namely 2.7 − 2.12 with acid dissociation rate constant (2.12) changed to acetic acid value following the reaction:

$$CH_3COOH \; \rightleftharpoons \; CH_3COO^- + H^+ \tag{4.1}$$

The model gives a good agreement in a closed system mimicking the shape of the pH − time curve (Fig.4.12 a). Also again it is confirmed that the higher the acid concentration, the longer the clock time (Fig. 4.12 b).
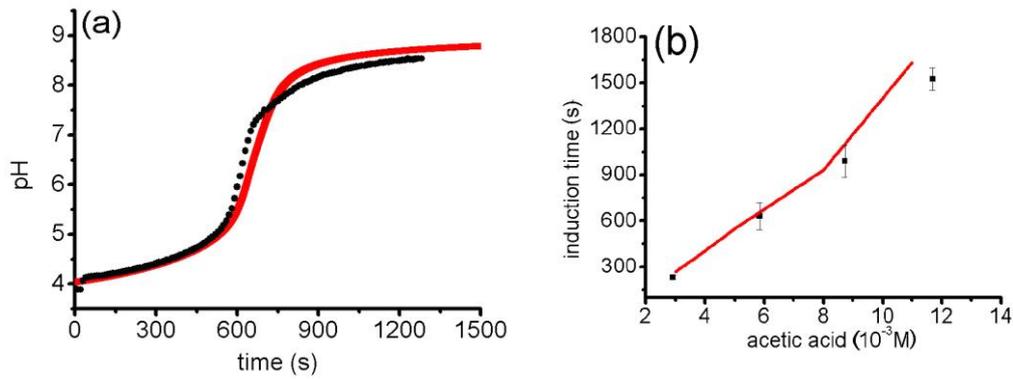
Figure 4.12 Comparison of experimental (black) and modelled (red) data for (a) pH changes in time, $[urease]_0$ = 1.4 unit/mL, $[urea]_0$ = 0.005 M, $[acetic\ acid]_0$ = 5.85 × 10^{-4} M, (b) induction time dependence on acetic acid concentration

The rate of change of pH is slower in acetic acid than in sulphuric acid, which is correlated with formation of the acetic acid/acetate buffer, as shown in Fig.4.13:
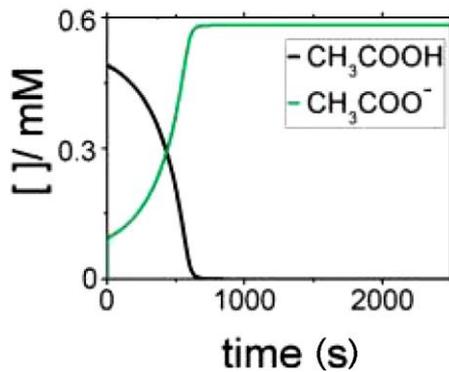
Figure 4.13 Modelled changes of concentrations in acetic acid and acetate during a clock. $[urease]_0$ = 1.4 unit/mL, $[urea]_0$ = 0.005 M, $[acetic\ acid]_0$ = 5.85 × 10^{-4} M

In flow, the model predicts only a small region of bistability (as shown in Fig. 4.13), but no oscillations are seen in the simulations.
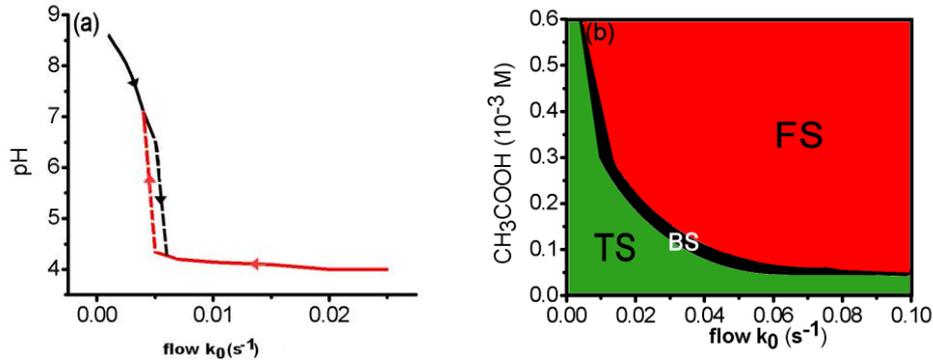
Figure 4.14 (a) Modelled behaviour of the urea/urease/acetic acid system in flow for [urease]$_0$ = 1.4 unit/mL, [urea]$_0$ = 0.005 M, [acetic acid]$_0$ = 5.85 × 10^{-4} M, with a small region of bistability. (b) acetic acid - flow rate phase diagram where TS = thermodynamic state; OSC = oscillations; FS = flow state

It was also possible to construct a bifurcation diagram where bistability was seen with two stable branches and one unstable as shown in Fig. 4.15. The model did not show any other types of steady states in this range of conditions.
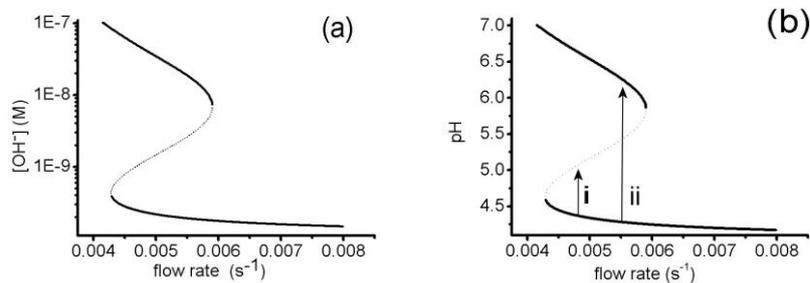
Figure 4.15 Modelled bifurcation diagram of the urea/urease/acetic acid system in terms of (a) concentration of OH-, (b) pH, where i – subcritical perturbation, ii – supercritical perturbation. [urease]$_0$ = 1.34 unit/mL, [urea]$_0$ = 0.005 M, [acetic acid]$_0$ = 5.85 × 10^{-4} M, solid lines – stable branches, dotted line – unstable branch

In the region where the coexistence of three steady states is seen, i. e. k_0 = 0.005 s^{-1}, it was possible to examine the system with respect to its sensitivity to perturbations in pH (Fig. 4.15 b). This was achieved by increasing the initial concentration of base from steady state value and observing how the system decays above or below the threshold. By comparison to the sulphuric acid system (Fig. 4.16

c and d) it is clear that the urea/urease/acetic acid system (Fig. 4.16 a and b) takes much more time (~ 4000 s) to reach either high or low pH steady state (in sulphuric acid it is ~250 s) though in both cases after a perturbation the system goes directly into its final steady state.
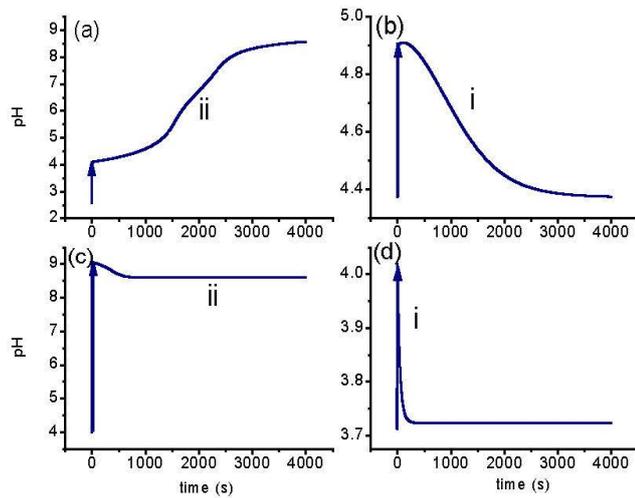
Figure 4.16 Modelled responses of the urea/urease/ (a), (b) acetic acid, or (c), (d) sulphuric acid system to perturbations in pH. $[urease]_0 = 1.34$ unit/mL, $[urea]_0 = 0.005$ M, $[acetic acid]_0 = 5.85 \times 10^{-4}$ M, $[sulphuric acid]_0 = 2.0 \times 10^{-4}$ M, $k_0 = 0.005$ s^{-1} i – subcritical perturbation, ii – supercritical perturbation

As there was no obvious source of negative feedback and initial attempts to obtain oscillations with removal of OH⁻ were not successful, it was assumed that one of possible reasons for the presence of these oscillations is sensitivity of the urea/urease/weak acid system to noise as it is known that noise can cause oscillations in bistable systems[125]. This pathway was followed because it has been shown that in enzyme-catalyzed reactions without feedback, noise may induce apparent bistable and oscillatory behaviour[126].

The basic (Langevin) equation that describes temporal changes of the variable x that contains noise is[1]:

$$\frac{dx}{dt} = q(x,t) + g(x,t)\xi(t) \tag{4.2}$$

where q(x,t)-drift term, g(x,t)-diffusion term(amplitude), $\xi(t)$-noise term

The noise term is described as the difference between Wiener processes at time t and

$(t+h)$[1]: $w(t) = W(t+h) - W(t) = h^{0.5}u(t)$ (4.3)

where u(t)-set of independent Gaussian random variables.

The algorithm containing noise is described by equations (4.4)-(4.6)[1]:

$k = hq(t, x(t))$ (4.4)

$l = h^{0.5}u(t)g(t,x(t))$ (4.5)

$x(t+h) = x(t)+0.5h[q(t,x(t))+q(t+h,x(t)+l+k)]+0.5\ h^{0.5}u(t)[g(t+h,x(t)+k+l)]$ (4.6)

The standard formula for adding white noise in C is gasdev random number generator where the amplitude is the main parameter.

To add noise effects in the urea/urease model the integration method had to be changed from CVODE to Euler or Runge-Kutta. For this purpose the model was rewritten in C and the results compared with original XPP version (with no noise). The codes are included in Appendix IV. Then noise terms were added to the differential equations of urea, NH_3 and CO_2. Although there was a good agreement of results while using different integration methods, the problem that arises from Runge-Kutta is the time of modelling (that is around 12 hours) as the step needs to be very small to give a reasonable outcome. To accelerate the calculation first of all a reduction of variables was made that kept the general behaviour of the original model. Improvement in the time of calculation was not significant as the equations that were considered in the reduced model were still stiff. To make the reduced model less stiff, fast equilibria in reactions was considered and rate constants rewritten to give reduced equations keeping the same value of the equilibrium constants. This operation improved the velocity of the calculation significantly and gave interesting dependencies of the effects of white noise on the initial concentration of urea. However the rescaled model with added noise did not show

the difference in behaviour between the weak and strong acids, and also the bistability was lost.

4.5 Discussion

The results presented in this chapter show different types of behaviour, including large amplitude oscillations, in the urea/urease/acetic acid reaction in a batch reactor and a CSTR. In batch, the system supported clock behaviour within a wide range of initial concentrations of the acid. There was no fast acceleration of the reaction compared to with sulphuric acid which was due to a strong buffering effect in the weak acid system (Fig. 4.13). In flow, the system was examined under different sets of parameters, such as concentrations of reactants, temperature as well as the range and direction of change (increasing/decreasing) of flow rates. The oscillations appear under certain flow rates in the majority of initial concentrations apart from at high urea (0.03 M), which may indicate that there is a critical concentration of the reactants that changes the behaviour of the system significantly. The region of oscillations is always for a much broader range of flow rates and the oscillations have more constant shape and amplitude when increasing the flow rate rather than decreasing the flow which may indicate either an experimental shift in parameters or a hysteresis when approaching the steady states that needs further exploration. There was no example of stable oscillations with constant amplitude and period seen that suggests that the nature of these oscillations is transient. Due to experimental limitations, such as pump channels having different flow rates or decay of the stock solution, it was impossible to stabilise the behaviour over a longer timescale in a single run.

The model with acetic acid shows a good agreement with the experimental pH–time profile and the dependence of the clock time on concentration of the acid in

a batch reactor. In a CSTR the model shows a very small range of bistability compared to the sulphuric acid system. As no oscillations were seen, perturbations have been made which showed that the response time of the weak acid system is much longer than in the strong acid, though no instabilities have been seen.

There could be several reasons for the presence of oscillations in chemical systems. Classical nonlinear analysis of a chemical autocatalytic system leads to creation of a Jacobian matrix with coefficients being taken from derivatives of rate equations with respect to all of the reactants in the system. Depending on the complexity of the eigenvalues of the matrix and their signs the behaviour and stability of the system can be predicted[2]. Oscillations are modelled under three different solutions. First one is when the solution is complex and its real parts are negative, which is called stable focus. In this case after a perturbation the system goes back to its steady state in an oscillatory manner with decreasing the amplitude until a final stabilization. Another solution where oscillations appear is when eigenvalues are complex numbers with real parts positive. This leads to unstable focus, where the oscillations increase in amplitude. The last situation leading to oscillations is when real parts of eigenvalues = 0, and only imaginary part is left, which is called Hopf bifurcation point. Under these conditions a node becomes unstable leading to limit cycle appearance. Although both of the first quoted examples are rarely identified in the literature, the third one is the most common source of chemical oscillations. This is due to the fact that for Hopf bifurcation coupling of reactions expressing positive and negative feedback is needed which can be obtained by cross-shaped diagram strategy[3] which distinguishes whole regions of presence different states depending on kinetic parameters such as flow rate. A source of negative feedback for acid autocatalytic reactions is usually acid consuming

compound, such as ferrocyanide coupled to bromate – sulphite reaction[4,5]. In analogical way for base autocatalytic reaction, such as methylene – glycol, an acid producing reaction was needed as a negative feedback (in this case gluconolactone hydrolysis)[6]. Also an outflow of the autocatalyst can be a source of negative feedback, as seen in very narrow range of conditions of the bromate – bromide – catalyst system.[7] Another interesting example of systems undergoing Hopf bifurcation is iodate – sulphite – ferrocyanide reaction[8]. In this system different types of Hopf bifurcations have been seen depending on the calculation parameters. Subcritical Hopf bifurcation has been shown in range of parameters as oscillations appear in large amplitude and constant period. Also supercritical Hopf bifurcation has been shown in this reaction as small amplitude oscillations with low period were observed as well. Also there was a situation where limit cycle collided with a saddle-node which caused an Infinite-Period Hopf bifurcation with constant amplitude and infinitely increasing period oscillations.

Following this pathway there is a possibility of presence of negative feedback in the urea/urease/acetic acid system. The products of the reaction, CO_2 and NH_3, can possibly transfer to gas phase, where ammonia is one of the driving species of the autocatalysis here. This assumption could be confirmed by experiment, however it has not been measured quantitatively yet. These gas transfer reactions are obviously present in both strong and weak acids systems, however sulphuric acid is not as sensitive to these processes as acetic acid because in strong acid solution the rate of production of base is much faster without buffering effects taking place in such strong scale as in the weak acid case. If this is the driving force of the oscillations the oscillations should be constant in time, what is not seen in our experiments. However the change in amplitude and period of the oscillations could be explained by slow

decay or the stock solutions or a slight mismatch in flow rate in different channels. Also there might be an Infinite Period bifurcation, however is has not been found in the current model. Additional steps with gas phase transfer have been added to the current model, but no evidence of any instability has been found yet. This model still needs further exploration. Also in current model there was no evidence of presence of a focus, however this may be again caused by the range of parameters chosen and possibly could be seen in small region of parameter space that has not been not investigated yet.

Another source leading to oscillations in chemical systems is noise, which appears to be particularly important in enzymatic systems[9]. Again there could be several factors causing noise-induced oscillations. First one is when there is a stochastic resonance with periodic variation of parameters (which in our case could be the flow rate, very clearly seen by small amplitude oscillations). This causes cycling of a bistable loop, which was seen for example in the oxidation of ascorbic acid by copper (II) ions[10]. Another situation is when there is an excitable system with one stable steady state and two unstable steady states which leads to periodic oscillations when intermediate noise is applied[11]. Examples of this situation are found in biological systems such as *Bacillus Subtilis*, where noise induces cellular differentiation through changes in genes expression and protein degradation[12]. Finally noise may shift regions of oscillations when there are systems with Hopf bifurcation. This could be obtained in practise by poor mixing effects that influences majority of the systems, for example BZ[13] or chlorite – thiosulphate[14] reactions.

With respect to the urea/urease/acetic acid system only the first mentioned situation of noise influence is possible. The second is excluded as there has not been any proof of a single excitable state in the current model. The third scenario could

not be explained by current model as well as any region of oscillations has not been found yet. Cycling of bistable loop is still probable as there is a possibility of variation of the activity of the enzyme especially seen under this range of enzyme concentrations. In order to prove this theory there is a need of more sophisticated calculating techniques to examine the model. Another useful information regarding enzyme action and the sensitivity of its kinetics to noise in this system would be to map the urea/urease/acetic acid behaviour in CSTR in much higher concentrations of the enzyme, as were used in fronts experiments to prove if the kinetics in flow reactor changes as significantly as in the spatial reactor.

4.6 Conclusions

A study of the urea/urease reaction in unbuffered conditions with replacement of the strong acid (sulphuric) to a weak one (acetic) has been done. In a batch reactor clock behaviour has been found with a strong buffering effect taking place which was illustrated in the model of the reaction. In a CSTR the experiments resulted in oscillatory behaviour within a range of parameters. There was no evidence of the bistability which was predicted by the model. Techniques applied for the examination of noise and perturbations do not reproduce the behaviour of the urea/urease/acetic acid system in a CSTR. The model needs further development such as additional reaction steps to be incorporated.

4.7 References

(1)   Miguel MS, Toral R: Stochastic Effects in Physical Systems. In *Instabilities and Nonequilibrium Structures*; Dordrecht: Kluwer Academic Publishing, 1997.

(2)   Gray P., Scott S. K.: *Chemical Oscillations and Instabilities*; Oxford University Press: Oxford, 1994.

(3)   Boissonade, J.; Dekepper, P.: *J. Phys. Chem.* **1980**, *84*, 501-506.

(4)   Edblom, E. C.; Luo, Y.; Orban, M.; Kustin, K.; Epstein, I. R.: *J. Phys. Chem.* **1989**, *93*, 2722-2727.

(5)   Zagora, J.; Voslar, M.; Schreiberova, L.; Schreiber, I.: *PCCP Phys. Chem. Chem. Phys.* **2002**, *4*, 1284-1291.

(6)   Kovacs, K.; McIlwaine, R. E.; Scott, S. K.; Taylor, A. F.: *J. Phys. Chem. A* **2007**, *111*, 549-551.

(7)   Orban, M.; Dekepper, P.; Epstein, I. R.: *J. Am. Chem. Soc.* **1982**, *104*, 2657-2658.

(8)   Gaspar, V.; Showalter, K.: *J. Phys. Chem.* **1990**, *94*, 4973-4979.

(9)   Samoilov, M.; Plyasunov, S.; Arkin, A. P.: *Proc. Nat. Acad. Sci. U. S. A.* **2005**, *102*, 2310-2315.

(10)   Strizhak, P. E.; Demjanchyk, I.; Fecher, F.; Schneider, F. W.; Munster, A. F.: *Angew. Chem.-Int. Edit.* **2000**, *39*, 4573-4576.

(11)   Lindner, B.; Garcia-Ojalvo, J.; Neiman, A.; Schimansky-Geier, L.: *Phys. Rep.* **2004**, *392*, 321-424.

(12)   Suel, G. M.; Garcia-Ojalvo, J.; Liberman, L. M.; Elowitz, M. B.: *Nature* **2006**, *440*, 545-550.

(13)   Menzinger, M.; Jankowski, P.: *J. Phys. Chem.* **1986**, *90*, 1217-1219.

(14)   Epstein, I. R.: *Nature* **1995**, *374*, 321-327.

5. Kinetic study of autocatalytic hydrolysis of esters

5.1 Introduction

One of the first attempts to create a pH-enzyme oscillator was by hydrolysis of benzoyl-L-arginine ethyl ester catalyzed by papain in a system with a membrane as mentioned in section 1.3[1]. Ester hydrolysis may be autocatalytic either through acid catalysis or enzyme catalysis, but this approach has not been investigated much.

Hydrolysis of esters is generally known to undergo different reaction mechanisms depending on the initial pH. The general scheme of the reaction is shown in eq. 5.1, where the reaction of the ester with water leads to production of an alcohol and a carboxylic acid:

$$R-\overset{\overset{O}{\|}}{C}-O-R' \xrightarrow{H_2O} R-\overset{\overset{O}{\|}}{C}-O-H + O-R' \qquad (5.1)$$

Ester — Carboxylic acid — Alcohol
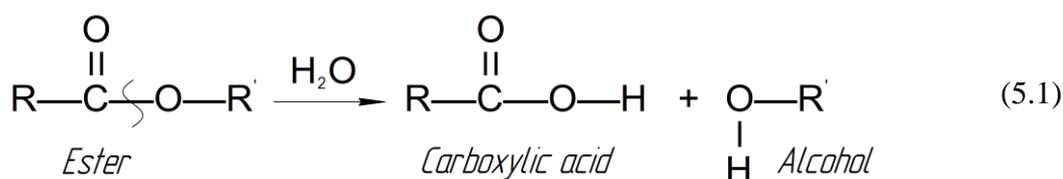
When the reaction is performed in acidic solution it is reversible and leads to equilibrium. The equilibrium can be shifted to the acid and alcohol products when performed in a large excess of water. The production of an ester is favoured when water is removed and in excess of alcohol solution. When the reaction is performed in a strong base solution, for example NaOH, the process becomes irreversible as it leads to the sodium salt, instead of the acid, that is not reactive with the alcohol.

Under conditions where the carboxylic acid product is favoured, the reaction may show autocatalytic behavior because of catalysis by acid:

$$(5.2)$$
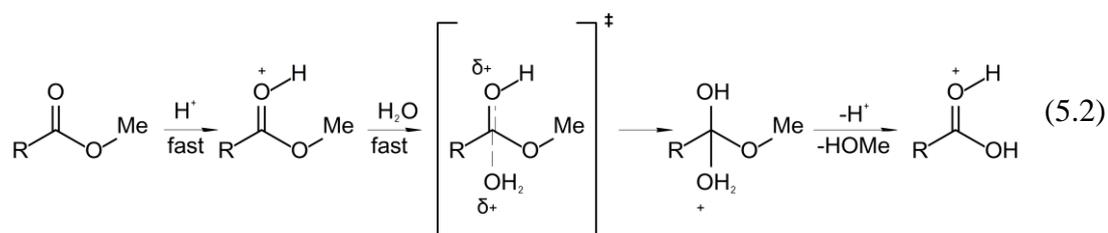
Apart from papain, ester hydrolysis processes can be catalyzed by other types of enzymes such as esterases[2]. Again as these enzymes have a bell-shape pH-rate curve and acid is one of the products of the reaction, so clock reactions from high to low pH should be expected, however because of experimental limitations such as very low solubility of esters in water and of enzymes in the oil phase evidence of acid autocatalysis taking place has not been clearly shown yet.

In this chapter firstly an analysis of the kinetic models of ester hydrolysis is done to indicate how different types of catalysis leads to pH clocks and bistability. Then the models are compared qualitatively with experimental results of several examples of enzyme-catalyzed and uncatalyzed ester hydrolysis is studied. In the final part, a model of aspirin hydrolysis is compared to experimental results as aspirin is one of the example esters investigated.

5.2 Modelling study

In the simplest model of ester hydrolysis three scenarios can be considered:
(A) Uncatalyzed:

$$S + H_2O \rightarrow P + P_2 \tag{5.3}$$

(B) Acid catalyzed:

$$S + H_2O \xrightarrow{H^+} P + P_2 \tag{5.4}$$

(C) Enzyme catalyzed:

$$S + H_2O \xrightarrow{enzyme} P + P_2 \tag{5.5}$$
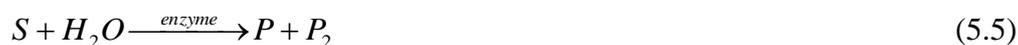
Where S = ester; P = carboxylic acid; P_2 = alcohol.

Two additional equilibria need to be included in each scenario:

$$P \rightleftharpoons P^- + H^+ \qquad pK_a \tag{5.6}$$

$$H_2O \rightleftharpoons H^+ + OH^- \tag{5.7}$$

The rate equations with flow term $(k_0([X_0] - [X])$ for reactions performed in CSTR are as follows:

$$\frac{d[S]}{dt} = -V + k_0([S_0] - [S]) \tag{5.8}$$

$$\frac{d[P]}{dt} = V - k_2[P] + k_{-2}[P^-][H^+] + k_0([P_0] - [P]) \tag{5.9}$$

$$\frac{d[P^-]}{dt} = k_2[P] - k_{-2}[P^-][H^+] + k_0([P_0^-] - [P^-]) \tag{5.10}$$

$$\frac{d[H^+]}{dt} = k_2[P] - k_{-2}[P^-][H^+] + k_3 - k_{-3}[OH^-][H^+] + k_0([H_0^+] - [H^+]) \tag{5.11}$$

$$\frac{d[OH^-]}{dt} = k_3 - k_{-3}[OH^-][H^+] + k_0([OH_0^-] - [OH^-]) \tag{5.12}$$

Where: k_2, k_{-2} – carboxylic acid equilibrium constants (5.6),

k_3, k_{-3} – water equilibrium constants (5.7),

k_0 – flow rate,

V_0 – hydrolysis rate, that varies in each scenario:

In model (A) $V_0 = k_1 S$, in model (B) $V_0 = (k_1 + k_{1a}[H^+])S$,

in model (C) $V_0 = \dfrac{V_{max} S}{(K_M + S)\left(1 + \dfrac{K_{es2}}{[H^+]} + \dfrac{[H^+]}{K_{es1}}\right)}$.

Where: k_1 – rate constant of uncatalyzed ester hydrolysis (reaction 5.3),

k_{1a} – rate constant of catalyzed ester hydrolysis (reaction 5.4).

The rate constants, adjusted in order to show different types of behaviour, are shown in Table 5.1, though in different models k_{1a}, k_1 and k_2 are varied.

Table 5.1 Rate constants used in the ester model, unless otherwise stated

Rate constants	k_1 s^{-1}	k_1a M s^{-1}	k_2 s^{-1}	k_{-2} M^{-1} s^{-1}	pK_a	k_3 M s^{-1}	k_{-3} M^{-1} s^{-1}
	1×10^{-4}	100	1×10^{-6}	1	3	1×10^{-3}	1×10^{11}
Enzyme constants	V_{max} M s^{-1}	K_M M	K_{es1}	K_{es2}			
	1×10^{-5}	1	1×10^{-4}	1×10^{-8}			

The maximum rate V_{max} depends on the total enzyme concentration $[E_0]$, K_M is the Michaelis constant, K_{es2} and K_{es1} are protonation equilibria of the substrate-enzyme complex (see Appendix 1). In each case the initial conditions are: S = 1 M, initial pH = 10. In the enzyme-catalyzed case, the pH dependence of relative enzyme rate,

calculated as $V_0 = \dfrac{V_{max} S}{(K_M + S)\left(1 + \dfrac{K_{es2}}{[H^+]} + \dfrac{[H^+]}{K_{es1}}\right)}$, is a bell-shape curve with

maximum at pH = 6:
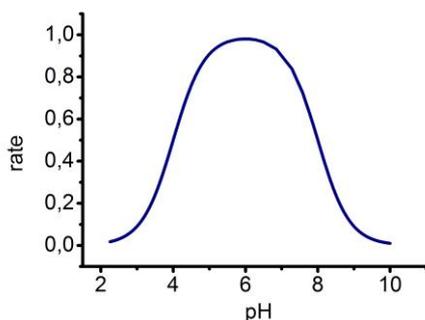
Figure 5.1 Modelled enzyme rate dependence on pH

The codes are included in Appendix V.

5.2.1 Results

(A) Uncatalyzed ester hydrolysis, $k_{1a} = 0$ M s^{-1}

In the uncatalyzed case it is still possible to see a clock reaction in terms of pH, though no direct acceleration in terms of H$^+$ production or substrate consumption is seen as shown in Fig.5.2. Also no evidence of bistability in flow is seen.
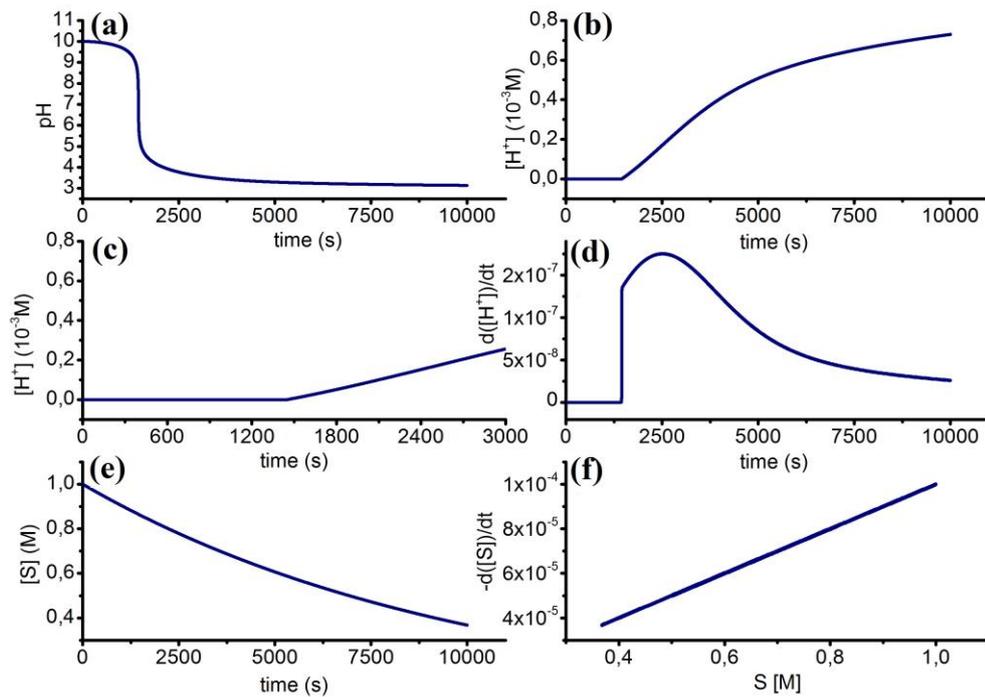
Figure 5.2 (a) pH – time plot, (b) $[H^+]$ changes in time, (c) enlarged region of $[H^+]$ production (d) reaction rate with respect to $[H^+]$, (e) $[S]$ changes in time, (f) reaction rate dependence on concentration of substrate. Model parameters: $k_{1a} = 0$ M s^{-1}

(B) Acid catalyzed ester hydrolysis

When acid catalysis is considered in the mechanism of ester hydrolysis the pH-time profile looks the same as in the uncatalyzed case with a sudden change of pH ~1700 s. However acceleration of the reaction is also seen with respect to the other species such as $[H^+]$ and $[S]$ (Fig. 5.3 b – e). Additionally a small region of bistability $(0.0003 – 0.0036 \text{ s}^{-1})$ is seen in the flow reactor as shown in Fig. 5.4.
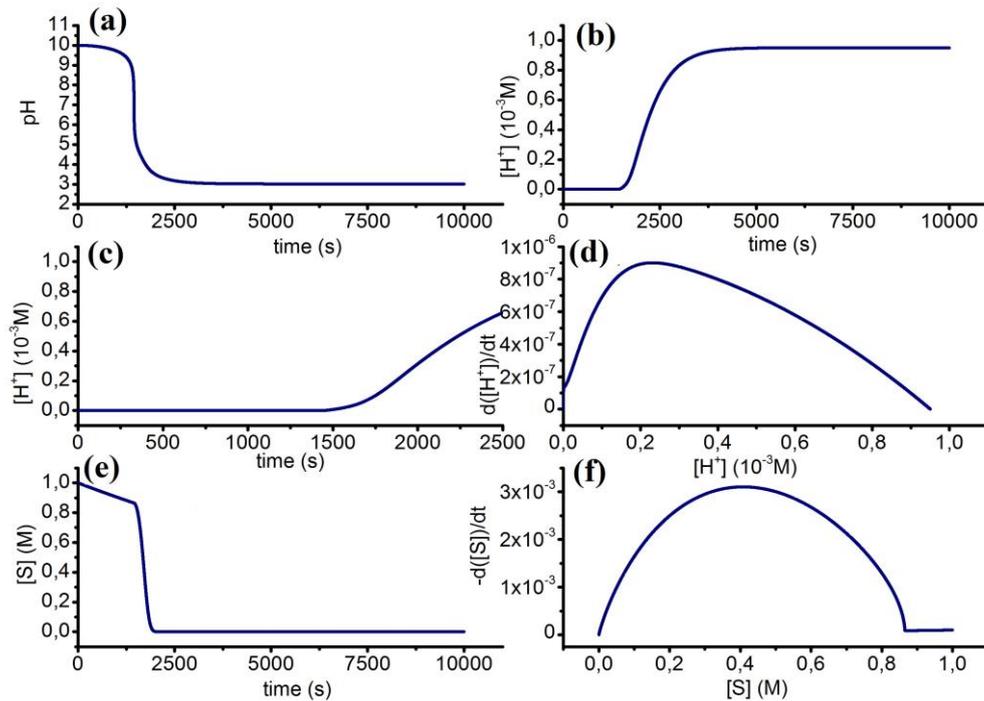
Figure 5.3 (a) pH-time plot, (b) [H$^+$] changes in time, (c) enlarged region of [H$^+$] production (d) dependence of reaction rate with respect to [H$^+$] on the concentration of acid, (e) [S] changes in time, (f) reaction rate dependence on concentration of substrate. Model parameters: $k_{1a} = 100$ M s^{-1}
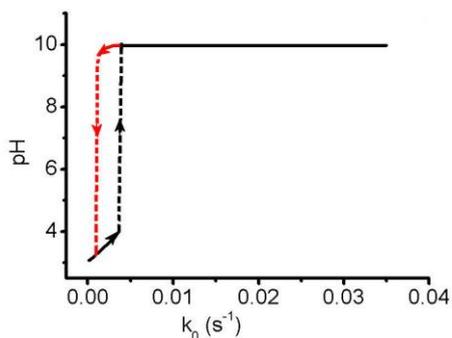
Figure 5.4 Modelled region of bistability in a flow reactor in acid catalyzed ester hydrolysis, conditions as stated in table 5.1

When the rate constants are changed to: $k_1 = 1 \times 10^{-5}$ s^{-1}, $k_{1a} = 1$ M s^{-1}, $k_2 = 1 \times 10^{-3}$ s^{-1} the pH change is bigger (the final pH goes to 1.50) and proceeds in two steps – the first one is from 10 to 5.5, the second one from 5.5 to 1.5 (as shown in Fig. 5.5 a). Also changes in the concentrations of [H$^+$] and [S] become sharper and their

derivatives more symmetrical than for higher values of k_1 and k_{1a} and a lower value of k_2. Additionally a much broader range of bistability is seen – from 0.008 to 0.030 s^{-1} as shown in Fig. 5.6.
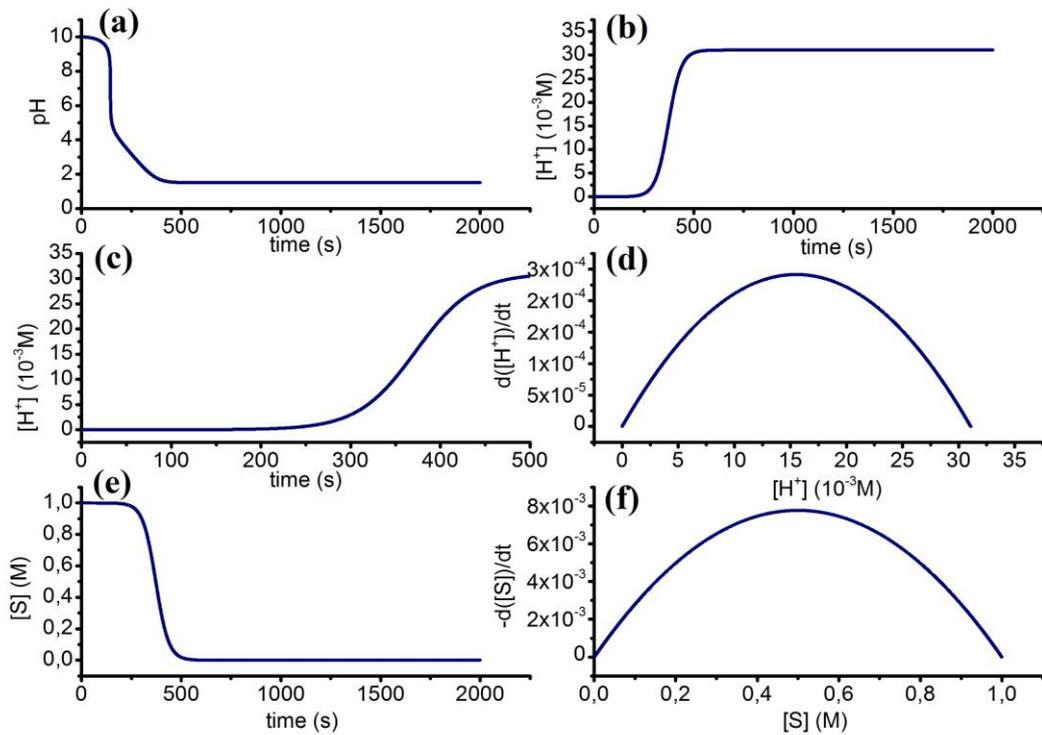
Figure 5.5 (a) pH-time plot, (b) $[H^+]$ changes in time, (c) enlarged region of $[H^+]$ production (d) dependence of reaction rate with respect to $[H^+]$ on concentration of acid, (e) $[S]$ changes in time, (f) reaction rate dependence on concentration of substrate. Model parameters: $k_1 = 1\times10^{-5}\,s^{-1}$, $k_{1a} = 1\,M\,s^{-1}$, $k_2 = 1\times10^{-3}\,s^{-1}$
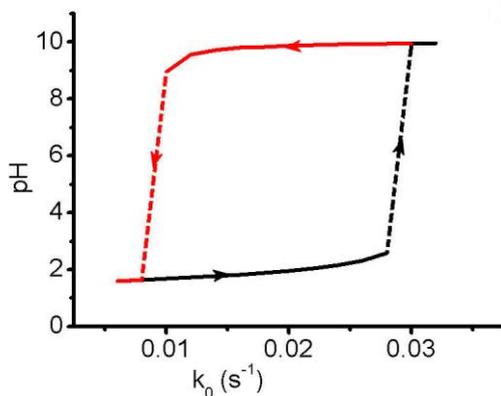
Figure 5.6 Modelled region of bistability in flow reactor in acid catalyzed ester hydrolysis,
$k_1 = 1\times10^{-5}\,s^{-1}$, $k_{1a} = 1\,M\,s^{-1}$,
$k_2 = 1\times10^{-3}\,s^{-1}$

(C) <u>Enzyme catalyzed ester hydrolysis</u>

When the catalysis is performed via a pH-sensitive enzyme with $k_1 = 1 \times 10^{-2}$ s^{-1}, $k_{1a} = 0$ M s^{-1}, $k_2 = 1 \times 10^{-4}$ s^{-1} the pH – time profile and production of acid look similar to the acid catalyzed case shown in Fig. 5.2, though the clock time is shorter. The major difference is that the substrate is consumed only to ~30% after 2000 s and exhibits a sharp maximum of reaction rate close to the initial concentration of the substrate (Fig. 5.7 f).
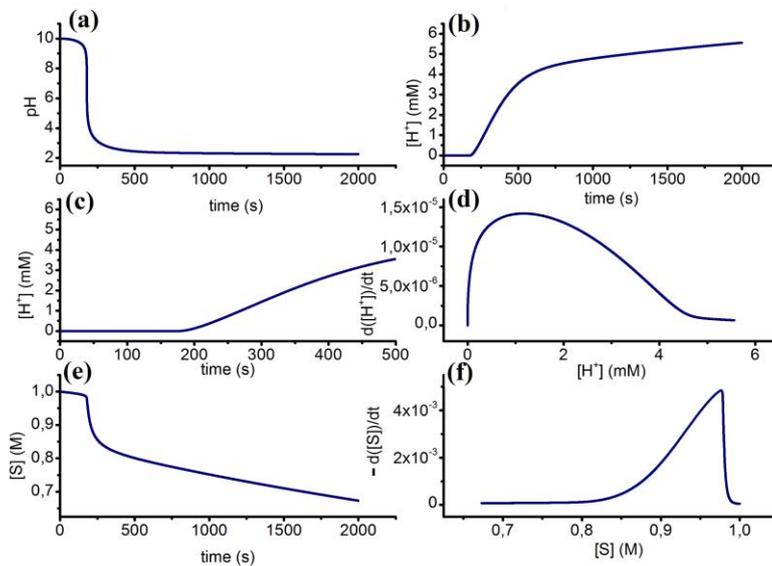
Figure 5.7 (a) pH-time plot, (b) $[H^+]$ changes in time, (c) enlarged region of $[H^+]$ production (d) dependence of reaction rate with respect to $[H^+]$ on concentration of acid, (e) [S] changes in time, (f) reaction rate dependence on concentration of substrate. Model parameters: $k_1 = 1 \times 10^{-2}$ s^{-1}, $k_{1a} = 0$ M s^{-1}, $k_2 = 1 \times 10^{-4}$ s^{-1}

In a flow reactor bistability is observed in flow rates between 0.15 and 0.70 s^{-1}, which is much broader than in the first acid catalyzed case with lower rate constants of catalysis and a higher acid dissociation constant (Fig. 5.3). It is also broader compared to the second acid catalyzed case (Fig. 5.5) and shifted to higher flow values.
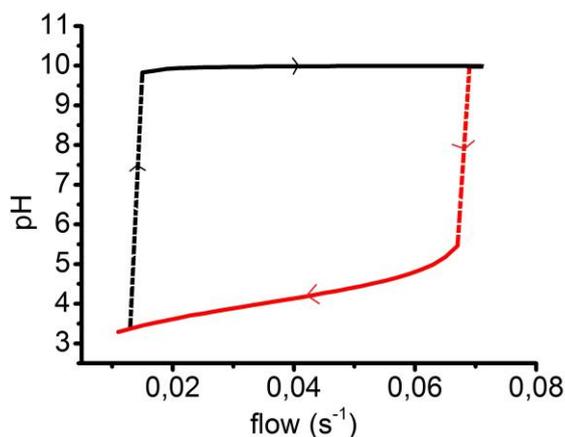
Figure 5.8 Modelled bistability region for enzyme catalyzed ester hydrolysis in a flow reactor with $k_1 = 1\times10^{-2}$ s^{-1}, $k_{1a} = 0$ M s^{-1}, $k_2 = 1 \times10^{-4}$ s^{-1}

5.3 Experimental

In the previous section, we have seen that with the addition of carboxylic acid catalysis to ester hydrolysis, we observe an increasingly more exponential growth in acid (Fig. c in each model). In the experiments we look for evidence of this trend. All reactions have been performed in a closed well-stirred reactor, where the solution consisted of 15 mL either of base (NaOH) or water. Then pH measurements were taken in the same way described in section 2.3.2 starting from the moment of addition of either solid ester or alcohol solution in p-nitrophenol acetate case. Attempts to monitor the substrate consumption or product appearance by UV-VIS spectrophotometry failed as the wavelengths of absorption lie in the noisy region of the spectrum of the equipment available which made the results inconsistent. The temperature during measurements was 20 ºC unless otherwise stated.

As a result of experimental difficulties it was not possible to perform the reactions in a CSTR in order to investigate the presence of bistability. Attempts to use other solvents for the esters failed as mixing with water during the pumping process caused volume contraction and significant heat release that makes the parameters in the CSTR impossible to control.

5.3.1 Hydrolysis of gluconolactone

One of the examples of compounds undergoing hydrolysis with generation of acid is gluconolactone. The reaction leads to opening the heterocyclic ring and production of gluconate ion:

$$+ H_2O \rightleftharpoons \qquad + H^+ \qquad (5.13)$$
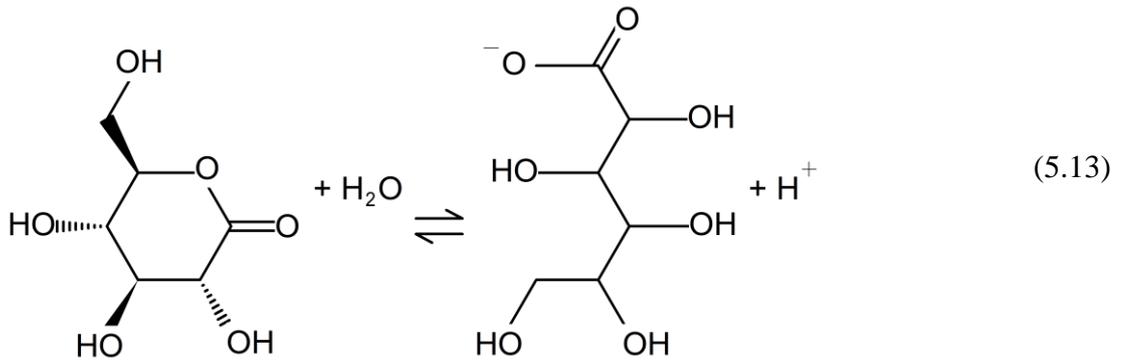
When performed in a batch reactor, where D-gluconic acid lactone undergoes dissolution and reaction, the major change of pH takes place in first 300 s (Fig. 5.9 a), and acid is produced faster starting from ~120 s (Fig. 5.9 c). The reaction rate has its maximum from 120 s till 350 s then the rate decelerates slowly.
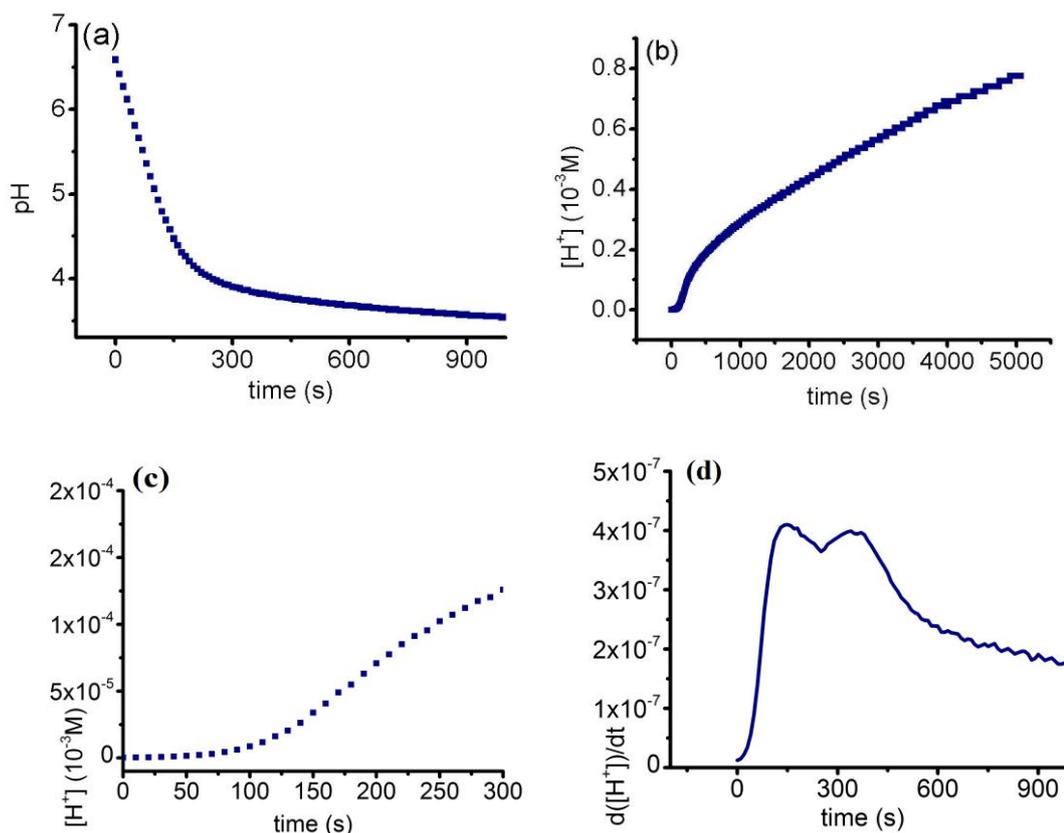
Figure 5.9 Hydrolysis of gluconolactone. (a) pH-time plot, (b) long-time [H$^+$] changes, (c) enlarged region of initial increase of [H$^+$], (d) changes of the rate of the reaction in time

5.3.2 Hydrolysis of lactide

Another compound that undergoes hydrolysis with production of acid is lactide. Again both opening of the ring and dissociation takes place:

$$+ H_2O \rightleftharpoons H^+ +2 \qquad (5.14)$$
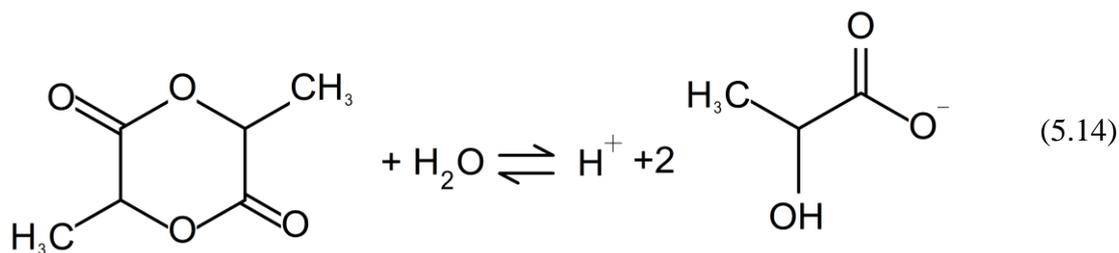
The changes of pH and concentration of H$^+$ look very different from the previous case. In the pH-time plot in Fig. 5.10 it is shown that two major changes of

pH take place: the first one between pH = 12 and 7, and the second between pH = 6

and 4. The concentration of hydrogen ion shows that only the second change, after

1300 s, contributes to acceleration in the production of acid significantly. The

reaction rate starts to accelerate at that point to become constant ~1900 s (Fig. 5.10

d).
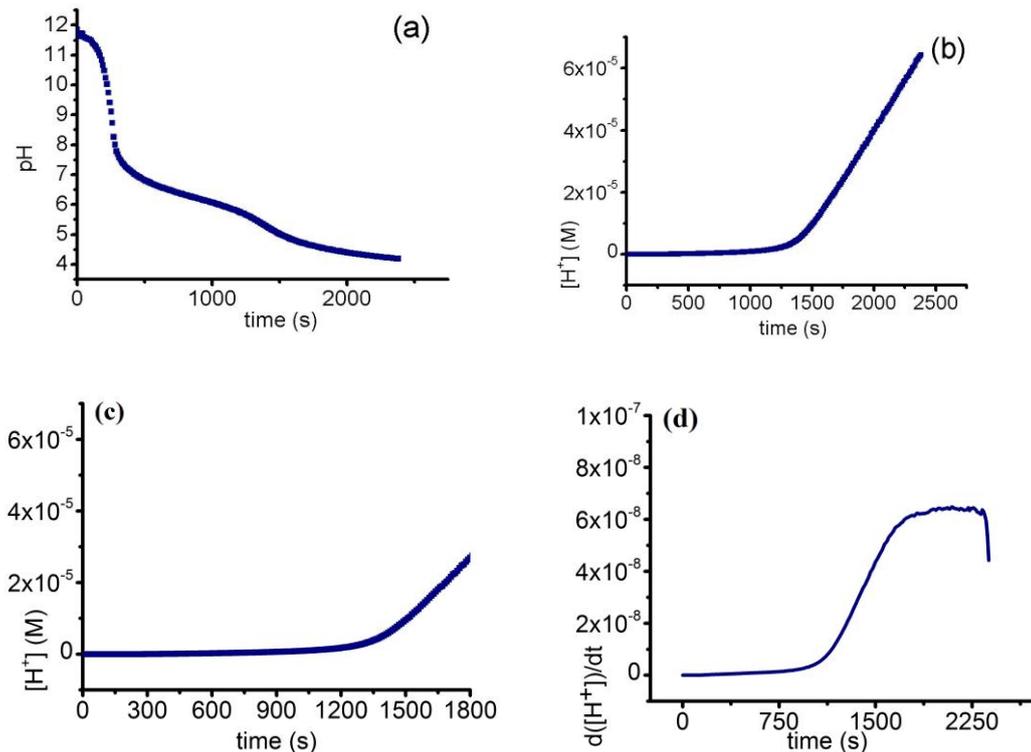
Figure 5.10 Dissolution and hydrolysis of 0.06 g of lactide in 15 mL of 0.016 M NaOH. (a) pH-time and (b) concentration of H^+ changes (c) enlarged region of initial increase of $[H^+]$, (d) changes of rate of the reaction

The same two steps in the production of acid are seen when the reaction is performed

in presence of enzyme butyrylcholinesterase, but also it is seen that the second

change of pH takes place earlier (of ~ 550 s) compared to the uncatalyzed case. Also

the rate of production is higher than in the previous case (Fig. 5.11 d).
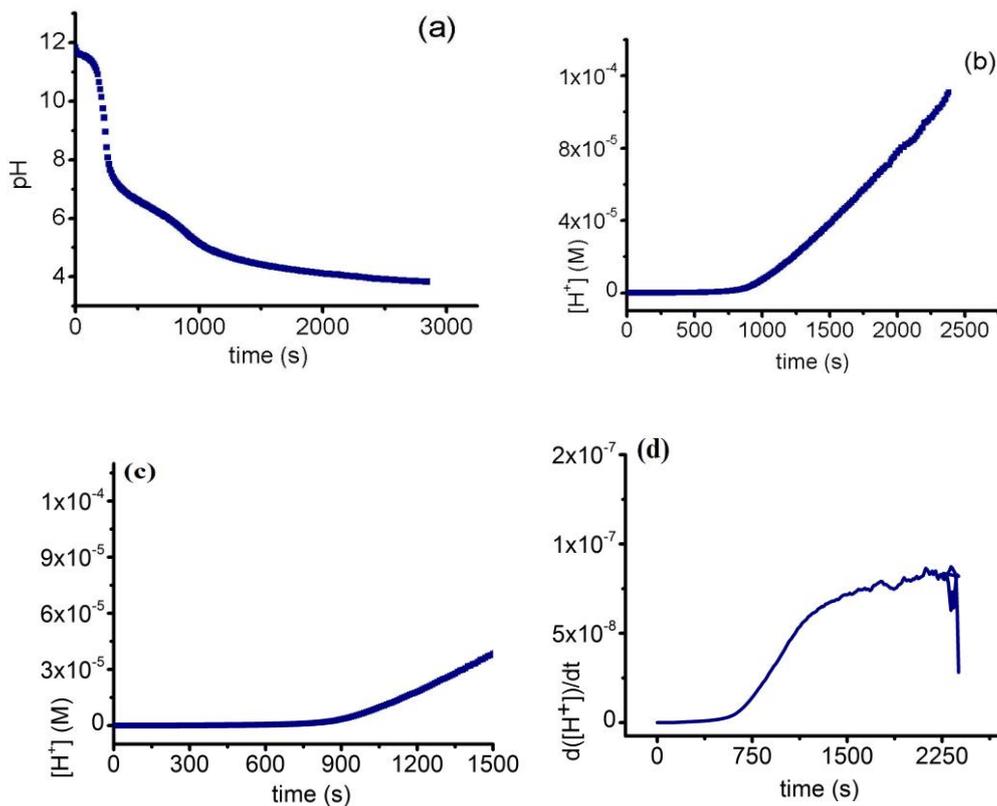
Figure 5.11 Dissolution and hydrolysis of 0.06 g of lactide in 15 mL of 0.016 M NaOH in presence of [butyrylcholinesterase]$_0$ = 2 unit/mL. (a) pH-time and (b) concentration of H$^+$ changes (c) enlarged region of initial increase of [H$^+$], (d) changes of rate of the reaction

5.3.3 Hydrolysis of p-nitrophenyl acetate catalyzed by chymotrypsin

A promising example of an enzyme-catalyzed hydrolysis of ester providing H$^+$ production is p-nitrophenyl acetate (PNPA) catalyzed by chymotrypsin[3]:

(5.16)

$$CH_3COOH \rightleftharpoons CH_3COO^- + H^+ \qquad\qquad pK_a = 4.8 \qquad\qquad (5.17)$$
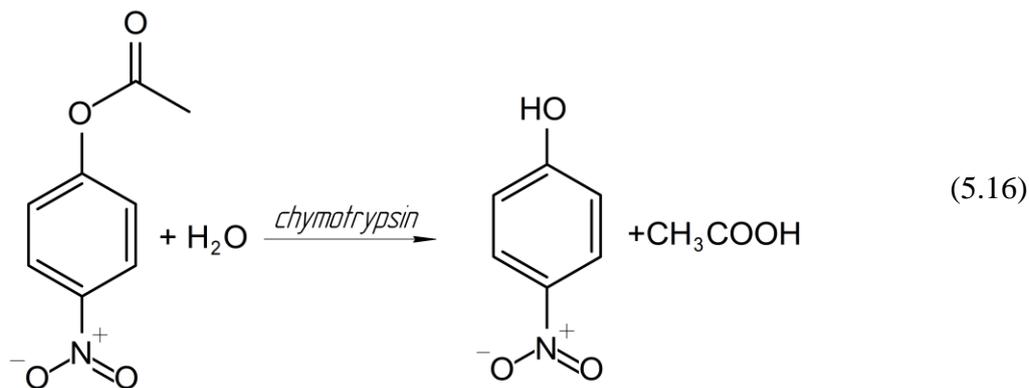
where the activity of the enzyme depends on pH as a bell shape curve with maximum at pH = 8. However, because of enzyme/substrate solubility issues, the reaction was performed in two phases: PNPA was dissolved in 100 % ethanol, chymotrypsin in 50/50 mixture of ethanol and 0.017 M NaOH. Both the pH and [H+] changes in time show the same trend as in the gluconolactone case, only the range of pH change is only in highly basic conditions. The main change of pH happens during the first minute, to become much slower in next 40 minutes in order to reach equilibrium:
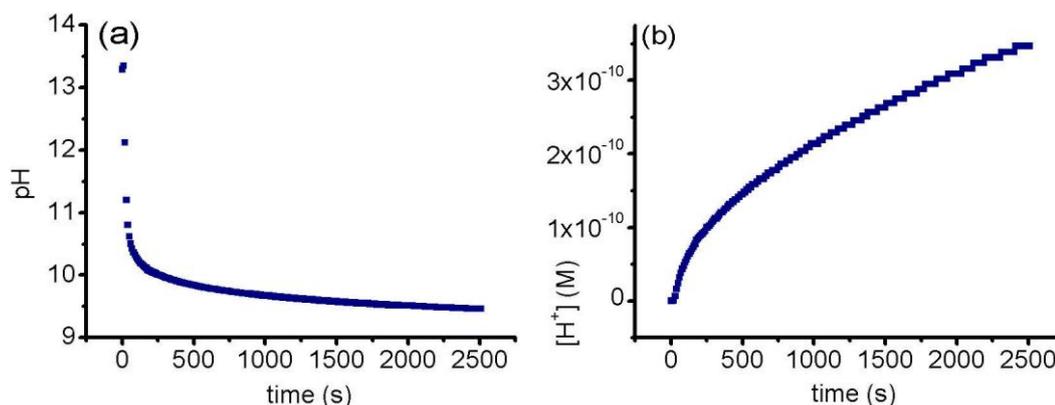
Figure 5.12 Hydrolysis reaction of $[PNPA]_0 = 0.05$ M, $[chymotrypsin]_0 = 0.59$ unit/mL. (a) pH- time and (b) concentration of H^+ changes

5.3.4 Hydrolysis of aspirin

Another ester reaction that is acid catalyzed is the hydrolysis of a popular drug aspirin[4]:

$$HCOOH - C_6H_4 - COOCH_3 + H_2O \rightleftharpoons HOOC - C_6H_4 - OH + CH_3COOH \quad (5.18)$$

$$CH_3COOH \rightleftharpoons CH_3COO^- + H^+ \qquad\qquad pK_a = 4.8 \qquad\qquad (5.19)$$

$$HOOC - C_6H_4 - OH \rightleftharpoons {}^-OOC - C_6H_4 - OH + H^+ \qquad pK_a = 3.0 \qquad\qquad (5.20)$$
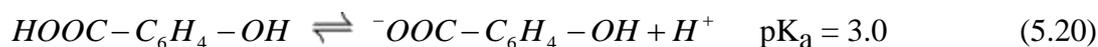
Addition of aspirin to NaOH leads to a sudden change of pH from 12.5 to 4.0 after 300 s as shown in Fig. 5.13 a. The concentration of H^+ profile (Fig. 5.13 b) shows significant growth after 400 s with slight acceleration.
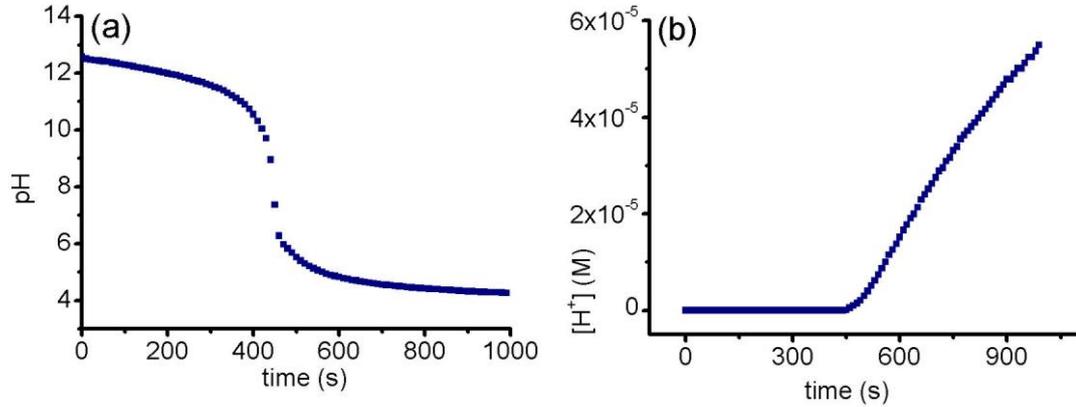
Figure 5.13 Example of pH "clock-type" behaviour when 0.05 g of aspirin is dissolved in 15 mL of 0.016 M NaOH

The dissolution of aspirin was observed to be slow and the solubility is 3 mg/mL at 20 °C, hence we investigated the reaction at different temperatures. This clock-type behaviour is seen in wide range of temperatures and the clock time can be varied from 100 s in 60 ℃ to 1250 s in 5 ℃ as shown in Figure 5.14.
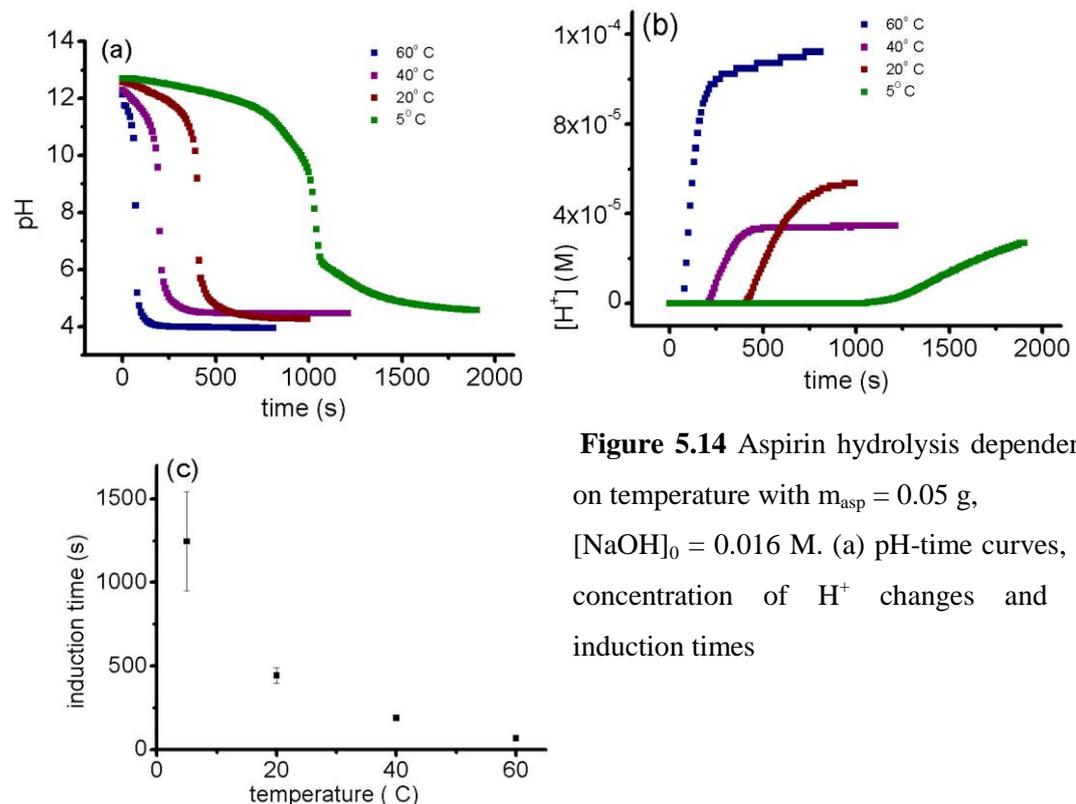
Figure 5.14 Aspirin hydrolysis dependence on temperature with $m_{asp} = 0.05$ g, $[NaOH]_0 = 0.016$ M. (a) pH-time curves, (b) concentration of H^+ changes and (c) induction times

The clock-type behaviour depends on the mass of aspirin dissolved, as when the mass is decreased to 0.03 g (below solubility limit) the final pH is only 8.5 after 7500 s at 20 ºC (as shown in Fig. 5.14 a) and no significant production of H^+ ions is seen. A temperature increase up to 60 ºC does not change the behaviour significantly as for the same mass of aspirin equivalent final pH values are seen (Fig. 5.15 c and d).
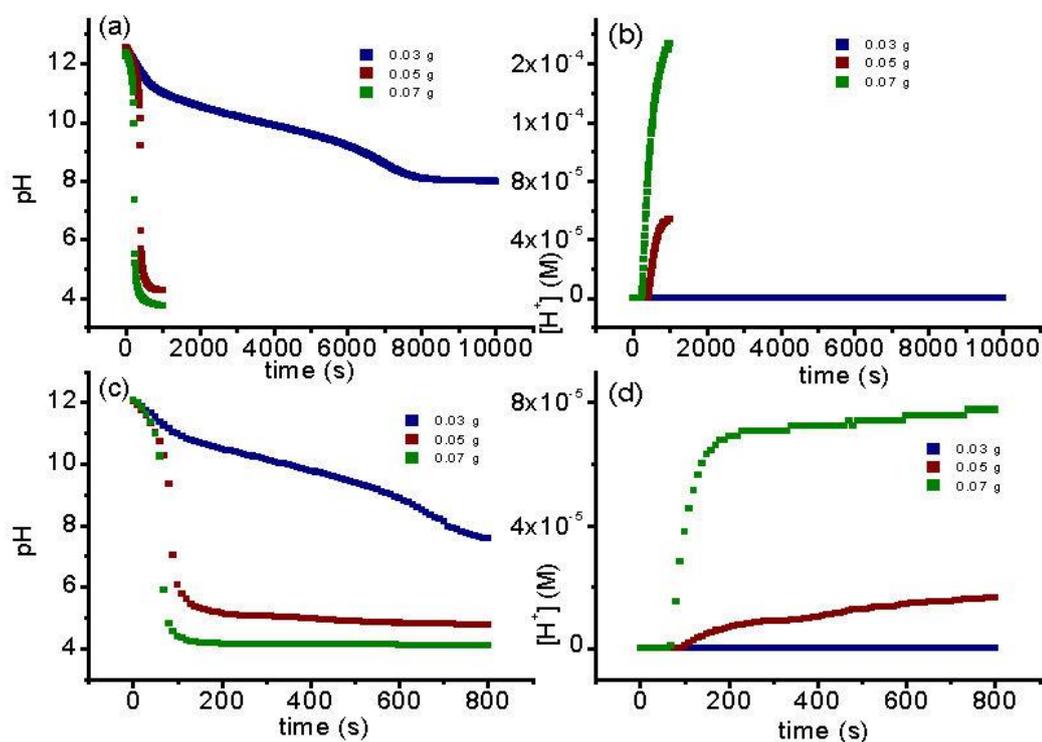
Figure 5.15 (a), (c) pH – time curves and (b), (d) concentration of H^+ changes during aspirin hydrolysis depending on the amount of aspirin added performed in (a), (b) 20 ºC, and (c), (d) 60 ºC

5.4 Model of aspirin hydrolysis

As the aspirin shows a pH clock but we were unable to follow the substrates by UV-VIS in experiments a model of aspirin hydrolysis was used to determine whether the reaction is autocatalytic.

The known established mechanism of aspirin hydrolysis consists of six irreversible steps (5.21 – 5.26) and four acid – base equilibria (5.27 – 5.30)[4]:

$$CH_3COOC_6H_4COOH + H^+ + H_2O \xrightarrow{k_1} HOC_6H_4COOH + CH_3COOH + H^+ \quad (5.21)$$

$$CH_3COOC_6H_4COOH + H_2O \xrightarrow{k_2} HOC_6H_4COOH + CH_3COOH \quad (5.22)$$

$$CH_3COOC_6H_4COOH + OH^- \xrightarrow{k_3} HOC_6H_4COOH + CH_3COO^- \quad (5.23)$$

$$CH_3COOC_6H_4COO^- + H^+ + H_2O \xrightarrow{k_4} HOC_6H_4COOH + CH_3COOH \quad (5.24)$$

$$CH_3COOC_6H_4COO^- + H_2O \xrightarrow{k_5} HOC_6H_4COOH + CH_3COO^- \quad (5.25)$$

$$CH_3COOC_6H_4COO^- + OH^- \xrightarrow{k_6} HOC_6H_4COO^- + CH_3COO^- \quad (5.26)$$

$$H_2O \rightleftharpoons H^+ + OH^- \qquad k_7, k_{7r} \quad pKa = 14 \qquad (5.27)$$

$$CH_3COOC_6H_4COOH \rightleftharpoons CH_3COOC_6H_4COO^- + H^+ \quad k_8, k_{8r} \quad pKa = 3.5 \quad (5.28)$$

$$HOC_6H_4COOH \rightleftharpoons HOC_6H_4COO^- + H^+ \qquad k_9, k_{9r} \quad pKa = 3 \qquad (5.29)$$

$$CH_3COOH \rightleftharpoons CH_3COO^- + H^+ \qquad k_{10}, k_{10r} \quad pKa = 4.8 \qquad (5.30)$$

As in the experiments, the dissolution process needs to be considered as well:

$$CH_3COOC_6H_4COOH \ (s) \rightleftharpoons CH_3COOC_6H_4COOH \ (aq) \qquad k_0, k_{0r}, \qquad (5.31)$$

The rate constants are known from the literature[4] and are shown in Table 5.2:

	day-1	s-1
k0		1.5e-3
k0r		1e-10
k1	1.9	2.19907E-05
k2	0.117	1.35417E-06
k3	1.00E+03	0.011574074
k4	46.7	0.000540509
k5	2.11E-03	2.44213E-08
k6	7.50E+03	0.086805556
k7		1.00E-03
k-7		1.00E+11
k8		3.16E+05
k-8		1.00E+09
k9		1.00E+06
k-9		1.00E+09
k10		8.00E+05
k-10		4.50E+10

Table 5.2 Rate constants used in modelling of aspirin hydrolysis

The only parameters possible to vary in this model are: the initial mass of aspirin to be dissolved and the initial pH. In Fig. 5.17 an example of a relatively fast "clock-type" change of pH is shown (~420 s) with the H^+ profile and its derivative. When compared to the situation with a lower mass of aspirin dissolved, shown in Fig. 5.18, it is clear that with a decrease of the substrate, the system loses its clock character with less sharp conversion and much smaller H^+ production (only to pH ~6.8). As in the experiments, slight changes of the initial mass of aspirin dissolved can lead to big quantitative changes in H^+ production (of several orders of magnitude). The values of masses leading to certain clock times are 2.5 times lower than in experiment, this may be caused by imperfect dissolution and mixing in the real system. A lower initial pH only accelerates the conversion.
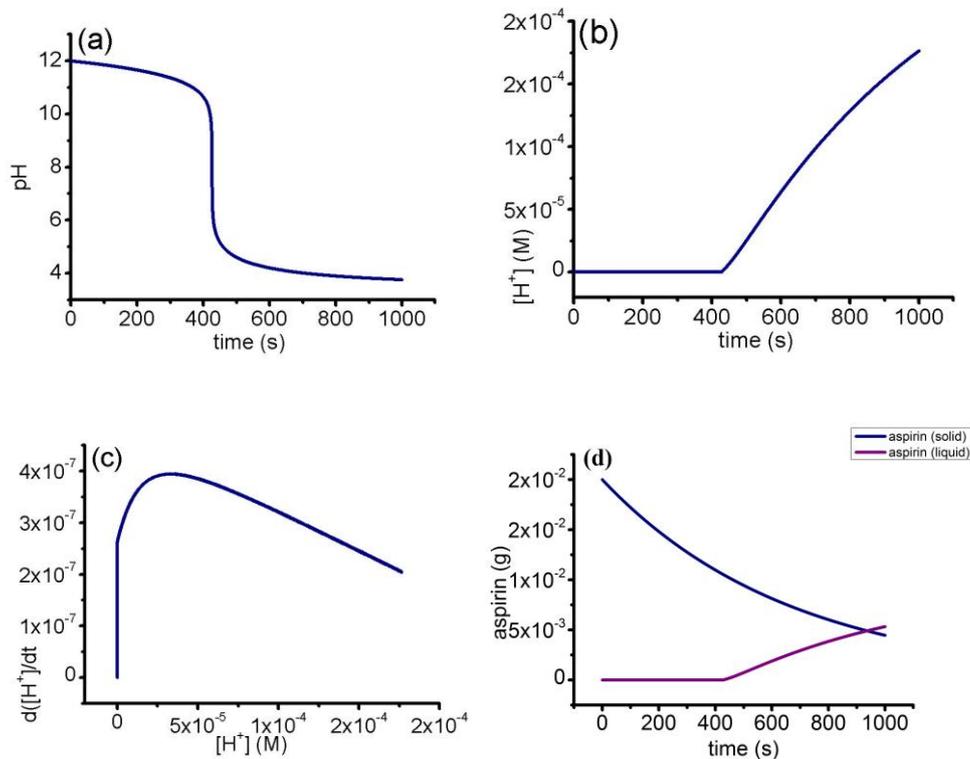
Figure 5.16 Modelling results of (a) pH, (b) concentration of H^+ changes in time and (c) reaction rate with respect to concentration of H^+, (d) aspirin profile in solid state and in solution with $m_{asp} = 0.020$ g, $pH_{init} = 12$
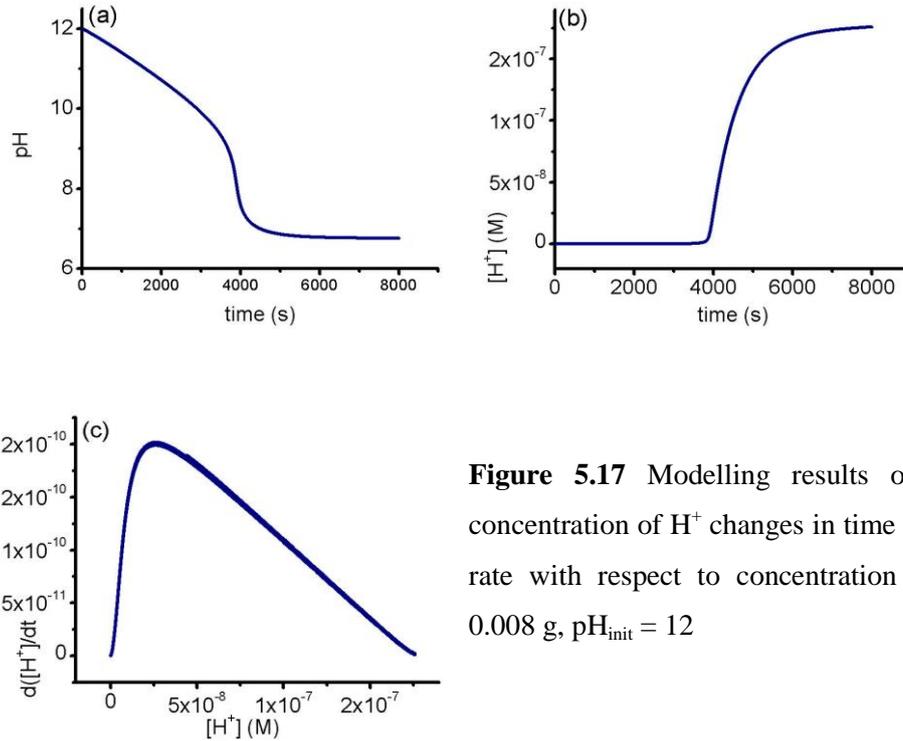
Figure 5.17 Modelling results of (a) pH, (b) concentration of H$^+$ changes in time and (c) reaction rate with respect to concentration of H$^+$, m_{asp} = 0.008 g, pH_{init} = 12

When $k_1 = 0$ s^{-1} (so that the acid catalytic step is "switched off") the pH-time plot still exhibits clock type behavior (Fig. 5.18a), and H$^+$ production looks similar to the case with catalysis (Fig. 5.16). The main difference is a sharper decrease of reaction rate after initial very fast production (Fig. 5.18 c) and slower transfer of aspirin into solution (Fig. 5.18 d).
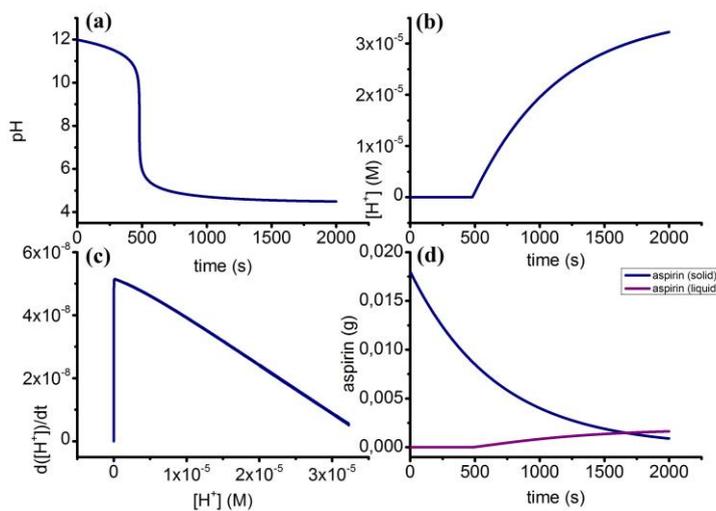
Figure 5.18 Modelling results of (a) pH, (b) concentration of H$^+$ changes in time and (c) reaction rate with respect to concentration of H$^+$, (d) aspirin profile in solid state and in solution, with m_{asp} = 0.020 g, pH_{init} = 12, $k_1 = 0$ s^{-1}

Additionally when $k_1 = 2.2 \times 10^4$ s^{-1} the behaviour of the system changes significantly. The pH-time plot exhibits a second step in the range of pH between 5.0 and 4.2 which causes a sharper increase of H$^+$ (Fig. 5.18 b) and a bell-shape rate dependence on acid concentration (Fig. 5.19 c) as well as changing the profile of aspirin dissolution into a sharp peak that takes place within this range of pH (Fig. 5.19 d).
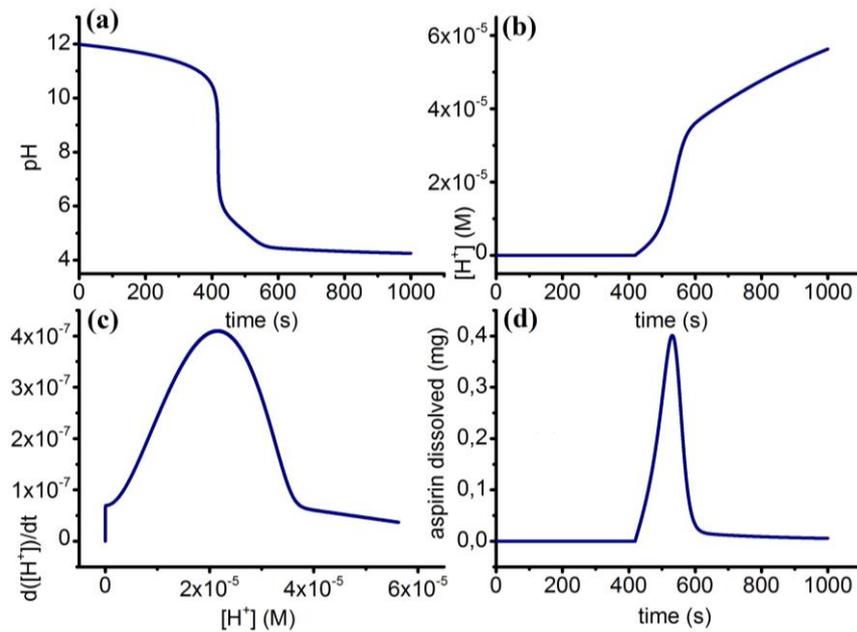
Figure 5.19 Modelling results of (a) pH, (b) concentration of H$^+$ changes in time and (c) reaction rate with respect to concentration of H$^+$, (d) aspirin in solution with $m_{asp} = 0.020$ g, pH$_{init} = 12$, $k_1 = 2.2 \times 10^4$ s^{-1}

It was also possible to construct clock times and final pH dependencies on initial mass of aspirin dissolve, shown in Fig. 5.20. Both of the dependencies show exponential character.
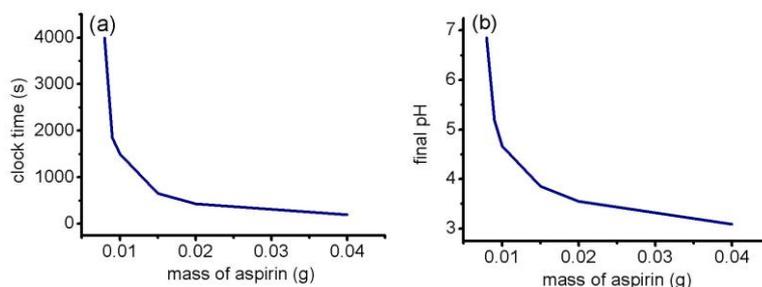
Figure 5.20 (a) Clock time, (b) final pH dependencies on initial mass of aspirin

5.5 Discussion

Our goal was to find the conditions for which autocatalysis might be observed in ester hydrolysis and therefore evidence of autocatalysis in new experimental systems. Up to now there are no literature reports of autocatalysis in an experimental study of acid-catalyzed ester hydrolysis.

The results in this chapter show a theoretical and experimental analysis of hydrolysis of organic compounds producing acid, namely open and cyclic esters (lactone). A pH clock is observed in the model with no catalysis due to consumption of initial OH^- present. It is clearly shown in the model that the addition of the acid catalytic step plays a major role in the kinetics and causes a much sharper production of acid and consumption of products with little effect on the pH-time plot (clock time). Additionally the second evidence of feedback in the system appears − bistability, that is not seen in the uncatalyzed case. When the acid equilibrium constant is increased, a second step of pH changes appears in the pH-time plot and although it is smaller in range than the first one, it contributes significantly to H^+ production and substrate consumption. Also the range of bistability becomes much wider than in the previous case. When additionally enzyme catalysis is considered the main effects are an increase in the region of bistability in the flow reactor with a decrease of consumption of the product, but with sharp maximum of reaction rate at the beginning of substrate consumption.

Experimental investigation allowed only trends in changes of pH to be shown. It is necessary to monitor changes in substrates to clearly see the presence of autocatalysis. However it is still possible to comment on the possibility of autocatalysis from the experimental data shown in the four examples of ester hydrolysis in this chapter. Two types of behaviour can be distinguished. In the first

one, seen in gluconolactone and p-nitrophenyl acetate hydrolysis, there is a direct decrease of pH below 500 s with a further slower production of H^+ that proceeds during next few thousands seconds. This H^+ curve looks very similar to the uncatalyzed model case, though the timescale in the simulations is much longer to show the clock behavior, which is not seen in the experiments. In the p-nitrophenyl acetate case the pH change is very small even in the presence of the enzyme as probably additional reactions are taking place between the product (acetic acid) and solvent (ethanol) which makes any autocatalysis impossible to be detected.

The second behaviour is visible in lactide hydrolysis where the H^+ production curve resembles the modeled acid-catalyzed case with increased dissociation constant: there are two pH jumps. Additionally when lactide hydrolysis is performed in the presence of the enzyme it is shown that only the second jump is influenced by the enzyme catalyst leaving the first pH decrease unchanged. No additional modelling has been done, though from literature[5] it is known that hydrolysis of polylactic acid exhibits rate acceleration in terms of both weight loss and pH after several days of the degradation process[6]. Following these observations it could be assumed that the cyclic dimer derivative of polylactic acid exhibits a similar rate acceleration due to the same mechanism on a shorter timescale.

In the case of aspirin hydrolysis we observed a pH clock and could not rule out feedback hence the model investigation. A full model of aspirin hydrolysis with consideration of all of the known steps including dissolution has been investigated. It has shown the same trends as in the experiments: several thousands seconds difference of clock times and several units of final pH difference caused by a decrease of the initial mass of aspirin in the order of 0.03 g, which is 1.67×10^{-4} moles change. The values of masses leading to certain clock times in simulations are lower

than in the experiment, which may be caused by imperfect dissolution and mixing in the real system. However there was no evidence of feedback in the model, probably as the acid catalysis is too weak, therefore the pH clock was seen because of consumption of initial OH⁻. When the rate of acid catalysis was increased in the model, the pH-time curve resembles the case of lactide with 2 pH jumps.

5.6 Conclusions

Models of ester hydrolysis show that in spite of the observation of pH clocks in all cases in a closed reactor, bistability is only seen in acid catalyzed and enzyme catalyzed cases in a flow reactor. In experiments, a pH clock is observed in the case of aspirin hydrolysis, but the model suggests that the acid catalysis does not play a role here. The most promising example of autocatalysis in the systems studied is the hydrolysis of lactide with two pH jumps rather than a characteristic pH clock, similar to the acid catalyzed model result, which should be the subject of further investigation.

5.7 References

(1)   Caplan, S. R.; Naparstek A.; Zabusky, N. J.: *Nature* **1973**, *245*, 364-366.

(2)   Quinn, D. M.: *Chem. Rev.* **1987**, *87*, 955-979.

(3)   Verma, S. K.; Ghosh, K. K.: *Colloid. Surface. A* **2010**, *368*, 154-158.

(4)   Edwards, L. J.: *Trans. Farad. Soc.* **1952**, *48*, 696-699.

(5)   Drumright, R. E.; Gruber, P. R.; Henton, D. E.: *Adv. Mater.* **2000**, *12*, 1841-1846.

(6)   Li, S. M.; McCarthy, S.: *Biomater.* **1999**, *20*, 35-44.

6. Self-propelled motion of aspirin crystals

6.1 Introduction

During investigation of the kinetics of hydrolysis of aspirin an intriguing behavior of self-motion of the crystals placed in unstirred water solution was noticed. This led to further investigation of this behavior in context of chemical locomotion. This field has been intensively investigated recently[1] in order to explain the motion of cells and organisms, such as bacteria[2], with possible applications for drug delivery. Similar type of behavior has been deeply studied in the case of camphor boats, where the driving force is the surface tension[3]. More recently self-motion has been designed in microparticles with asymmetric catalyst[4]. In this chapter a set of experimental results on the motion of aspirin crystals under different conditions is shown and a discussion on possible mechanisms of the motion is presented.

6.2 Experimental

The experiments were performed in 16 mL of water poured on a Petri Dish, with diameter $d = 5$ cm and height $h = 0.7$ cm. The Petri Dish was thermostated to 20 °C by CC3 Polystat. The pH of the solutions was adjusted by dilution of 0.1 M NaOH or 0.1 M H_2SO_4. Aspirin crystals were used as purchased from Sigma Aldrich of typical length $l = 1$ mm. Differences in shape were determined by pictures taken under a microscope (Olympic). Typically they had either a rod-like (Fig. 6.1 a), an oval (Fig. 6.1 b) or an asymmetrical (Fig. 6.1 c) shape. Additionally the mass of each crystal was measured on a microbalance (Sartorius). For each solution with a different pH the experiments were repeated at least 10 times.
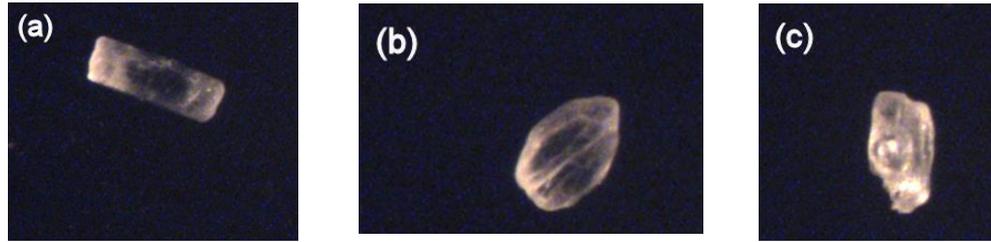
Figure 6.1 Illustration of different shapes of aspirin crystals with length (long axis): (a) rod-like (1.9 mm), (b) oval (1.5 mm), (c) asymmetrical (1.5 mm)

The movement of a particle was registered for 1000 of frames at 0, 5, 10, 15 and 20 mins counted from the moment of addition of a crystal to the solution. The pictures were taken every 0.02 s by a CCD camera coupled with the MATLAB program (The MathWorks, Natick, MA). Also the MATLAB program was used to track the particle and calculate the angular velocity. The code is attached in Appendix VI. The linear velocity was calculated for each time step and gave an average for 999 steps. The angular velocity in a single experiment was taken as an average value of slopes as shown in an example in Fig. 6.2. In all of the experiments only the slopes giving repeatable trend were used to calculate the average value, as in Fig. 6.2 for example 1-14 were taken for average and 15-16 were omitted. Then the average angular velocity was calculated for whole set of experiments under certain pH.
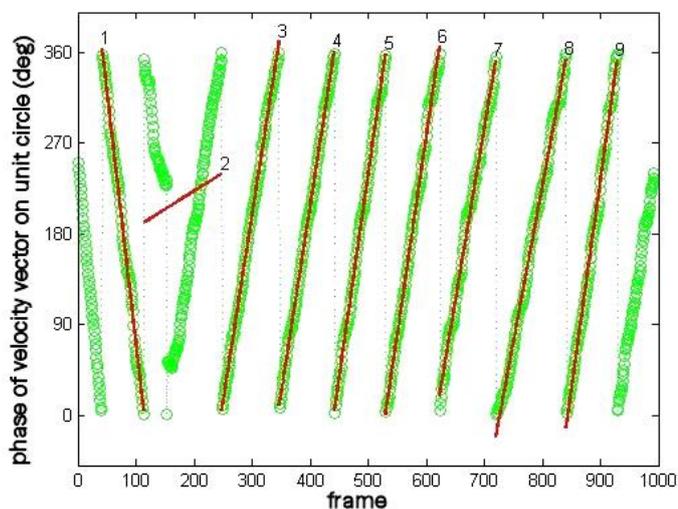
Figure 6.2 Example of fitting of slopes (red line) of phase of velocity vector per frame (green circles) which results in angular velocity (degrees per frame)

6.3 Results

6.3.1 Motion of a crystal

In a single run of 1000 frames, a particle may exhibit different types of motion and change linear and angular speed signifcantly. In Fig. 6.3 a typical example is shown, where the evolution of the color from dark blue through yellow to red represents the position of the particle from the first frame captured to the last (1000th). This example shows how the character of the motion evolves from an irregular pathway (0 – 300 frames) into small circles (300 – 500 frames) to finish with large radius of motion (1000 frames). It is clearly seen in Fig. 6.3 b that the critical change of linear velocity takes place with increasing radius significantly at ~870th frame. With angular motion analysis it is easy to see the turning point and change of direction of motion of the particle (~350 s), though slopes of the function of phase velocity vector change gradually, which may not be perfectly visible in Fig. 6.3 c.
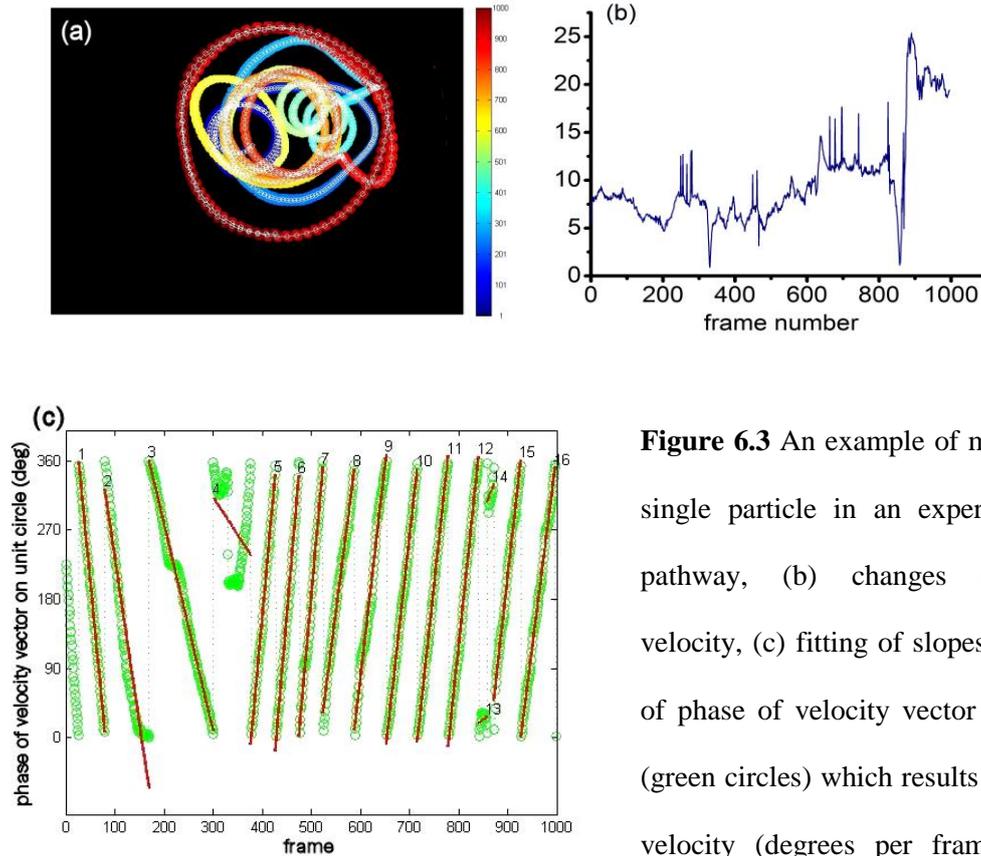
Figure 6.3 An example of motion of a single particle in an experiment. (a) pathway, (b) changes of linear velocity, (c) fitting of slopes (red line) of phase of velocity vector per frame (green circles) which results in angular velocity (degrees per frame) during 1000 frames taken, pH = 2.6

6.3.2 Specific types of motion

Although in the majority of experiments the nature of motion changes during the recording time, as shown in the section above, some of the results showed a repeatable trend in a single experiment. Three major types of motion could be distinguished: large radius cycle (periodic), small radius cycle (periodic), and translational motion coupled with small radius cycle (quasiperiodic).

In the first case, a big and regular reproducible pathway leads to high linear velocity values as shown in Fig. 6.4. The angular velocity in this example is 3.71 degrees per frame.
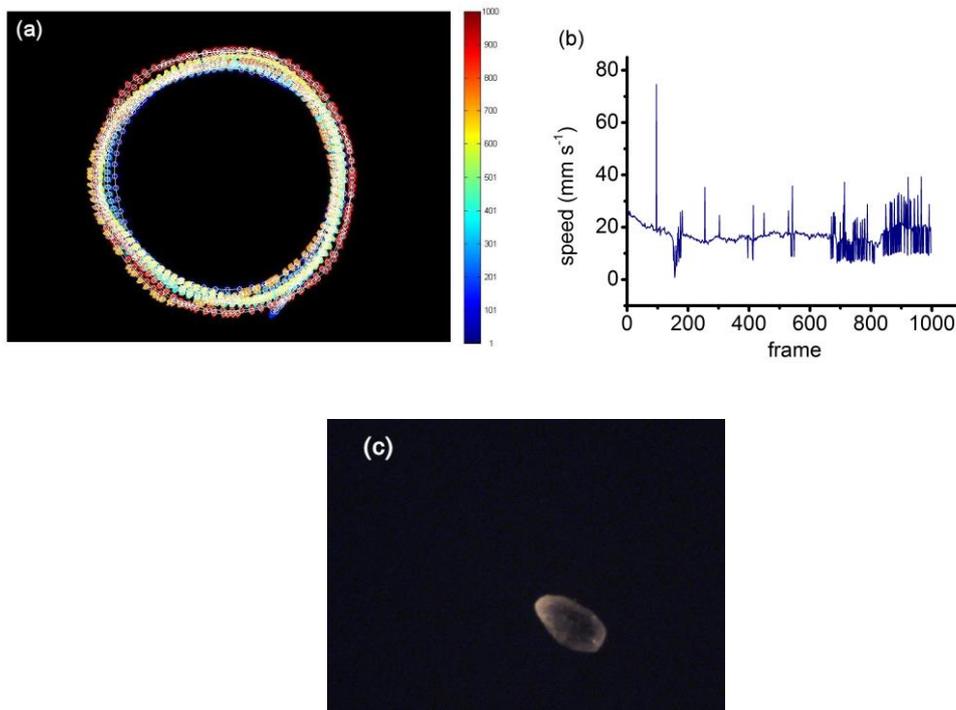
Figure 6.4 An example of a particle exhibiting circular motion with large radius. (a) the path of the motion (field of view = 50 x 67 mm^2), (b) linear velocity, and (c) shape of the particle (length = 1.6 mm), pH = 0.95

The second case is when the particle exhibits small-radius and low linear velocity as shown in Fig. 6.5. The linear velocity decreases by ~10 mm s^{-1}, though the angular velocity rises up to 29.3 degrees per frame.
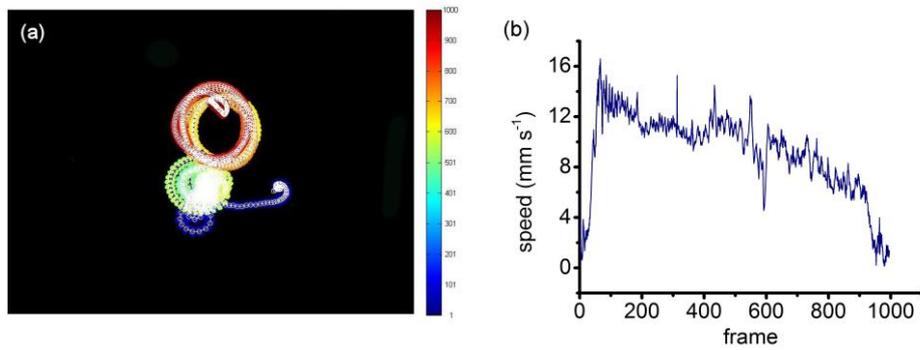
Figure 6.5 An example of a particle exhibiting small radius motion. (a) the path of the motion (field of view = 50 x 67 mm^2), (b) linear velocity, length of the particle = 1.6 mm, pH = 2.6

Another example of specific type of motion registered was a combination of translational and circular motion. The linear speed analysis shows in this case reproducible trends of spikes of slower and faster motion. Spikes can be as large as 55 mm s^{-1} as shown in Fig. 6.6 b. In this case it is almost impossible to calculate rotational velocity because of complex shape of the motion.
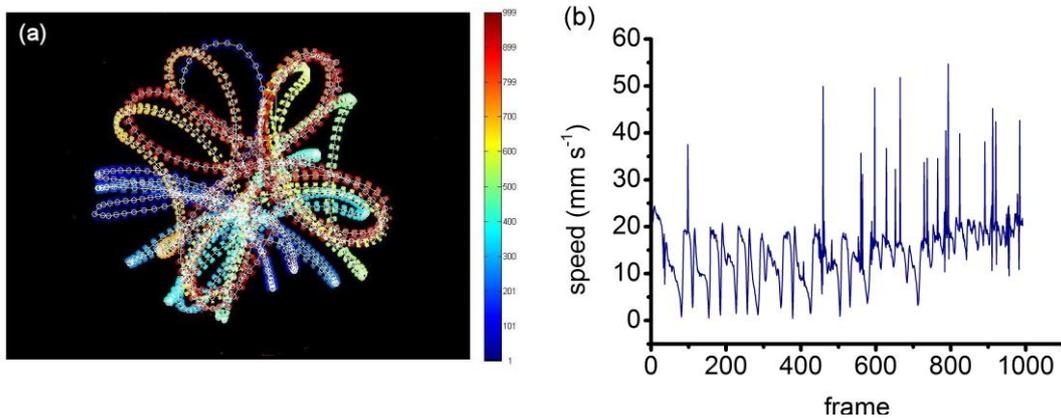
Figure 6.6 An example of a particle exhibiting circular motion with large radius. (a) the pathway captured (field of view = 50 x 67 mm^2), (b) linear velocity, length of the particle = 1.6 mm, pH = 7.1

Another specific example showing coupling of types of motion is the flower pattern with small-radius circular motion that is shown in Fig. 6.7 a.
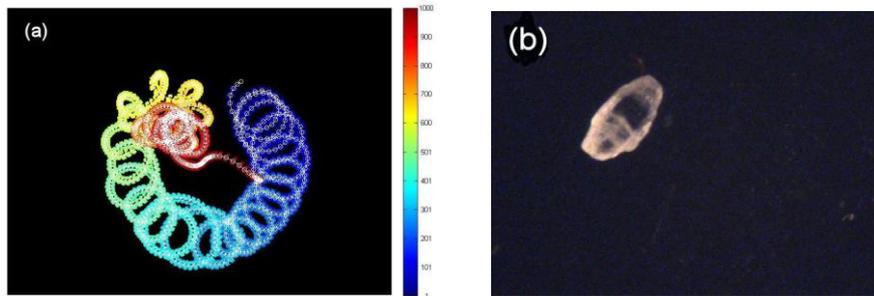
Figure 6.7 An example of a particle exhibiting coupled translational with small radius circular motion (a) the pathway captured (field of view = 50 x 67 mm^2), (b) shape of the particle, (length = 1.9 mm), pH = 5.44

6.3.3 Factors affecting motion

Several factors that could possibly affect velocity and trajectory of the motion, such as mass of the particle, pH of the solution or presence of other compounds, i.e. buffers or surfactants, were investigated. The first factor investigated was how angular velocity changes in time for set of particles with different masses. Fig. 6.8 shows that no significant trend can be defined from the experimental data. The velocity may increase significantly as in the most extreme case at 30 mins is 11 times bigger than at the beginning (m = 0.43 mg), but also for crystal with similar mass (m = 0.47 mg) the angular velocity may remain almost unchanged. There is also no definite linear increase of the angular velocity as in most of the cases particles have by turns faster and slower periods of motion.
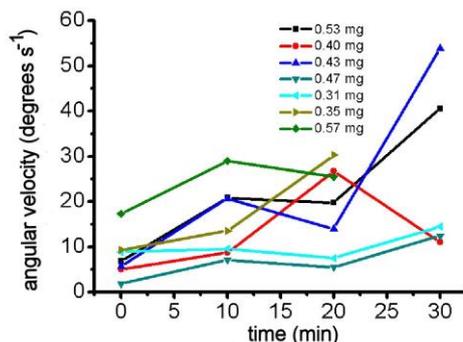
Figure 6.8 Angular velocity change in time for particles with different masses, pH = 5.44

In the same conditions mass – velocity plots were constructed. As shown in Fig. 6.9 there is a very weak correlation for first 1 min 30 s and even weaker for 10 min – 11 min 30 s, so it is impossible to define any influence of mass of a crystal on its angular velocity. Similar lack of correlation was found in solutions with lower and higher pH values.
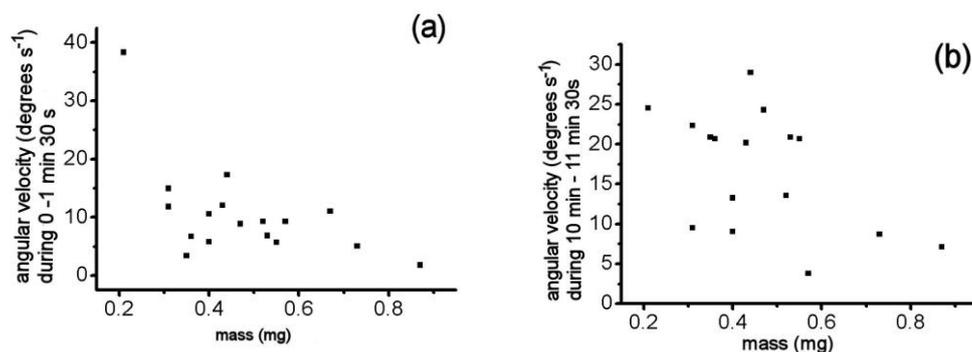
Figure 6.9 Angular velocity vs mass for first (a) and second (b) set of pictures in pH = 5.44

In more acidic solution although dissolution time was longer than in water, not enough of examples possible to be analysed in long term velocity measurements for pH = 0.85. There was a possibility to construct a plot of angular velocity change in time for pH = 2.60. Again no definite trend was found as the angular velocity changes alternately and the amplitude varies without definite dependence on the mass: for example the velocity of the crystal with m = 1.29 mg changes only of ~2.5 units, when for the crystal with slightly lower mass, m = 1.10 mg, changes 6 times.
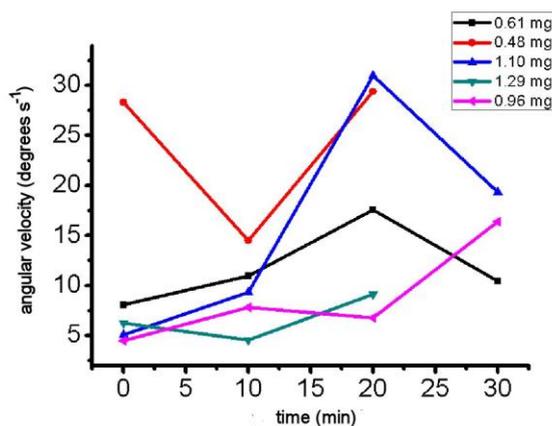
Figure 6.10 Angular velocity change in time for experiments in pH = 2.60

In pH > 10 almost no movement of particles and very fast dissolution takes place. For pH = 9.27 and pH = 7.11 dissolution of particles is faster than in lower pH values. Only two examples of long term measurements with increase of angular velocity in time could have been analyzed in long term measurements for pH = 7.11, that are shown in Fig. 6.11. In both cases the velocity did not change significantly for first 20 mins, but only exhibited significant increase after 30 mins.
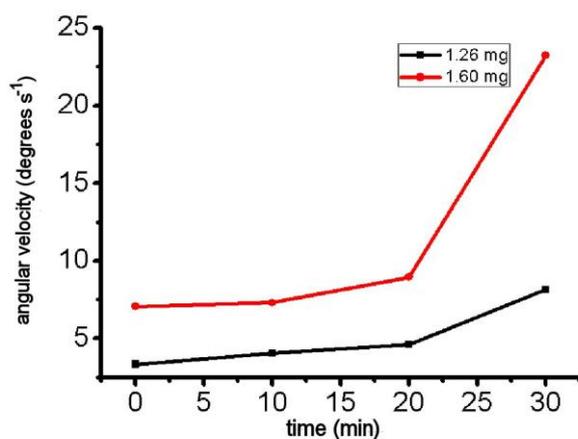
Figure 6.11 Angular velocity change in time for experiments in pH = 7.11 adjusted by dilution of NaOH

In order to analyze the trend of angular velocity depending on pH either maximum velocity (Fig. 6.12 a) or the average (Fig. 6.12 b) of all velocities for each set of particles for first 1 min 30 s were compared. The average angular velocity indicates that the crystals move the fastest in more acidic solution, than maximum angular velocity analysis states. The velocity decreases significantly already in slightly basic solution in both ways of analysis. Both of the approaches to compare the velocity can contain some errors caused by differences in shape of particles or average mass shifted in each set of 10 particles for experiments under different pHs that influenced the velocity significantly.
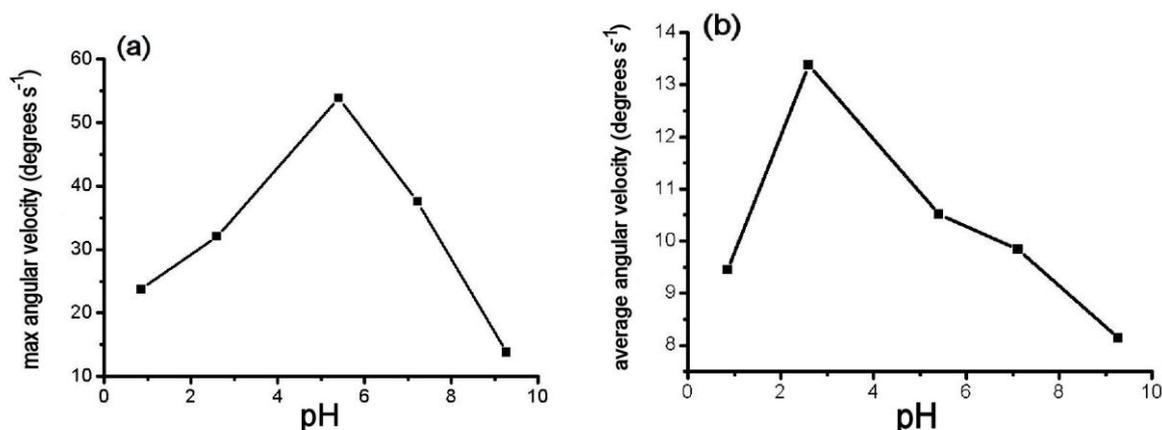
Figure 6.12 (a) Maximum angular velocity vs pH and (b) average angular velocity vs pH plots calculated for a set of 10 particles under each pH

Apart from pH several factors that might have influenced the motion of particles have been investigated. In order to determine whether buffering has an impact on the dynamic motion of aspirin crystal experiments in phosphate buffer (5 mL of 0.2 M KH_2PO_4 + 4.68 mL of 0.2 M NaOH diluted in 20 mL of H_2O, giving pH = 7.8) were performed. No movement of crystals was found in these conditions. When the buffer was diluted 10 times crystals started to exhibit jumping motion only.

When surfactant, such as CTAB powder, was added to the solution, crystals stop moving suddenly, although they have been moving continuously in the same solution before. When the solution is either saturated with aspirin (0.018 M) or contains large amount of sodium salicylate (0.31 M) the crystals hardly move at all. Addition of weak organic acid (acetic acid to make pH = 3.48), does not influence the motion significantly. The same situation is when ionic strength is increased by dissolution of NaCl to create 1.71 M solution.

6.3.4 Motion of other crystals

A number of solid compounds that have significantly similar or completely different chemical structure to aspirin were investigated in terms of their behaviour

in water. The results are presented in Table 6.1. The main similarity is that all of the compounds with benzene ring float and exhibit at least very little movements. From heterocycles only lactide floats and moves, ribose or gluconic acid lactone do not confirm this trend as they sink, though their solubility is much larger than in case of lactide which may play an important role in the behavior. Also all of the inorganic compounds sink and dissolve quickly as their solubility in water is much larger than the organic compounds investigated.

Further experiments in different pHs have been done also for sodium salicylate and salicylic acid. In both cases fastest dissolution takes place in water. For sodium salicylate in water and NaOH solution (pH = 12.04) wave motion of the surface and oil formation while dissolution of the powder is observed. In acid intense motion of parts of the surface is seen.

For salicylic acid expansion of the crystal powder and creation of network on the surface is noticed in all pHs. The closest interactions of crystals were in base and the fastest motion in water.

Table 6.1 Results of investigating behavior of crystals of other compounds on the surface of water

Compound	Structure	Behaviour	Solubility in water (g L^{-1})
Sodium oxalate		Sinks	3.7

Table 6.1(continuation) Results of investigating behavior of crystals of other compounds on the surface of water

Compound	Structure	Behaviour	Solubility in water (g L^{-1})
Bromomethoxy benzaldehyde		Floats, only very little moves	0.19
Benzoyl peroxide		Moves as esters, nice visible shape, a lot of circulation	0.03
2-bromo-5-methoxy benzoic acid		Floats, some synchronized moves	0.22
Benzamide		Floats, some synchronized moves	28.24
D-ribose		Sinks and dissolves	1000
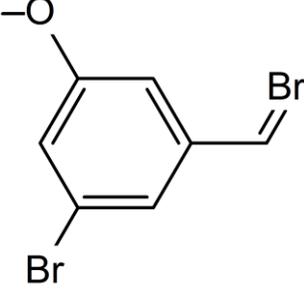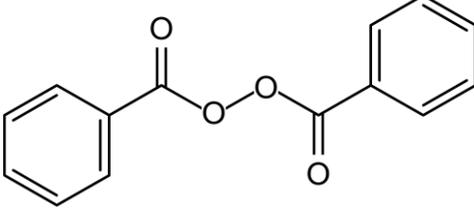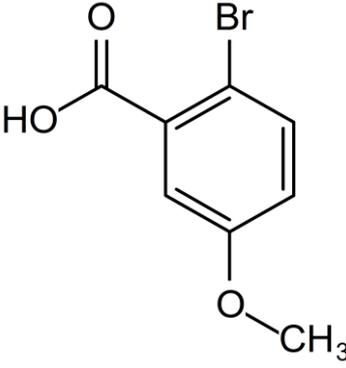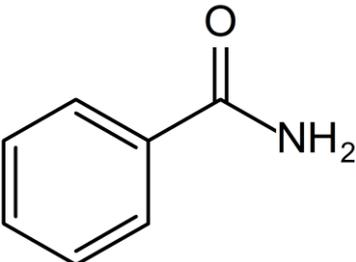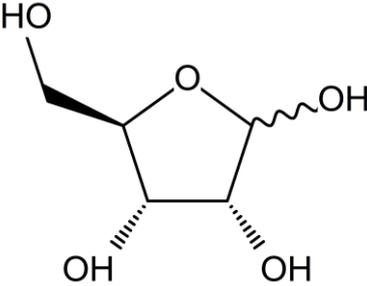
Table 6.1(continuation) Results of investigating behavior of crystals of other compounds on the surface of water

Compound	Structure	Behaviour	Solubility in water $(g\ L^{-1})$
4-bromobenzaldehyde		Moves as esters	1.5
D-galactose		Sinks and dissolves	1000
5-bromo-3-nitrosalicyl aldehyde		Floats, some synchronized moves	0.04
Methylhydroxy benzoate		Floats and moves	5.98
Lactide		Floats and moves	3.16
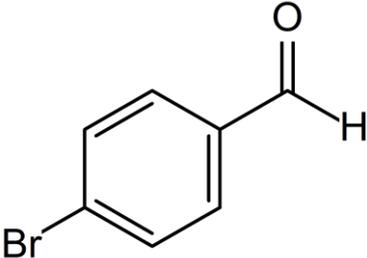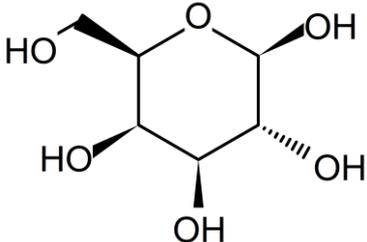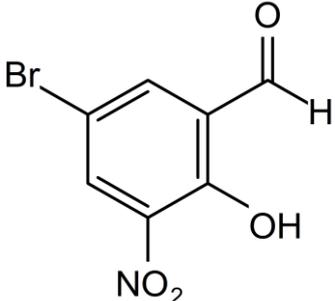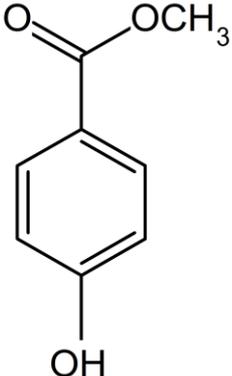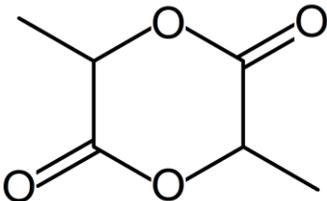
Table 6.1(continuation) Results of investigating behavior of crystals of other compounds on the surface of water

Compound	Structure	Behaviour	Solubility in water (g L^{-1})
Nitrophenyl acetate		Floats and moves	1.16
Salicylic acid		Floats and moves	3.81
Aspirin		Floats and moves	4.6
Arginine		Sinks	87.1
Gluconic acid lactone		Sinks	1000
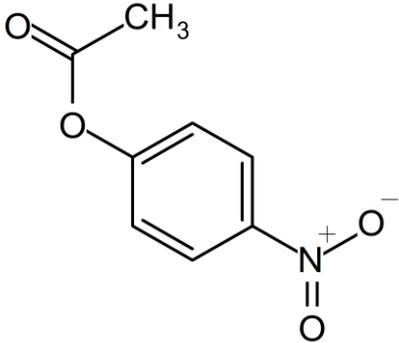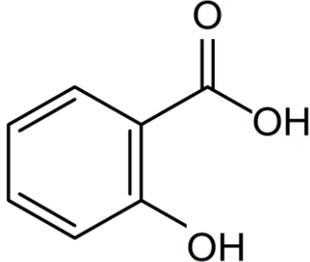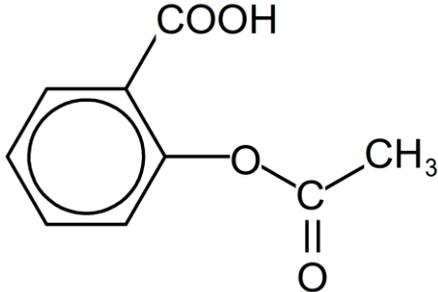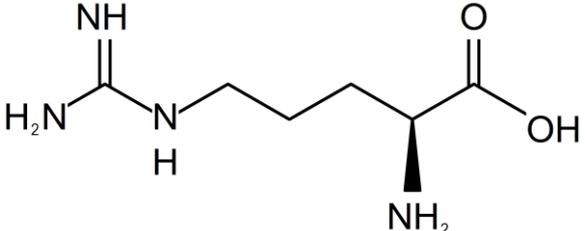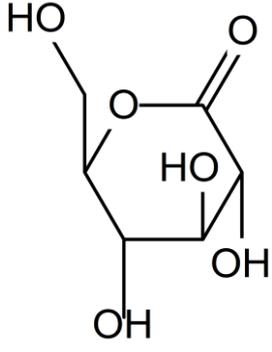
Table 6.1(continuation) Results of investigating behavior of crystals of other compounds on the surface of water

Compound	Structure	Behaviour	Solubility in water (g L^{-1})
Sodium salicylate		Floats and very quickly dissolves	110
All inorganic compounds		Sink and dissolve	>1000
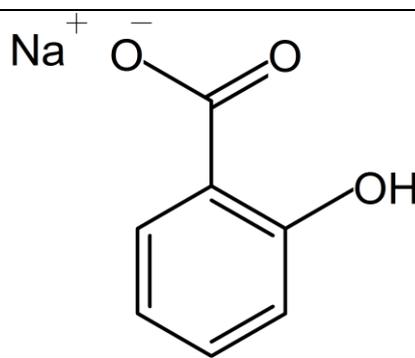
6.3.5 Multiple aspirin experiments

Additionally experiments investigating behavior with more than one aspirin crystal were performed. The results show that the nature of motion of more crystals is influenced by both pH and number of particles put in the system. In pH > 10 the movement is only to stick together already for two particles as shown in Fig.6.13.
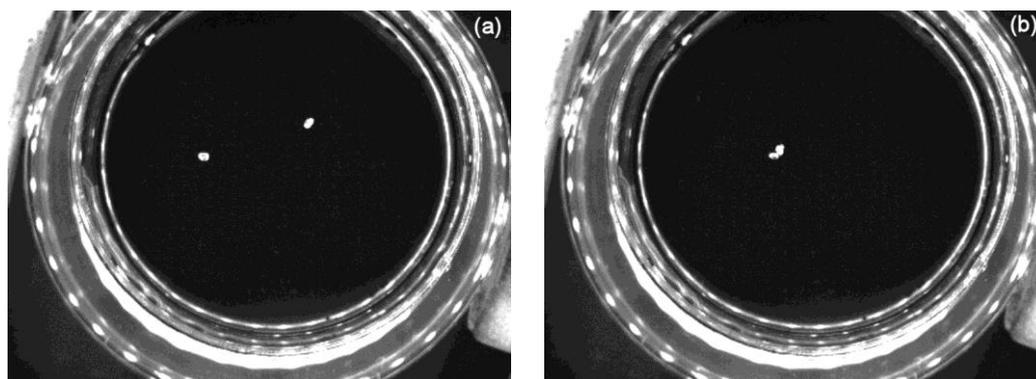
Figure 6.13 Behaviour of two particles in basic solution of pH = 11.84, (a) 0 s, (b) 78 s

In less basic solution, pH = 8.50, two or three particles move independently, though they do not stick together even in longer timescale. A cluster is created only for much bigger number of crystals as shown in Fig.6.14.
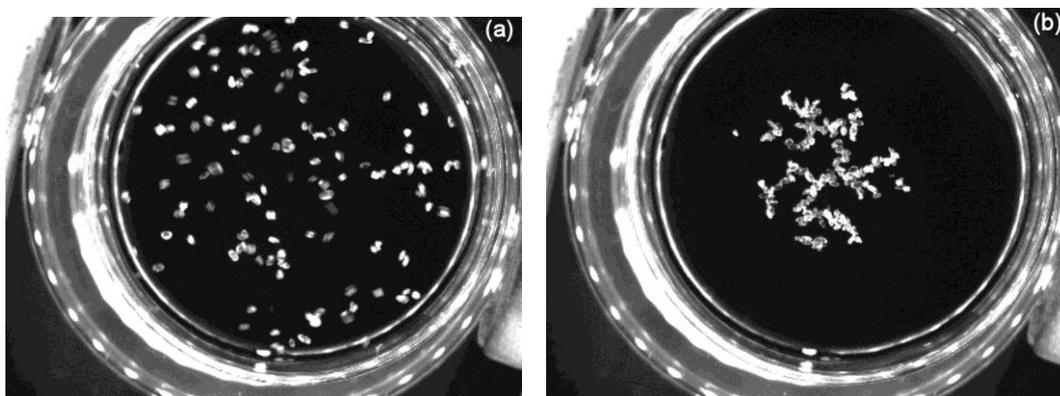
Figure 6.14 Creation of cluster of aspirin crystals in pH = 8.50, (a) 0 mins, (b) 5 mins

In neutral conditions, pH = 7.05, even with more than 50 crystals there is no definite attraction of all of the particles or one cluster created, but only smaller groups of crystals sticking together (as shown in Fig. 6.15) and ceasing of the motion in time.
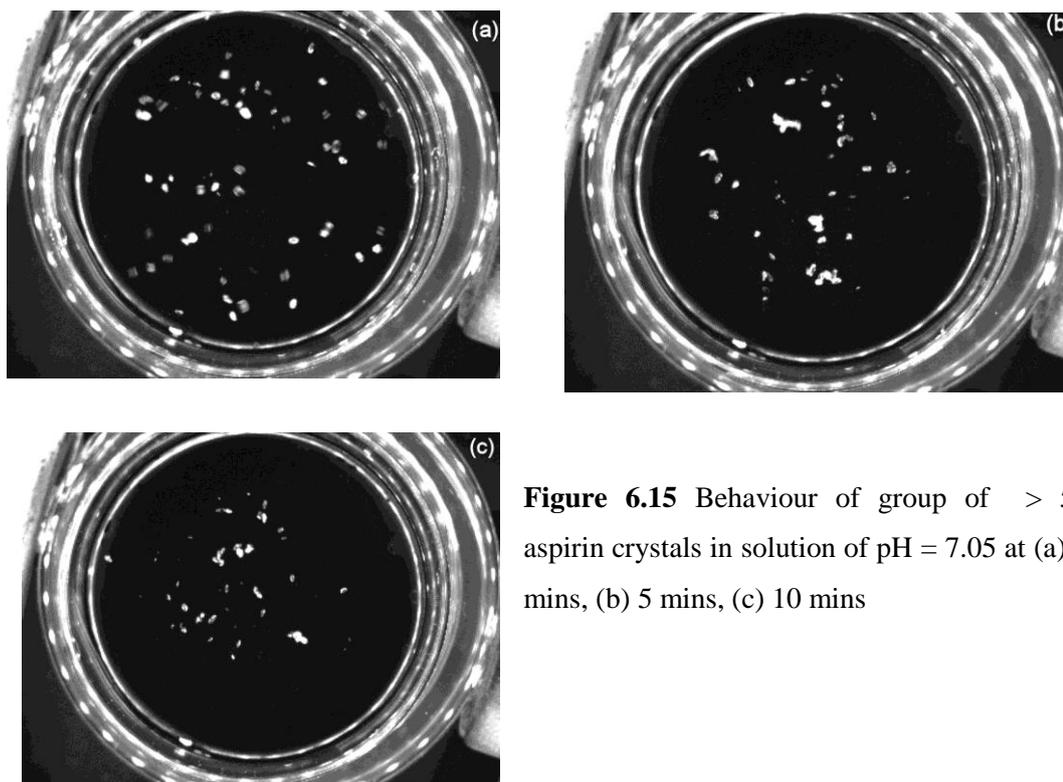
Figure 6.15 Behaviour of group of > 50 aspirin crystals in solution of pH = 7.05 at (a) 0 mins, (b) 5 mins, (c) 10 mins

In very acidic solution, pH = 0.72, fast motion is noticed in first minute after addition of aspirin crystals, than decrease of velocity until definite stoppage. For 15-20 particles the cluster was created from very first seconds to as shown in Fig. 6.16.
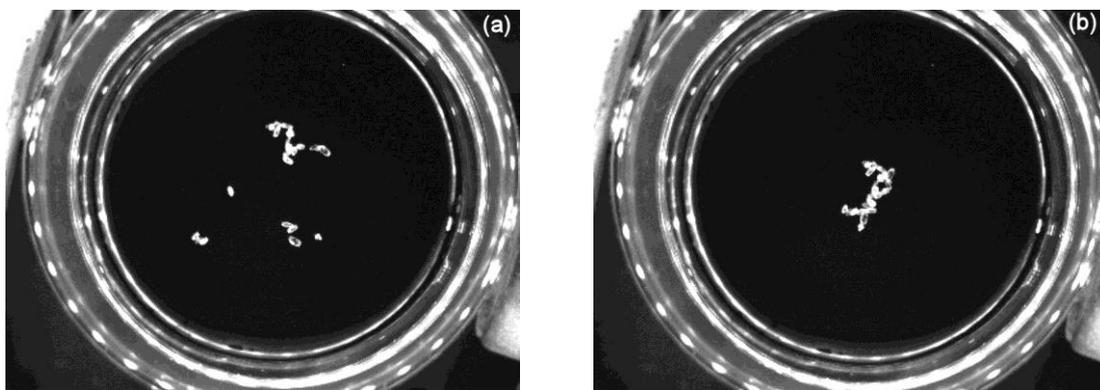
Figure 6.16 Behaviour of group of 17 aspirin crystals in solution of pH = 0.72 at (a) 5 s, (b) 70 s

6.4 Discussion

Self-motion of aspirin crystals during the period of dissolution and hydrolysis reaction has been shown together with differences in its nature depending on pH of the solution, size, shape and mass of the particle as well as modification of physicochemical properties of the solution such as ionic strength, surface tension or saturation. Other examples of similar compounds (esters with a benzene ring) show a similar kind of behavior in terms of floating and movement on the surface of water while being dissolved, though because of structure of solid aspirin supplied allowing to monitor and analyze the movement of a single particle dynamics as well as multiple particles interactions, the behavior of this ester was analyzed the most accurately.

From all of the types of chemical motors known before, such as: interfacial tension[5], diffusionophoresis[6], bioelectrochemical[7] or microcantilever[8] driven, an example of camphor boats[9] is the closest case to the aspirin propulsion. Main

similarities are the scale and the system where both compounds move as well as the range of velocities, both of them also can exhibit different modes of motion: rotational and translational.

The mechanism of camphor motion[10] involves firstly a dissolution of the solid and formation of a thin layer at the surrounding surface, secondly a gradient of the surface tension is created because of inhomogeneity in the surface density. Then the surface tension gradient induces an acceleration of the particle motion. Additionally as camphor particles evaporate the gradient in surface tension inducing the motion is maintained.

Since the motion of aspirin is similar to camphor, hydrolysis of aspirin should reduce the surface tension. This is probably due to the formation of hydrotropic products sodium salicylate or salicylic acid. Hydrotropes are compounds that contain hydrophobic aromatic or heteroaromatic ring and hydrophilic short chain or inorganic part[11,12]. The main difference between hydrotropes and surfactants is that because of difference in geometry of the hydrophobic part hydrotropes do not undergo selfaggregation in opposition to surfactants, where the hydrophobic chains aggregate spontaneously. However they are still known to lower the surface tension, it was experimentally proved that hydrotropes, such as sodium salicylate, toluenesulphonate, cumenesulphonate, xylenesulphonate or butyl monoglycol sulfate decrease the surface tension significantly (of even more than 50% in case of cumenesulphonate)[13]. Many of the crystals that exhibited motion are hydrotropes.

Although aspirin is denser than water (1.39 g cm^{-3}), when placed in water it floats on the surface (as shown in Fig. 6.17). This is connected with a structure of this compound (as well as all of the other esters that consist of an aromatic and

aliphatic parts), where the aromatic part from salicylic acid provides hydrophobic forces.
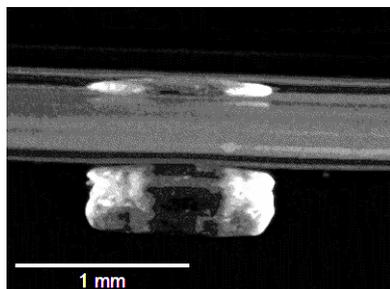
Figure 6.17 Side picture of an aspirin crystal floating at the surface of water

Additionally according to crystallographic investigation hydrophobicity[14,15] in aspirin crystals differ in each direction. For example in a schematic crystal shown in Fig. 6.18 hydrophobicity would increase as: $(001) > (100) > (011)$[14]. This would explain the complex motion depending on the crystal structure.

Figure 6.18 A schematic of crystal structure of aspirin
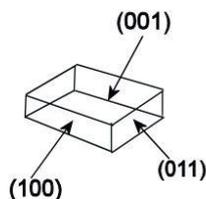
There are a few significant differences between camphor and aspirin. First of all, camphor is a ketone and while being put in water does not undergo a spontaneous hydrolysis, as aspirin does, but evaporates. Secondly the modes of motion in camphor can be easily influenced by changing the shape of the crystals[10], which directly allows to control the motion, whereas in aspirin the crystals have their natural anisotropy that drives the motion in different modes. This makes also collective motion of camphor to be predictable and possible to be controlled in different spatial set-ups[10,16].

6.5 Conclusions

A new chemical system exhibiting self-locomotion has been presented in this chapter. The analysis of the motion of a single particle has been done within a range of parameters in order to explain and control the motion of the crystals. The behaviour of other compunds within the same chemical family as well as from differents families has been investigated and compared. The collective behaviour of aspirin crystals under different pH conditions has been compared. The possible explanation of differences in motion and methods to control the behaviour can possibly be found in differences in crystal structure of aspirin and needs further experimental investigation.

6.6 References

(1)   Paxton, W. F.; Sundararajan, S.; Mallouk, T. E.; Sen, A.: *Angew. Chem.-Int. Edit.* **2006**, *45*, 5420-5429.

(2)   Budrene, E. O.; Berg, H. C.: *Nature* **1991**, *349*, 630-633.

(3)   Nakata, S.; Kirisaka, J.: *J. Phys. Chem. B* **2006**, *110*, 1856-1859.

(4)   Howse, J. R.; Jones, R. A. L.; Ryan, A. J.; Gough, T.; Vafabakhsh, R.; Golestanian, R.: *Phys. Rev. Lett.* **2007**, 048102-1 - 048102-4.

(5)   Paxton, W. F.; Kistler, K. C.; Olmeda, C. C.; Sen, A.; St Angelo, S. K.; Cao, Y. Y.; Mallouk, T. E.; Lammert, P. E.; Crespi, V. H.: *J. Am. Chem. Soc.* **2004**, *126*, 13424-13431.

(6)   Keh, H. J.; Wei, Y. K.: *Colloid Polym. Sci.* **2000**, *278*, 539-546.

(7)   Mano, N.; Heller, A.: *J. Am. Chem. Soc.* **2005**, *127*, 11574-11575.

(8)   Su, M.; Dravid, V. P.: *Nano Lett.* **2005**, *5*, 2023-2028.

(9)   Nakata, S.; Matsuo, K.: *Langmuir* **2005**, *21*, 982-984.

(10)   Nakata, S.; Iguchi, Y.; Ose, S.; Kuboyama, M.; Ishii, T.; Yoshikawa, K.: *Langmuir* **1997**, *13*, 4454-4458.

(11)   Subbarao, C. V.; Chakravarthy, I. P. K.; Bharadwaj, A.; Prasad, K.: *Chem. Eng. Technol.* **2012**, *35*, 225-237.

(12)   Eastoe, J.; Hatzopoulos, M. H.; Dowding, P. J.: *Soft Matter* **2011**, *7*, 5917-5925.

(13)   Balasubramanian, D.; Srinivas, V.; Gaikar, V. G.; Sharma, M. M.: *J. Phys. Chem.* **1989**, *93*, 3865-3870.

(14)   Heng, J. Y. Y.; Bismarck, A.; Lee, A. F.; Wilson, K.; Williams, D. R.: *J. Pharm. Sci.* **2007**, *96*, 2134-2144.

(15)   Olusanmi, D.; Roberts, K. J.; Ghadiri, M.; Ding, Y.: *Int. J. Pharm.* **2011**, *411*, 49-63.

(16)   Nakata, S.; Hayashima, Y.; Komoto, H.: *PCCP Phys. Chem. Chem. Phys.* **2000**, *2*, 2395-2399.

7. Future work

Each set of results introduced in this thesis can be built upon in future work. In chapter 2, the urea/urease reaction was shown to give pH clocks and bistability. Although the behaviour of the urea/urease reaction in a closed system was well characterized in a range of conditions, still the occasional low values of final pH could be explained either by monitoring of other species, such as CO_2 or NH_3, during the reaction, or more accurate characterization of the urease activity. A confirmation of the presence of autocatalysis in the urea/urease/sulphuric acid has been shown by bistability when the reaction was performed in a CSTR, however shifts of the range and pH of bistability have been noticed. More experimental runs are needed to find the average behavior. Also performing the reaction in a CSTR for a broader set of conditions will allow the regions of bistability, flow and thermodynamic states to be mapped out experimentally, and check the validity of the model.

Propagation of the pH fronts was shown in a range of conditions in the urea/urease reaction, which for high enzyme concentration was confirmed by the proposed model. For a lower urease concentration, fronts were not supported anymore, whereas the model still showed propagation. The model should be revised including non-mass action kinetics or with respect to sensitivity of the system to mixing effects. Additionally the boarder of the behavior where the fronts are supported/not supported should be investigated further experimentally.

When the acid was changed to weak one, the behavior of the system changed significantly especially in a CSTR, where oscillations have been observed. The attempts to model these oscillations have not mimicked the experimental results, so further investigation of the possible influence of noise or mixing effects on the system is needed with more sophisticated modeling tools. Also further mapping of the behavior under higher urease concentrations and investigation of the nature of the

oscillations on a longer timescale will contribute significantly to understanding of the system.

A group of compounds that undergo acid catalyzed hydrolysis and might show acid autocatalysis were investigated. The main experimental problem encountered was lack of solubility of the substrates in water which needs to be solved by performing the reaction at a water-oil interface. Also a confirmation of the autocatalysis present in these systems is needed by monitoring the time profiles of the reactant species by UV-VIS or different analytical tools.

Motion of aspirin crystals on the surface of water has been investigated under different conditions. The origin of the types of motion observed lies probably in the asymmetry of the crystal structure, especially the position of the hydrophobic parts of aspirin which needs a proper investigation by X-ray crystallography to establish the connection between types of motion and the structure of a certain particle. Additionally experiments with designed crystals with a regular structure would possibly allow control over the motion more accurately. A more detailed and quantitative analysis of the motion of group of aspirin crystals will give a useful contribution towards understanding the nature of the motion of the particles.

Appendix I Enzyme reaction mechanism and rate

The reaction is of the Michaelis-Menten type:

(1) $EH + U \rightleftharpoons EHU$

(2) $EHU \rightleftharpoons P + EH$

where EH is the active protonated form of the enzyme, U is the substrate, urea, EHU is the enzyme-substrate complex and P is $2NH_3$ and CO_2 formed via carbamic acid: NH_2COOH.[91] Applying the steady state approximation to EHU and setting $E_0 = E + EHU$ where $E_0 =$ the total enzyme concentration yields the Michaelis-Menten expression for the rate:

$$V = \frac{V_{max} U}{K_M + U}$$

where the maximum rate $V_{max} = k_7 E_0$ and the Michaelis constant $K_M = (k_{-6} + k_7)/k_6$.

pH dependence of the reaction

The reaction shows a typical bell-shaped curve which can be explained by the presence of 2 acid equilibria giving inactive forms of enzyme:

(3) $EH \rightleftharpoons E^- + H^+$ $\quad\quad\quad\quad\quad\quad\quad$ K_{e2} pK2 = 8.7

(4) $EH_2^+ \rightleftharpoons EH + H^+$ $\quad\quad\quad\quad\quad\quad\quad$ K_{e1} pK1 = 5.3
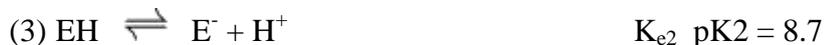
and inactive forms of enzyme-substrate complex:

(5) $EHU \rightleftharpoons EU^- + H^+$ $\quad\quad\quad\quad\quad\quad\quad$ K_{es2}

(6) $EH_2U \rightleftharpoons EHU + H^+$ $\quad\quad\quad\quad\quad\quad\quad$ K_{es1}

It is found that K_M changes little with acid concentration implying that $K_{e1} = K_{es1}$ and $K_{e2} = K_{es2}$ (i.e. the protonation equilibria do not change in the presence of the substrate). Taking into consideration equilibria (9 – 12), the rate expression becomes:

$$V = \frac{V_{max} U}{(K_M + U)\left(1 + \dfrac{K_{es2}}{H^+} + \dfrac{H^+}{K_{es1}}\right)}$$

Product inhibition

The ammonium ion is found to inhibit the reaction by non-competive mechanism[91]:

(7) $EHPS \rightleftharpoons EHS + P$ $\qquad$ K_P

(8) $EHP \rightleftharpoons EH + P$ $\qquad$ K_p

This equilibrium may be incorporated into the Michaelis rate expression to give:

$$V = \frac{V_{max} U}{(K_M + U)\left(1 + \dfrac{P}{K_p}\right)}$$

Substrate inhibition

The urea inhibits the reaction by an uncompetitive mechanism[91]:

(9) $EHS_2 \rightleftharpoons EHS + S$ $\qquad$ K_s
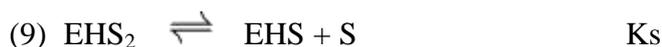
This equilibrium may be incorporated into the rate expression to give:

$$V = \frac{V_{max} U}{(K_M + U\left(1 + \dfrac{U}{K_U}\right))}$$

Combining:

$$v_0 = \frac{V_{max} U}{\left(K_M + U(1 + \dfrac{U}{K_U})\right)\left(1 + \dfrac{P}{K_P}\right)\left(1 + \dfrac{K_{es2}}{[H^+]} + \dfrac{[H^+]}{K_{es1}}\right)}$$

Appendix II Ode file for XPPaut

Developed by Annette Taylor

```
#urea-urease reaction
f(U,H,NHf)=-Vm*U/((KM*(1+Ke2/H+H/Ke1)+U*(1+U/KS))*(1+NHf/Kp))
g(U,H,NHf,NHt)=2*Vm*U/((KM*(1+Ke2/H+H/Ke1)+U*(1+U/KS))*(1+NHf/
Kp))+k2*NHf-k2r*NHt*H
h(NHt,H,NHf)=-k2*NHf+k2r*NHt*H
k(U,H,NHf,COt,HCO)=Vm*U/((KM*(1+Ke2/H+H/Ke1)+U*(1+U/KS))*(1+NH
f/Kp))-k3*COt+k3r*HCO*H
l(H,COt,COe,HCO)=k3*COt-k3r*HCO*H-k4*HCO+k4r*COe*H
m(HCO,H,COe)=k4*HCO-k4r*COe*H
n(H,NHf,NHt,COt,COe,HCO,OH,HA,A)=k2*NHf-k2r*NHt*H-
k3r*H*HCO+k3*COt+k4*HCO-k4r*COe*H+k5-k5r*H*OH+k6*HA-k6r*A*H
o(OH,H)=k5-k5r*H*OH
p(H,HA,A)=-k6*HA+k6r*A*H
q(H,HA,A)=k6*HA-k6r*A*H

#parameters
par Vm=1.3e-4,KM=0.003,KS=3,KP=0.002,Ke1=5e-6,Ke2=2e-9, k2=24,
k2r=4.3E10,k3=0.037,k3r=7.9e4, k4=2.8,k4r=5e10,k5=1e-3,
k5r=1e11, k6=1.2e9,k6r=1e11

# spatial parameters
par r=0.2,Dx=2.0e-3,Doh=5e-3,Dh=9e-3

# initial data
init U[1..2]=0.010
init NHt[1..2]=0.012
init NHf[1..2]=0.022
init COt[1..2]=0.00028
init HCO[1..2]=0.016
init COe[1..2]=0.0009
init H[1..2]=9.9e-10
init OH[1..2]=1.01e-5
init HA[1..2]=1.4e-10
init A[1..2]=0.0017

init U[3..100]=0.03
init NHt[3..100]=0
init NHf[3..100]=0
init COt[3..100]=0
init HCO[3..100]=0
init COe[3..100]=0
init H[3..100]=2e-3
init OH[3..100]=1e-14/2e-3
init HA[3..100]=2e-3
init A[3..100]=0

#boundary conditions
U0=U1
NHt0=NHt1
NHf0=NHf1
COt0=COt1
```

```
HCO0=HCO1
COe0=COe1
H0=H1
OH0=OH1
HA0=HA1
A0=A1
U101=U100
NHt101=NHt100
NHf101=NHf100
COt101=COt100
HCO101=HCO100
COe101=COe100
H101=H100
OH101=OH100
HA101=HA100
A101=A100

#reaction-diffusion
%[1..100]
U[j]'=f(U[j],H[j],NHf[j])+Dx*(U[j+1]-2*U[j]+U[j-1])/(r*r)
NHt[j]'=g(U[j],H[j],NHf[j],NHt[j])+Dx*(NHt[j+1]-
2*NHt[j]+NHt[j-1])/(r*r)
NHf[j]'=h(NHt[j],H[j],NHf[j])+Dx*(NHf[j+1]-2*NHf[j]+NHf[j-
1])/(r*r)
COt[j]'=k(U[j],H[j],NHf[j],COt[j],HCO[j])+Dx*(COt[j+1]-
2*COt[j]+COt[j-1])/(r*r)
HCO[j]'=l(H[j],COt[j],COe[j],HCO[j])+Dx*(HCO[j+1]-
2*HCO[j]+HCO[j-1])/(r*r)
COe[j]'=m(HCO[j],H[j],COe[j])+Dx*(COe[j+1]-2*COe[j]+COe[j-
1])/(r*r)
H[j]'=n(H[j],NHf[j],NHt[j],COt[j],COe[j],HCO[j],OH[j],HA[j],A[
j])+Dh*(H[j+1]-2*H[j]+H[j-1])/(r*r)
OH[j]'=o(H[j],OH[j])+Doh*(OH[j+1]-2*OH[j]+OH[j-1])/(r*r)
HA[j]'=p(H[j],HA[j],A[j])+Dx*(HA[j+1]-2*HA[j]+HA[j-1])/(r*r)
A[j]'=q(H[j],HA[j],A[j])+Dx*(A[j+1]-2*A[j]+A[j-1])/(r*r)
%

@ total=1000,dt=1,tol=1e-14, atol=1e-14,
meth=cvode,bandup=10,bandlo=10
@ xplot=t,yplot=OH,xhi=1000,ylo=1e-8,yhi=1e-3
@ maxstor=100000
#
done
```

Appendix III Matlab code front speed

Developed by Tamas Bansagi

```
close all
clear all
%===============================PARAMETERS
==============================
rfn='Y:\CHM\Physical\AFT\MMW\ureapetri60\ureapetri60_'; % root of file
names
```

```
bg=1;       % background file
fi=50;       % first file
li=200;      % last file
mf=5;       % median filter radius
smf=10;     % smoothing factor for 1D cut
d=10;       % range of diff
sp_res=13.2; % pixel/mm because 735 pixel corresponds to 50 mm
dt=5;       % time elapsed between consecutive frames (in seconds)
dxf=3;       % increment for space axis in figure 2 (in mm)
nc=9;        % number of cuts: 4,9,16 etc
ir=30;      % radius of the omitted area around origin
%=======================================================================
====
t=fi*dt:dt:li*dt;
fc=sqrt(nc);
af=360/2/pi;
ar=linspace(0,(360-360/nc),nc)/af;
filename=[rfn,num2str(bg),'.jpg'];
bg=imread(filename);
bg2=medfilt2(bg(:,:,2), [mf mf]);
filename1=[rfn,num2str(fi),'.jpg'];
i=imread(filename1);
i_fi=i(:,:,2);
filename2=[rfn,num2str(li),'.jpg'];
i=imread(filename2);
i_li=i(:,:,2);
i_si=uint8((double(i_fi)+double(i_li))/2);
imshow(i_si,'Border','tight');
text(1,10,[filename1,' + ',filename2],'BackgroundColor',[1 1 1]);
[xl,yl] = ginput(2); length_of_cut=pdist([xl yl]);
xp=round(xl(1)+cos(ar)*length_of_cut);
yp=round(yl(1)+sin(ar)*length_of_cut);
xps=round(xl(1)+cos(ar)*ir);
yps=round(yl(1)+sin(ar)*ir);
xpt=round(xl(1)+cos(ar)*(length_of_cut+10));
ypt=round(yl(1)+sin(ar)*(length_of_cut+10));
cl=length(improfile(i,[xps(1) xp(1)],[yps(1) yp(1)])); % length in
pixels for length correction of oblique cuts for p=1:nc
    line([xps(p) xp(p)],[yps(p) yp(p)],'LineWidth',2,'Color',[0 0 0]);
    hold on
    quiver(xps(p),yps(p),(xp(p)-xps(p)),(yp(p)-
yps(p)),0.55,'MaxHeadSize',1/cl*100,'LineWidth',2,'Color',[0 0 0])

text(xpt(p),ypt(p),num2str(p),'HorizontalAlignment','Center','Color',[1
1 1]) end hold off for n=fi:li
    filename=[rfn,num2str(n),'.jpg'];
    i=imread(filename);
    i_f=medfilt2(i(:,:,2),[mf mf]);
    ima(n-fi+1,:,:)=double(i_f)-double(bg2);
end
figure
for ang=1:nc
    subplot(fc,fc,ang)
    for n=fi:li
        c=improfile(squeeze(ima(n-fi+1,:,:)),[xps(ang)
xp(ang)],[yps(ang) yp(ang)],'bicubic');
```

```
        csm=smooth(c,smf);
        ds=round(d/2);
        for x=1:length(c)-d
            dcsm(x+ds)=csm(x+d)-csm(x);
        end
%       plot(c,'-k')
%       hold on
%       plot(csm,'-r')
%       hold on
%       plot(dcsm,'-ob')
%       hold on
        max_dcsm=max(dcsm);
        dcsm(dcsm < max_dcsm) = 0;
        fp=find(dcsm);
        frpo(n-fi+1)=mean(fp);
        dcsm_frpo(n-fi+1)=mean(dcsm(fp));
%       plot(frpo(n-fi+1),dcsm_frpo(n-fi+1),'og')
    end

    lc=length(c);
    real_frpo=frpo/sp_res*cl/lc;
    fpifpf(ang,:)=[real_frpo(1) real_frpo(length(real_frpo))];
    plot(t,real_frpo,'ok')
    xlabel('Time (sec)')
    ylabel('Space (mm)')
    [fit_lin_par, stat] = polyfit(t,real_frpo,1);
    lin = fit_lin_par(1).*t+fit_lin_par(2);
    slope(ang)=fit_lin_par(1)*60;
    hold on
    set(gcf,'Color','white')
    plot(t, lin,'-r','LineWidth',2);
    xtick=get(gca, 'XTick');
    ytick=get(gca, 'YTick');
    xtl=length(xtick);
    ytl=length(ytick);
    text_str=['\bf',num2str(ang),'\rm  slope =
',num2str(fit_lin_par(1)*60)];
    text((xtick(1)+xtick(2))/2,(ytick(ytl)+ytick(ytl-
1))/2,text_str,'HorizontalAlignment','Left');
    axis([xtick(1) xtick(xtl) ytick(1) ytick(ytl)]);
    % ===== MS Excel output (comment out if not needed)
==================
    data_matrix(1,1:3)={'time','front position','fitted front
position';};
    for dat=1:li-fi+1
    data_matrix(dat+1,1:3)={t(dat),real_frpo(dat),lin(dat);};
    end
    %
========================================================================
    filename_xls=[rfn,'rad_',num2str(ang),'.xls'];
    xlswrite(filename_xls, data_matrix);
    clear max_dcsm dcsm frpo dcsm_frpo fp c csm real_frpo xtick ytick
data_matrix
    hold off
end
set(gcf,'Color','white')
```

```
figure
subplot(1,2,1)
plot(slope,'ok')
msl=mean(slope);
axis([0 nc+1 min(slope)*0.9 max(slope)*1.1]) hold on
line([0 nc+1],[msl msl],'LineWidth',2,'Color','red');
xlabel('Cut')
ylabel('Front velocity (mm/min)')
set(gcf,'Color','white')
std_err_sl=std(slope)/sqrt(nc);
text((nc+1)/2,min(slope)*0.95,['\fontsize{9}v_{fr} = ',num2str(msl),'
\pm ',  num2str(std_err_sl,'% 10.5f'),'
mm/min'],'HorizontalAlignment','Center');
legend('fr. vel. along cut','avg. fr vel.')
subplot(1,2,2)
axis([0 nc+1 0 max(max(fpifpf))*1.1])
mfp=mean(fpifpf(:,2)-fpifpf(:,1));
for ang=1:nc
line([ang ang],[fpifpf(ang,1)
fpifpf(ang,2)],'LineWidth',2,'Color','green');
line([ang+0.15 ang+0.15],[0 fpifpf(ang,2)-
fpifpf(ang,1)],'LineWidth',2,'Color','blue');
line([ang+0.3 ang+0.3],[mfp fpifpf(ang,2)-
fpifpf(ang,1)],'LineWidth',2,'Color','red');
line([0 nc+1],[mfp mfp],'LineWidth',2,'Color','red');
end
hold on
plot(1+0.3:nc+0.3,fpifpf(:,2)-fpifpf(:,1),':r')
legend('fr. position','fr. range','fr. range dev.') grid on
xlabel('Cut')
ylabel('initial and final front positions (mm)')
set(gcf,'Color','white')
```

Appendix IV XPP and C models with noise

XPP model with added noise:
Developed by Annette Taylor

```
#urea-urease reaction: rate equations
wiener w
U'=-
k8*E*U/((1+d*Kes2/H+d*H/Kes1)*(0.003+U*(1+b*U/3))*(1+c*NH4/0.002))+k
0*(U0-U)+g*w
NH3'=2*k8*E*U/((1+d*Kes2/H+d*H/Kes1)*(0.003+U*(1+b*U/3))*(1+c*NH4/0.
002))+k2*NH4-c*NH3*H-k0*NH3+g*w
NH4'=-k2*NH4+c*NH3*H-k0*NH4
CO2'=k8*E*U/((1+d*Kes2/H+d*H/Kes1)*(0.003+U*(1+b*U/3))*(1+c*NH4/0.00
2))-k0*CO2+g*w
H'=k2*NH4-c*NH3*H+k6*HA-k6r*H*A+k0*(H0-H)
HA'=-k6*HA+k6r*A*H+k0*(HA0-HA)
A'=k6*HA-k6r*A*H-k0*A

aux pH=-log(H)/log(10)
#parameters
par k2=1e-9, k6=1,k6r=1e-3
par k8=3.7e-6,E=1.34,Kes1=5e-6,Kes2=2e-9,d=1,b=1, c=1, g=0
```

```
par k0=0,U0=0.005,H0=1e-4,HA0=1e-4


#initial conditions
init U=0.005,NH3=0,NH4=0,CO2=0,H=1e-4,HA=1e-4,A=0


#numerical stuff
@ total=20000,dt=0.1,tol=1e-12, atol=1e-8, meth=euler
@ xplot=t,yplot=pH,xhi=20000,ylo=1,yhi=14
@ maxstor=10000000
Done
```

C model with added noise:
Developed by Annette Taylor

```
    /****************************/
   //  Urea-Urease reaction

#include <stdio.h>
#include <stdlib.h>
#include <math.h>

#define max(a,b) ((a)>(b)?(a):(b))
#define IA 16807
#define IM 2147483647
#define AM (1.0/IM)
#define IQ 127773
#define IR 2836
#define NTAB 32
#define NDIV (1+(IM-1)/NTAB)
#define EPS 1.2e-7
#define RNMX (1.0-EPS)

// noise
float gasdev(long *idum);
long seed=-101;
double r; // random number
double l; // eq 2.128
double g=0;  // amplitude

/*****************/
//parameters
double Ui=5e-3;
double NH3i=0.0;
double NH4i=0.0;
double CO2i=0.0;
double HCO3i=0.0;
double CO3i=0.0;
double Hi=1e-7;
double OHi=1e-7;
double HAi=5.83e-4;
double Ai=0.0;

double k0;   //flow rate
```

```c
double k0step=0.001;   // step size increase in k0
double k0loop=10;     // total number of steps in k0
double k8=3.7e-6;
double k2=24;
double k2r=4.3e10;
double k3=0.037;
double k3r=7.9e4;
double k4=2.8;
double k4r=5e10;
double k5=1e-3;
double k5r=1e11;
double k6=7.8e5;
double k6r=4.5e10;
double E=1.34;
double KM=0.003;
double Ks=3;
double Kp=0.002;
double Kes1=5e-6;
double Kes2=2e-9;

double dt=1e-7;   // time step
long total=1000;  //total time in s
long nstep=1e7;  // number of timesteps in 1 s
long istep;
int icount=0;
int iicount=0;
int time;  //time in s
/**********************************/
// variables

double U;
double NH3;
double NH4;
double CO2;
double HCO3;
double CO3;
double H;
double OH;
double HA;
double A;
double funcHi;

//data files

FILE *out;
FILE *out2;

/****************************************************/


void report_parameters ( void )
{
 printf ( "dt=%f\n", dt );
 printf ( "U=%f", Ui );
}
```

```
/**************************************************/

void initial_conditions(void)

{
         U=Ui;
      NH3=NH3i;
      NH4=NH4i;
      CO2=CO2i;
      HCO3=HCO3i;
      CO3=CO3i;
      H=Hi;
      OH=OHi;
      HA=HAi;
      A=Ai;

}

/*******************************************/

void reaction ( )
{
 double  funcUi, funcNH3i, funcNH4i, funcCO2i, funcHCO3i, funcCO3i, funcOHi;
 double funcHAi, funcAi;
 double  funcUb, funcNH3b, funcNH4b, funcCO2b, funcHCO3b, funcCO3b, funcOHb;
 double funcHAb, funcAb, funcHb;

  r = gasdev(&seed);
  l = sqrt(dt)*r*g;

funcHi=H+dt*(k2*NH4-k2r*NH3*H+k3*CO2-k3r*H*HCO3+k4*HCO3-k4r*CO3*H+k5-
      k5r*H*OH+k6*HA-k6r*A*H+k0*(Hi-H));
funcUi=U+dt*(-k8*E*U/((1+Kes2/H+H/Kes1)*(KM+U*(1+U/Ks))*(1+NH4/Kp))+k0*(Ui-
      U));

      funcNH3i=NH3+dt*(2*k8*E*U/((1+Kes2/H+H/Kes1)*(KM+U*(1+U/Ks))*(1+NH
      4/Kp))+k2*NH4-k2r*NH3*H-k0*NH3);
funcNH4i=NH4+dt*(-k2*NH4+k2r*NH3*H-k0*NH4);
funcCO2i=CO2+dt*(k8*E*U/((1+Kes2/H+H/Kes1)*(KM+U*(1+U/Ks))*(1+NH4/Kp))-
      k3*CO2+k3r*H*HCO3-k0*CO2);
funcHCO3i=HCO3+dt*(k3*CO2-k3r*H*HCO3-k4*HCO3+k4r*CO3*H-k0*HCO3);
funcCO3i=CO3+dt*(k4*HCO3-k4r*CO3*H-k0*CO3);
funcOHi=OH+dt*(k5-k5r*H*OH-k0*OH);
funcHAi=HA+dt*(-k6*HA+k6r*A*H+k0*(HAi-HA));
funcAi=A+dt*(k6*HA-k6r*A*H-k0*HA);

funcHb=H+dt*(k2*funcNH4i-k2r*funcNH3i*funcHi+k3*funcCO2i-
      k3r*funcHi*funcHCO3i+k4*funcHCO3i
    -k4r*funcCO3i*funcHi+k5-k5r*funcHi*funcOHi+k6*funcHAi-
      k6r*funcAi*funcHi+k0*(Hi-H));
funcUb=U+dt*(-
      k8*E*funcUi/((1+Kes2/funcHi+funcHi/Kes1)*(KM+funcUi*(1+funcUi/Ks))*(1+fu
      ncNH4i/Kp))+k0*(Ui-U));
```

```
        funcNH3b=NH3+dt*(2*k8*E*funcUi/((1+Kes2/funcHi+funcHi/Kes1)*(KM+funcU
        i*(1+funcUi/Ks))*(1+funcNH4i/Kp))
+k2*funcNH4i-k2r*funcNH3i*funcHi-k0*NH3i);
funcNH4b=NH4+dt*(-k2*funcNH4i+k2r*funcNH3i*funcHi-k0*NH4i);

        funcCO2b=CO2+dt*(k8*E*funcUi/((1+Kes2/funcHi+funcHi/Kes1)*(KM+funcUi*(
        1+funcUi/Ks))*(1+funcNH4i/Kp))
    -k3*funcCO2i+k3r*funcHi*funcHCO3i-k0*CO2i);
funcHCO3b=HCO3+dt*(k3*funcCO2i-k3r*funcHi*funcHCO3i-
        k4*funcHCO3i+k4r*funcCO3i*funcHi-k0*HCO3i);
funcCO3b=CO3+dt*(k4*funcHCO3i-k4r*funcCO3i*funcHi-k0*CO3i);
funcOHb=OH+dt*(k5-k5r*funcHi*funcOHi-k0*OHi);
funcHAb=HA+dt*(-k6*funcHAi+k6r*funcAi*funcHi+k0*(HAi-HA));
funcAb=A+dt*(k6*funcHAi-k6r*funcAi*funcHi-k0*HAi);

    U = (funcUi+funcUb)/2+l;
    NH3 = (funcNH3i+funcNH3b)/2+l;
    NH4 = (funcNH4i+funcNH4b)/2;
    CO2 = (funcCO2i + funcCO2b)/2+l;
    HCO3 = (funcHCO3i + funcHCO3b)/2;
    CO3 = (funcCO3i + funcCO3b)/2;
    H = (funcHi + funcHb)/2;
    OH = (funcOHi + funcOHb)/2;
    HA = (funcHAi + funcHAb)/2;
    A = (funcAi +funcAb)/2;


}

/****************************************************/

void simulate (void)
{

 reaction (  );

 icount++;

 if(icount==nstep){
  fprintf(out,"%d %g %g %g  %g  %g %g %g %g %g %g %g %g\n",time, l, U, NH3,
  NH4, CO2, HCO3, CO3, H, OH, HA, A);

  fflush(out);
   icount=0;
 }

 if (funcHi==0) {
        time = total;
        }

}

/****************************************************/
void doit ( void )
```

```
{

  for (time = 0; time <=total; time++) {
 for ( istep = 1; istep <= nstep; istep++ ) {
    simulate ();
 }
 }


}
/***************************************************/
main ()

{char fname[30];
 int i;

    report_parameters ();
    initial_conditions();

    out2=fopen("ss.dat","wt");

    for (i=0; i<=k0loop; i++){

   k0=i*k0step;

  sprintf(fname,"out_%d.dat",i);
  out = fopen(fname,"wt");

    doit ();

    fclose(out);
    fprintf(out2, "%f %g\n", k0, H);
    fflush(out2);

    }

    fclose(out2);


}

/*****************************************************/

/* Random number generator
/* To generate real random numbers 0.0-1.0 */
/* Should be seeded with a negative integer */

float ran1(long *idum) {
   int j;
   long k;
   static long iy=0;
   static long iv[NTAB];
   float temp;
```

```
    if (*idum <= 0 || !iy) {
       if (-(*idum) < 1) *idum=1;
       else *idum = -(*idum);
       for (j=NTAB+7;j>=0;j--) {
          k=(*idum)/IQ;
          *idum=IA*(*idum-k*IQ)-IR*k;
          if (*idum < 0) *idum += IM;
          if (j < NTAB) iv[j] = *idum;
       }
       iy=iv[0];
    }
    k=(*idum)/IQ;
    *idum=IA*(*idum-k*IQ)-IR*k;
    if (*idum < 0) *idum += IM;
    j=iy/NDIV;
    iy=iv[j];
    iv[j] = *idum;
    temp=(float)AM*iy;
    if (temp > RNMX) return (float)RNMX;
    else return temp;
}

// gasdev returns a normally distributed deviate with zero mean and unit variance.
// idum -  set to any negative integer to initialize or reinitialize the random number generator.

float gasdev(long *idum)
{

    static int iset=0;
    static double gset;
    double fac,rsq,v1,v2;

    if (iset == 0) {
       do {
          v1=2.0*ran1(idum)-1.0;
          v2=2.0*ran1(idum)-1.0;
          rsq=v1*v1+v2*v2;
       } while (rsq >= 1.0 || rsq == 0.0);
       fac=sqrt(-2.0*log(rsq)/rsq);
       gset=v1*fac;
       iset=1;
       return (float)(v2*fac);
    } else {
       iset=0;
       return (float)gset;
    }
```

Appendix V XPP models for ester hydrolysis

Developed by Annette Taylor

#acid ester hydrolysis

```
S'=-(k1+k1a*H)*S+k0*(S0-S)
P'=(k1+k1a*H)*S-k2*P+k2r*Pm*H-k0*P
Pm'=k2*P-k2r*Pm*H-k0*Pm
H'=k2*P-k2r*Pm*H+k3-k3r*H*OH+k0*(H0-H)
OH'=k3-k3r*H*OH+k0*(OH0-OH)

aux pH=-log(H)/log(10)

#parameters
par k1=1e-5,k1a=1e-1,k2=1e-3,k2r=1
par k3=1e-3,k3r=1e11
par k0=0,S0=1,H0=1e-10,OH0=1e-4


#initial conditions
init S=1,P=0,Pm=0,H=1e-10,OH=1e-4

#numerical stuff
@ total=2000,dt=0.1,tol=1e-12, atol=1e-8, meth=stiff
@ xplot=t,yplot=pH,xhi=2000,ylo=1,yhi=14
@ maxstor=10000000
done
```

#enzyme ester hydrolysis

```
S'=-k1*S/((1+d*Kes2/H+d*H/Kes1)*(KM+S))+k0*(S0-S)
P'=k1*S/((1+d*Kes2/H+d*H/Kes1)*(KM+S))-k2*P+k2r*Pm*H-k0*P
Pm'=k2*P-k2r*Pm*H-k0*Pm
H'=k2*P-k2r*Pm*H+k3-k3r*H*OH+k0*(H0-H)
OH'=k3-k3r*H*OH+k0*(OH0-OH)

aux pH=-log(H)/log(10)

#parameters
par k1=1e-2,KM=1,Kes1=1e-4,Kes2=1e-8,k2=1e-4,k2r=1
par d=1,k3=1e-3,k3r=1e11
par k0=0,S0=1,H0=1e-10,OH0=1e-4


#initial conditions
init S=1,P=0,Pm=0,H=1e-10,OH=1e-4

#numerical stuff
@ total=2000,dt=0.1,tol=1e-12, atol=1e-8, meth=stiff
@ xplot=t,yplot=pH,xhi=2000,ylo=1,yhi=14
```

```
@ maxstor=10000000
done
```

#the aspirin clock

```
#AH = aspirin (solution), A=aspirin anion, H = acid, OH =
base, SH =salicyclic acid, S = anion,CH =acetic acid, C =
anion

AHs'=-k0*AHs^n+k0r*AH^n
AH'=k0*AHs^n-k0r*AH^n-k1*AH*H-k2*AH+k3*OH*A-k8*AH+k8r*A*H
A'=-k4*A*H-k5*A+k6*OH*A+k8*AH-k8r*A*H
SH'=k1*AH*H+k2*AH+k4*A*H-k9*SH+k9r*S*H
S'=k3*AH*OH+k5*A+k6*OH+k9*SH-k9r*S*H
CH'=k1*AH*H+k2*AH+k3*OH*AH+k4*A*H+k5*A-k10*CH+k10r*C*H
C'=k6*A*OH+k10*CH-k10r*C*H
H'=-k4*A*H+k7-k7r*OH*H+k8*AH-k8r*A*H+k9*SH-k9r*S*H+k10*CH-
k10r*C*H
OH'=-k3*AH*OH-k6*A*OH+k7-k7r*OH*H

#pH
aux pH=-log(H)/log(10)

#parameters
par n=1,k0=1.5e-3,k0r=1e-10,k1=2.2e-5,k2=1.4e-6,k3=0.012,
k4=5.4e-4,k5=2.44e-8,k6=0.087, k7=1e-
3,k7r=1e11,k8=3.2e5,k8r=1e9,k9=1e6,k9r=1e9,k10=8e5,k10r=4.5e10

#some initial conditions
init AHs=0.018,OH=1e-2,H=1e-12,AH=0,A=0,SH=0,S=0,CH=0,C=0

#numerical
@ total=1000,dt=0.01,tol=1e-12, atol=1e-8, meth=stiff
@ xplot=t,yplot=pH,xhi=1500,ylo=5,yhi=14
@ maxstor=10000000
Done
```

Appendix VI Matlab code for particle tracking

Developed by Tamas Bansagi

```
clear all
close all
%============================== PARAMETERS
==============================
n=100;        % number of pictures (background excluded)
bg=1;        % background image
z='C:\Users\chmtb\Desktop\RESEARCH_LEEDS\particle3\particle3a_'; % root
of file names
res=11.1;    % resolution pixel/mm
dt=0.08;     % time elapsed between frames in seconds (12.5 image/sec)
th=80;       % brightness threshold for filtering
```

```
dbp=30;     % assumed minimum distance between bright objects (BO) in
pixels
aop=40;     % assumed area of particle(s) in pixels
%========================================================================
====
filename=[z,num2str(bg),'.jpg'];
if n > 256 % colorbar works nicely only for fewer than 256 images
therefore colorbar needs some rescaling
    cl=256;
else
    cl=n;
end
cb_label= num2str(round(linspace(1,n,11)')); %set color bar label
jet_bck=colormap(jet(cl)); % set colormap jet_bck(1,1:3)=0; % set
colormap ibg=double(imread(filename)); i=ibg-ibg; %way of creating a
matrix of zeros pc=0; for y=(bg+1):n
    acl=y/n; %set color value for BO
    filename=[z,num2str(y),'.jpg'];
    j=double(imread(filename))-ibg; %load image as double precision
array
    j(j < th) = 0; % pixels with brightness below "th" are set to zero
    j(j >= th) = acl; % pixels with brightness above "th" are set to
predefined color
    i=i+j; % the act of superposition
    i(i > acl) = acl; % when BO overlap some pixels become greater than
"acl" therefore they need resetting to proper "acl" value
    [m(:,1) m(:,2)]=find(j); % identify non-zero elements, i.e. BOs in
image
    sm=size(m);
    d=zeros(sm(1)-1,1); %define a vector to hold distances between
pixels of BOs
    for e=1:sm(1)-1
        d(e)=sqrt(sum((m(e,:)-m(e+1,:)).^2)); %calculate distances
between pixels of BOs
    end
    d(d < dbp) = 0; % set distances above the assumed minimum distance
between BO in pixels to zero
    dz=find(d); % get indices of distances grater than "dbp"
    ldz=length(dz)+1;
    az(1)=0; % create "az" an auxilary vector for boundaries of BOs in
"m"
    az(2:ldz)=dz;
    az(ldz+1)=sm(1);
    for bl=1:ldz
        if (az(bl+1)-az(bl)+1) > aop
            pc=pc+1;

sp(pc,:)=[mean(m((az(bl)+1):(az(bl+1)),1)),mean(m((az(bl)+1):(az(bl+1))
,2))]; %average row and column indices of BOs between bounds stored in
"az"; "sp" is likely to store the coordinates of center points of
particles
        end
    end
    clear m az % clear them because in the next round they might have
different size end dx=diff(sp(:,2)); % calculate dy (note that
coordinates are reversed because matrix notation and pixel layout are
```

```
different) dy=-diff(sp(:,1)); % calculate dx dydx=dy./dx; %slope of
movement len=sqrt(dx.^2+dy.^2)/res; % lenght of movement % juggling
with numbers to make the phase of velocity vectors fall on unit circle
ndx=dx; ndx(ndx >= 0) = 0; ndx(ndx < 0) = 180;
ang=atan(dydx)*180/pi+ndx; nang=ang; nang(nang >= 0) = 0; nang(nang <
0) = 360; ang=ang+nang; % display results
imshow(i)
colormap(jet_bck)
colorbar('YTickLabel',cb_label);
set(gcf,'color','white')
hold on
plot(sp(:,2),sp(:,1),'-wo')
figure
subplot(3,1,1)
plot(len,':ko')
xlabel('frame');
ylabel('distance (mm)');
subplot(3,1,2)
plot(len/dt,':ro')
xlabel('frame');
ylabel('Speed (mm/sec)');
subplot(3,1,3)
plot(ang,':go')
xlabel('frame');
ylabel('ph. of vel. vec. on unit circle (deg)');
set(gca,'YTick',[0 90 180 270 360])
set(gcf,'color','white')
disp(['Number of frames (b.g. excluded): ',int2str(n-1)]) disp(['Number
of particle positions identified: ',int2str(pc)]) d_ang=diff(ang);
d_ang(abs(d_ang)<300)=0; phj=find(d_ang); % phj=[1; phj]; % comment out
if you want to include the first bit of the % experiment in the fitting
figure
plot(ang,':go')
xlabel('frame');
ylabel('ph. of vel. vec. on unit circle (deg)');
set(gca,'YTick',[0 90 180 270 360])
set(gcf,'color','white')
hold on
for i=1:length(phj)-1
    [fit_lin_par, stat] =
polyfit(phj(i)+1:phj(i+1),ang(phj(i)+1:phj(i+1))',1);
    lin = fit_lin_par(1).*(phj(i):phj(i+1))+fit_lin_par(2);
    slope(i)=fit_lin_par(1);
    plot(phj(i):phj(i+1),lin,'-r','LineWidth',2)
    hold on
    if fit_lin_par(1) < 0
        pozy=lin(1);
        pozx=phj(i);
    else
        pozy=lin(length(lin));
        pozx=phj(i+1)-1;
    end
    text(pozx,pozy+10,[num2str(i)])
    clear lin
end
hold off
```

```
% ===== MS Excel output (comment out if not needed) ==================
% SLOPES data_matrix(1,1:2)={'NOTE:','Unit of slopes: deg/frame';};
data_matrix(2,1:2)={'line#','slope';};
for i=1:length(phj)-1
    data_matrix(i+2,1:2)={i,slope(i);};
end
filename_xls=[z,'rev_slope','.xls'];
dos_command=['del ',filename_xls];
dos(dos_command);
xlswrite(filename_xls,data_matrix);
% DISTANCE TRAVELLED BY PARTICLE & SPEED BETWEEN FRAMES
dist_data_matrix(1,1:3)={'distance(n)=location(n+1)-
location(n)','Speed=dist(n)/dt',''};
dist_data_matrix(2,1:3)={'frame#','distance (mm)','speed (mm/sec)'};
for i=1:length(len)-1
    dist_data_matrix(i+2,1:3)={i,len(i),len(i)/dt};
end
filename_xls=[z,'dist_speed','.xls'];
dos_command=['del ',filename_xls];
dos(dos_command);
xlswrite(filename_xls,dist_data_matrix);
% ======================================================================
```